Title

Measurements of differential cross sections of Higgs boson production through gluon fusion in the H→WW∗→eνμν final state at s=13 TeV with the ATLAS detector

Authors

Aad, G
Abbott, B
Abeling, K
et al.

THE EUROPEAN
PHYSICAL JOURNAL C

Regular Article - Experimental Physics

Measurements of differential cross sections of Higgs boson production through gluon fusion in the $H \rightarrow WW^* \rightarrow e\nu\mu\nu$ final state at $\sqrt{s} = 13$ TeV with the ATLAS detector

ATLAS Collaboration[*]

CERN, 1211 Geneva 23, Switzerland

Abstract Higgs boson production via gluon–gluon fusion is measured in the $WW^* \rightarrow e\nu\mu\nu$ decay channel. The dataset utilized corresponds to an integrated luminosity of $139 \, \text{fb}^{-1}$ collected by the ATLAS detector from $\sqrt{s} = 13$ TeV proton–proton collisions delivered by the Large Hadron Collider between 2015 and 2018. Differential cross sections are measured in a fiducial phase space restricted to the production of at most one additional jet. The results are consistent with Standard Model expectations, derived using different Monte Carlo generators.

Contents

1 Introduction

Since the discovery of the Higgs boson in 2012, by the ATLAS [1] and CMS [2] collaborations, measurements of Higgs boson properties have remained consistent with the expectations of the Standard Model (SM). The Higgs boson mass has been determined, measurements of the Higgs coupling to fermions and gauge bosons have been performed (see, e.g. Refs. [3,4]), and differential cross sections have been measured by the ATLAS and CMS collaborations. Since the differential cross sections of the Higgs boson can be predicted with high precision, these measurements can be used to search for deviations from the Standard Model and probe the effect of higher-order corrections in perturbation theory.

This paper presents measurements of differential cross sections for Higgs boson production via gluon–gluon fusion (ggF) and decay into $WW^* \rightarrow e\nu\mu\nu$. Measuring the decay of the Higgs boson in the WW channel is an important component of fully characterising Higgs measurements in all of its decay states. The measurements are reported in a fiducial phase space, which minimizes extrapolations and therefore the model dependence of the results. Measurements of Higgs boson decays into WW bosons are well motivated because the large branching fraction makes the measurement competitive with the cleaner $\gamma\gamma$ and ZZ channels. Although the presence of neutrinos in the WW final states makes it impossible to fully reconstruct the final state kinematics, the high branching fraction makes the measurement competitive with fully leptonic final states. In addition, the Higgs boson's $WW^* \rightarrow e\nu\mu\nu$ decay mode has an advantage when compared with the decay into b-quark pairs, since the Higgs boson produced via ggF is not required to be highly boosted, allowing a detailed study of the full Higgs transverse momentum spectrum. Finally, the $e\nu\mu\nu$ final state is considered in order to avoid large backgrounds from Drell–Yan production that appear in the same flavour channels.

The analysis is performed using the full Run 2 dataset, corresponding to an integrated luminosity of $139 \, \text{fb}^{-1}$, collected with the ATLAS detector during 2015–2018 at a centre-of-mass energy $\sqrt{s} = 13$ TeV. Final states with at most one jet are considered. Final states with two jets are not considered in order to avoid large backgrounds from top production processes. The small expected contributions from Higgs

[*] e-mail: atlas.publications@cern.ch

production in the vector-boson fusion (VBF) and associated production (*VH*) processes are fixed to their SM expectations and considered as background. Previous ATLAS measurements of the differential cross section in this channel were performed on 20.3 fb^{-1} of data collected at a centre-of-mass energy of $\sqrt{s} = 8$ TeV [5], while the inclusive cross-section measurement in this channel was performed on 139 fb^{-1} of $\sqrt{s} = 13$ TeV data [6]. The CMS Collaboration published a measurement of the differential and inclusive cross sections in this channel using 137 fb^{-1} of data collected at a centre-of-mass energy of $\sqrt{s} = 13$ TeV [7]. Compared to the previous ATLAS result, the present measurement introduces a refinement in that the signal in each interval of the observable under consideration is extracted by means of a fit to a kinematic variable. Compared to the previous results obtained by subtracting expected background contributions from the data, the current method, which employs a fitting procedure gives an improved sensitivity and allows for a more comprehensive treatment of systematic uncertainties. The ATLAS and CMS collaborations have also performed differential cross-section measurements for the cases where the Higgs boson decays into $ZZ \rightarrow 4\ell$ and $\gamma\gamma$ [8,9].

The measurements of the differential cross sections are corrected for detector effects to a fiducial phase space defined at the particle level, through a procedure referred to as unfolding. Defining the selection criteria at the particle level removes the dependence on the theoretical modelling and facilitates direct comparison with a wide variety of theoretical predictions. The measurements are almost insensitive to the uncertainties on the ggF SM predictions to which they are compared.

The theoretical prediction of the differential cross section as a function of the Higgs boson transverse momentum (p_T^H) is calculated at next-to-next-to-leading order (NNLO) in quantum chromodynamics (QCD). In ggF production, the transverse momentum of the Higgs boson is balanced by soft quark and gluon emission, enabling the low-momentum region of this distribution to test the non-perturbative effects, the modelling of soft-gluon emissions calculated using resummation, and loop effects sensitive to the Higgs–Charm Yukawa coupling. The low p_T^H region is also sensitive to the interactions of the charm and bottom quarks with the Higgs boson. The high p_T^H region is sensitive to perturbative QCD effects, as well as possible contributions from 'beyond the Standard Model' (BSM) physics, and higher-dimensional effective operators in BSM Lagrangians [10,11].

The production kinematics of the Higgs boson produced in gluon fusion in a *pp* collision can be described by jet kinematic variables that include the number of jets and the rapidity of the leading jet ($|y_{j0}|$).[1] The $|y_{j0}|$ distribution probes

the theoretical modelling of hard gluon and quark emission. Measuring the cross section as a function of the number of jets provides information about the relative contributions of different Higgs production mechanisms. Processes with at most one jet are dominated by ggF and probe the higher-order QCD contributions to this production mechanism. In addition to measuring quantities sensitive to Higgs boson production, observables sensitive to its $WW^* \rightarrow e\nu\mu\nu$ decay are also explored. These include leptonic kinematic observables such as the leading lepton's transverse momentum ($p_T^{\ell 0}$) and the dilepton system's transverse momentum ($p_T^{\ell\ell}$), invariant mass ($m_{\ell\ell}$), rapidity ($y_{\ell\ell}$), azimuthal opening angle ($\Delta\phi_{\ell\ell}$), and also $\cos\theta^*$, defined as $\cos\theta^* = |\tanh(\frac{1}{2}\Delta\eta_{\ell\ell})|$ (where $\Delta\eta_{\ell\ell}$ is the lepton pseudorapidity difference). The observable $y_{\ell\ell}$ is highly correlated with the rapidity of the reconstructed Higgs boson (y_H), which is known to be sensitive to the parton distribution function (PDF) [12]. The observable $\cos\theta^*$ is longitudinally boost-invariant and sensitive to the spin structure of the produced diparticle pairs, as discussed in Ref. [13].

Finally, double-differential measurements are made, in which the Higgs production cross section is explored as functions of two variables simultaneously, with one sensitive to the production kinematics and the other to the decay kinematics. Specifically, the cross section is measured as a function of 0-jet and 1-jet bins versus $p_T^{\ell 0}$, $p_T^{\ell\ell}$, $m_{\ell\ell}$, $y_{\ell\ell}$, $\Delta\phi_{\ell\ell}$, and $\cos\theta^*$.

2 ATLAS detector

The ATLAS detector [14] is a multipurpose detector at the Large Hadron Collider at CERN, and almost fully covers the solid angle around the collision point. The innermost part of the detector covers the pseudorapidity range $|\eta| < 2.5$ and is used to gather information about the momentum and the sign of the charge of charged particles. This inner detector (ID) consists of a silicon Pixel detector, a silicon microstrip tracker, and a straw-tube transition-radiation tracker. The Pixel detector includes a new innermost layer, the insertable B-layer [15,16], added before Run 2. A thin superconducting solenoid surrounds the ID, providing it with a 2 T axial magnetic field. The inner detector is surrounded by electromagnetic and hadronic calorimeters. The electromagnetic (EM) calorimeter, consisting of lead absorbers and liquid argon

---

[1] ATLAS uses a right-handed coordinate system with its origin at the nominal interaction point (IP) in the centre of the detector and the *z*-

Footnote 1 continued

axis along the beam pipe. The *x*-axis points from the IP to the centre of the LHC ring, and the *y*-axis points upwards. Cylindrical coordinates (r, ϕ) are used in the transverse plane, ϕ being the azimuthal angle around the *z*-axis. The pseudorapidity is defined in terms of the polar angle θ as $\eta = -\ln\tan(\theta/2)$. Angular distance is measured in units of $\Delta R \equiv \sqrt{(\Delta\eta)^2 + (\Delta\phi)^2}$. Rapidity *y* is defined in terms of four-momentum as $y = \frac{1}{2}\ln((E + p_z)/(E - p_z))$.

(LAr), provides electromagnetic and hadronic energy measurements. It consists of a barrel component in the centre of the detector, covering $|\eta| < 1.475$, and two EM endcaps covering $1.375 < |\eta| < 3.2$. In addition, copper–LAr hadronic endcaps are placed behind the EM endcaps to capture hadronic energy in the $1.5 < |\eta| < 3.2$ region.

The EM calorimeter is surrounded by the steel and scintillator hadronic Tile calorimeter (TileCal), which measures the energy of hadrons. The Tile calorimeter consists of a central barrel covering $|\eta| < 1.0$, and two extended barrels in the forward regions, covering $0.8 < |\eta| < 1.7$. The regions closest to the beam pipe are covered by forward calorimeters (FCal), which cover $3.1 < |\eta| < 4.9$ and consist of three modules. The first module is made of copper–LAr and is used for electromagnetic measurements and the beginning of the hadronic shower. The other two modules consist of tungsten and LAr and complete the hadronic measurements.

The calorimeters are surrounded by a muon spectrometer (MS) with superconducting toroidal magnets made of eight air-core barrel loops and two endcaps. The toroid magnets produce a non-uniform magnetic field, resulting in a bending power ranging from 2.0 to 6.0 T m. The MS has a high-precision tracking chamber system covering $|\eta| < 2.7$ and consisting mainly of monitored drift tubes but complemented by cathode-strip chambers in the forward directions, where the background is highest. The MS uses resistive-plate chambers in the barrel and thin-gap chambers in the endcaps for triggering within $|\eta| < 2.4$ and to provide track coordinates in the non-bending plane.

A two-level trigger system is used to select events of interest. The first-level trigger is implemented in hardware and uses a subset of the detector information to accept events from the 40 MHz proton bunch crossings at a rate below 100 kHz. This is followed by a software-based trigger, which reduces the accepted event rate to 1 kHz on average depending on the data-taking conditions.

An exhaustive software suite [17] is used in data simulation, in the reconstruction and analysis of real and simulated data, in detector operations, and in the trigger and data acquisition systems of the experiment.

3 Signal and background modelling

The signal and background modelling is described using various generators to model the hard-scatter process, parton shower (PS), hadronization and underlying event (UE). The Higgs boson can be produced through ggF processes, vector-boson fusion (VBF), in association with a W or Z boson (VH) or with a top-quark pair ($t\bar{t}H$). There are other production modes as well, but those are not included in this analysis as their expected contributions are negligible. These include Higgs bosons produced with a bottom-quark pair

($b\bar{b}H$) or a single top quark (tH, with either an additional W boson, tWH, or an additional b-quark and light quark, $tHqb$). In the combined 0-jet and 1-jet signal regions (see Sect. 4), the non-ggF production modes make up 6.9% of the total expected Higgs boson event yield, with 60% of this contribution coming from VBF production.

The primary ggF signal process was modelled using POWHEG NNLOPS [18–22] interfaced with PYTHIA 8 [23]. The 0-jet, 1-jet and 2-jet cross sections are predicted at NNLO, NLO and LO, respectively. To obtain NNLO accuracy for observable distributions, the Higgs boson rapidity spectrum in HJ-MiNLO [24–26] was reweighted to that of HNNLO [27]. The resulting Higgs boson transverse momentum spectrum is compatible with the fixed-order HNNLO calculation and the HRES 2.3 calculation [28,29]. The AZNLO tune [30] of the parameter values was used for the PS, UE and hadronization. The ggF process is normalized to the N^3LO cross section in QCD with NLO electroweak corrections [31–41]. For the results, a comparison is made between the ggF process generated by POWHEG and an alternative generation performed by MADGRAPH5_AMC@NLO [42] with the NNPDF2.3LO [43] PDF set.

The VBF events were generated with POWHEG, interfaced with PYTHIA 8 and normalized to cross sections from NLO QCD with EW corrections, with an approximate NNLO QCD correction applied [44–46]. The VH production process was generated with POWHEG MiNLO, and interfaced with PYTHIA 8. The VH cross section is calculated at NNLO in QCD with NLO electroweak corrections for $q\bar{q}/qg \rightarrow VH$ and at NLO and next-to-leading-logarithm accuracy in QCD for $gg \rightarrow ZH$ [47–53].

For the ggF, VBF and VH predictions, the PDF4LHC15NNLO [54] PDF set was used. All of the Higgs boson cross sections and branching fractions are normalized in accordance with HDECAY [55–57] and PROPHECY4F [58–60] calculations, which provide NLO EW corrections and account for interference effects. The samples were generated assuming a Higgs boson mass of 125 GeV. The signal predictions described are not an extensive list of all available Monte Carlo simulations, and were chosen because of their applicability to this phase space.

The main sources of SM background that could resemble the signal process are the production of top quarks, dibosons, Z+jets, W+jets and multijets. The top-quark pair production process was simulated using POWHEG in the POWHEG BOX framework using the NNPDF3.0NLO PDFs, and interfaced with PYTHIA 8 using NNPDF2.3 PDFs for parton showering. The associated production of top quarks with W bosons, Wt, was modelled using the POWHEG BOX v2 generator at NLO in QCD, using the five-flavour scheme and the NNPDF3.0NLO set of PDFs. The diagram removal scheme [61] was used to remove interference between Wt and $t\bar{t}$ production. The $t\bar{t}$ process is normalized using cross

sections calculated at NNLO+NNLL [62], while the *Wt* process is normalized to NNLO. The alternative top-quark samples used to estimate certain systematic uncertainties were produced using MG5_aMC@NLO [42].

The *WW* background sample was generated using Sherpa 2.2.2 interfaced with NNPDF3.0nnlo PDFs [63]. The sample was generated with up to one jet at NLO accuracy and with two or three jets at LO accuracy. The loop-induced *gg*-initiated diboson processes were simulated by Sherpa 2.2.2 with up to one additional jet, interfaced with Sherpa 2.2.2 for the UE and PS, and used the NNPDF3.0nnlo PDF set.

The *WZ* and *ZZ* samples were generated with Sherpa 2.2.2, using the NNPDF3.0nnlo PDF set, at NLO accuracy for up to one jet and at LO accuracy for two or three jets. Events containing three vector bosons, *VVV*, were simulated with the Sherpa 2.2.2 generator, using the NNPDF3.0nnlo PDF set. The matrix elements are accurate to NLO for the inclusive process and to LO for up to two additional parton emissions.

Drell–Yan production was simulated with Sherpa 2.2.1 using the NNPDF3.0nnlo PDFs with dedicated parton shower tuning developed by the Sherpa authors.

Production of *Zγ* and *Wγ* events was modelled using Sherpa 2.2.8 at NLO accuracy for up to one jet, using the NNPDF3.0nnlo PDFs. They were interfaced with Sherpa 2.2.8 for the UE and PS.

The *W*+jets process modelling is based on a purely data-driven method. However, MC samples are used to validate the estimation as well as to estimate the sample composition uncertainties. The *V*+jets processes simulated in Powheg MiNLO interfaced with Pythia 8, are used for the validation of the *W*+jets modelling. The PDF set used in Powheg was CT14nnlo whereas the PDF set used in the parton shower was CTEQ6L1lo. The alternative *V*+jets samples used to estimate certain systematic uncertainties were produced using MadGraph5_aMC@NLO.

For the background processes, the AZNLO tune [30] is used for the diboson processes, while the A14 tune [64] is used for other processes.

The full list of Monte Carlo generators involved in the estimates used for this analysis is shown in Table 1.

All simulated samples include the effect of pile-up from multiple interactions in the same and neighbouring bunch crossings. This was achieved by overlaying each simulated hard-scatter event with minimum-bias events, simulated using Pythia 8 with the A3 tune. The Monte Carlo (MC) events were weighted to reproduce the distribution of the average number of interactions per bunch crossing ($\langle\mu\rangle$) observed in the data. The $\langle\mu\rangle$ value in data was rescaled by a factor of 1.03 ± 0.04 to improve agreement between data and simulation in the visible inelastic proton–proton (*pp*) cross-section [93].

All samples were processed through the ATLAS detector simulation [94] based on Geant4 [95], and reconstructed with the standard ATLAS reconstruction software. Data are removed if relevant detector components were not fully operational, or if other data integrity issues were identified, as described in Ref. [96].

4 Event selection

Events are selected using a combination of unprescaled single-lepton triggers and one *e*–*μ* dilepton trigger [97,98]. During the first year of data taking the single-electron (single-muon) trigger threshold was 24 (20) GeV, and was increased to 26 GeV for the remainder of Run 2. The dilepton trigger had p_T thresholds of 17 GeV for electrons and 14 GeV for muons. At least one of the leptons reconstructed offline is required to match the online object that was triggered on. If only the dilepton trigger was used, each reconstructed lepton is required to match the triggered object. The p_T of the reconstructed leptons that are matched to the trigger are required to be at least 1 GeV above the trigger-level threshold.

The analysis utilizes both the objects identified after the full detector reconstruction and objects identified at the particle level in simulation. The particle-level and reconstructed objects are selected in two stages. An overlap removal procedure is applied to the objects resulting from the first selection stage, to ensure that no object is counted twice. After the second selection stage, the objects are used to construct fiducial, signal and control regions.

4.1 Reconstructed objects

Reconstruction-level objects are built from the signals left in the detector by traversing particles. The overlap removal procedure performed on reconstructed objects after the first selection stage is complex, and is fully described in Ref. [6]. For reconstructed leptons, lepton identification is used in the signal selection and a separate lepton identification is used, with some selection criteria reversed, for the estimation of backgrounds with misidentified leptons.

Electrons are reconstructed as clusters of energy deposited in the EM calorimeter and associated tracks in the inner detector. At the first selection stage, electrons are required to have a transverse momentum of $p_T > 10$ GeV and $|\eta| < 2.47$. The longitudinal impact parameters must satisfy, $|z_0 \sin\theta| < 0.5$ mm, while the significance of the transverse impact parameters must satisfy $|d_0|/\sigma_{d_0} < 5$ [99]. A likelihood-based electron selection at the 'Very Loose' operating point is used [99]. At the second selection stage, electrons are required to have $p_T > 15$ GeV, and to be outside the transition region between the barrel and endcaps of the EM calorimeter, $1.37 < |\eta| < 1.52$. Electrons with

Table 1 Overview of simulation tools used to generate signal and background processes, as well as to model the UE and PS. The PDF sets are also summarized. Alternative event generators or quantities varied to estimate systematic uncertainties as well as alternative predictions used in the final-results comparison are shown in parentheses

Process	Matrix element (alternative)	PDF set	UE and PS model (alternative model)	Prediction order for total cross section
ggF H	POWHEG BOX v2 [18–22] NNLOPS [18,25,66] (MG5_AMC@NLO) [42,67]	PDF4LHC15NNLO [54]	PYTHIA 8 [65] (HERWIG 7) [68]	N^{3}LO QCD + NLO EW [31–41]
VBF H	POWHEG BOX v2 [20–22,66] (MG5_AMC@NLO)	PDF4LHC15NLO	PYTHIA 8 (HERWIG 7)	NNLO QCD + NLO EW [44–46]
VH excl. $gg \rightarrow ZH$	POWHEG BOX v2	PDF4LHC15NLO	PYTHIA 8	NNLO QCD + NLO EW [47–49, 51,52]
ttH	POWHEG BOX v2	NNPDF3.0NLO	PYTHIA 8	NLO [31]
$gg \rightarrow ZH$	POWHEG BOX v2	NNPDF3.0NLO	PYTHIA 8	NLO+NLL [50,53]
$qq \rightarrow WW$	SHERPA 2.2.2 [69] (Q_{cut})	NNPDF3.0NNLO [70]	SHERPA 2.2.2 [71–76] (SHERPA 2.2.2 [72,80]; μ_q)	NLO [77–79]
$qq \rightarrow WWqq$	MG5_AMC@NLO [42]	NNPDF3.0NLO	PYTHIA 8 (HERWIG 7)	LO
$gg \rightarrow WW/ZZ$	SHERPA 2.2.2	NNPDF3.0NNLO	SHERPA 2.2.2	LO [81]
$WZ/V\gamma^*/ZZ$	SHERPA 2.2.2	NNPDF3.0NNLO	SHERPA 2.2.2	NLO [82]
$V\gamma$	SHERPA 2.2.8 [69]	NNPDF3.0NNLO	SHERPA 2.2.8	NLO [82]
VVV	SHERPA 2.2.2	NNPDF3.0NNLO	SHERPA 2.2.2	NLO
$t\bar{t}$	POWHEG BOX v2 (MG5_AMC@NLO)	NNPDF3.0NLO	PYTHIA 8 (HERWIG 7)	NNLO+NNLL [83–89]
Wt	POWHEG BOX v2 (MG5_AMC@NLO)	NNPDF3.0NLO	PYTHIA 8 (HERWIG 7)	NNLO [90,91]
Z/γ^*	SHERPA 2.2.1 (MG5_AMC@NLO)	NNPDF3.0NNLO	SHERPA 2.2.1	NNLO [92]

$15 < p_T < 25$ GeV are required to satisfy a 'Tight' operating point, while electrons with $p_T > 25$ GeV must satisfy a 'Medium' operating point. Lower-energy electrons are required to satisfy a tighter operating point since they are more likely to originate from misconstructed objects. To reduce the number of misidentified electrons, these electrons must be well isolated from other objects, using the strictest isolation criteria as described in Ref. [100], which employ both calorimeter and tracking information. The approximate efficiency of identifying and isolating leading and subleading electrons in the phase space of this analysis is is 81% and 58%, respectively

Muons are reconstructed using tracking information from the inner detector and the muon spectrometer. The muon identification is defined by making two sets of requirements on the number of detector hits, the momentum resolution, the track goodness-of-fit, and other parameters [101]. At the first selection stage, muons with $p_T > 10$ GeV and $|\eta| < 2.7$ are considered if they are identified with the 'Loose' quality working point [102]. These muons must satisfy $|z_0 \sin\theta| < 1.5$ mm and $|d_0|/\sigma_{d_0} < 3$ requirements. At the second selection stage, muon track segments in the inner detector and muon spectrometer are required to match, as defined by the 'Tight' working point, which maximizes the muon purity. Additionally, muons selected at the second stage are required to have $p_T > 15$ GeV and pseudorapidity $|\eta| < 2.5$. These muons must also satisfy the strictest isolation requirement [101], which employ both calorimeter and tracking information and entail that the muons be well isolated from other objects in order to differentiate them from muons produced in background processes containing semileptonic decays of heavy-flavour hadrons. Finally, the muons selected at the second stage must satisfy $|z_0 \sin\theta| < 0.5$ mm and $|d_0|/\sigma_{d_0} < 3$ requirements. The approximate efficiency of identifying and isolating leading and subleading muons in the phase space of this particular analysis is 85% and 72%, respectively.

Jets are reconstructed using the anti-k_t algorithm [103] with a radius parameter $R = 0.4$, and corrections are applied to calibrate the jets to the particle-level energy scale, as described in Ref. [104]. Jets are then calibrated using the particle-flow algorithm as described in Ref. [105]. At the first selection stage, jets are required to have $p_T > 20$ GeV, be located within $|\eta| < 4.5$, and satisfy the 'jet vertex tagger' (JVT) requirements described in Ref. [106]. The JVT requirements are applied to jets in the range $20 < p_T < 60$ GeV and $|\eta| < 2.4$ in order to reduce the number of jets from pile-up. At the second selection stage, jets are required to have $p_T > 30$ GeV. Jets containing b-hadrons are identified using the DL1r b-tagging algorithm and are required to satisfy the 85% efficiency working point; they must also satisfy $p_T > 20$ GeV and be located within $|\eta| < 2.5$ [107].

The missing transverse momentum, defined as the negative vector sum of the transverse momenta of objects in the detector, measures the sum of the momenta of the neutrinos in the $WW^* \to e\nu\mu\nu$ decays. Two types of missing transverse momentum are used in the analysis. The first, denoted by E_T^{miss}, is described in Ref. [108] and accounts for the inclusion of electrically neutral objects by using jets directly in the calculation of E_T^{miss}. This E_T^{miss} definition is used in the calculation of all sensitive variables because it provides superior resolution for objects used to discriminate signal events from background events. The second is a track-based variable, denoted by $E_T^{\text{miss, track}}$ [108], which uses tracks matched to jets instead of the calorimeter jet energy and is used to suppress backgrounds from misidentified objects because it has better pile-up robustness than E_T^{miss}. Both types of missing transverse momentum use a 'Tight' working point [108], which is equivalent to the condition that forward jets must satisfy the $p_T > 30$ GeV requirement. The estimation of the lower energy components is based on tracks for both E_T^{miss} definitions.

4.2 Signal region selection

The signal region (SR) is defined using reconstructed objects at the second selection stage, and subdivided into categories of events that contain either no jets or one jet. The two categories share a common pre-selection and signal selection, but have partially different background rejection selections applied to reflect the variation in background composition between the jet multiplicity bins.

The signal region contains events with exactly two opposite-sign different-flavour leptons, with the leading (subleading) lepton required to satisfy $p_T > 22$ GeV ($p_T > 15$ GeV). The invariant mass of the two leptons, $m_{\ell\ell}$, is required to be greater than 10 GeV in order to remove low-mass meson resonances and Drell–Yan events. To ensure orthogonality with the VH (WH, ZH) phase space, events with additional reconstructed leptons with p_T greater than 15 GeV are removed. In order to suppress misreconstructed low-energy events, the $E_T^{\text{miss, track}}$ is required to be greater than 20 GeV. Events that contain a b-tagged jet with $p_T > 20$ GeV are removed to suppress backgrounds from top-quark processes. Additionally, a selection requiring a minimum value of 80 GeV is applied to the transverse mass (m_T), defined as:

$$m_T = \sqrt{\left(E_T^{\ell\ell} + E_T^{\text{miss}}\right)^2 - \left|\vec{p}_T^{\ell\ell} + \vec{E}_T^{\text{miss}}\right|^2}$$

where $E_T^{\ell\ell} = \sqrt{|\vec{p}_T^{\ell\ell}|^2 + m_{\ell\ell}^2}$. This requirement suppresses non-WW diboson background, as well as background from misidentified objects.

Table 2 Event selection criteria used to define the signal and fiducial region in the analysis. The E_T^{miss} definition described in Sect. 4.3 is used for the selection at particle level. The reconstructed electrons are required to have a pseudorapidity $|\eta| < 2.47$, excluding the transition region between the barrel and endcaps of the EM calorimeter, $1.37 < |\eta| < 1.52$

Category	$N_{\text{jet},(p_T>30\,\text{GeV})} = 0$	$N_{\text{jet},(p_T>30\,\text{GeV})} = 1$
Pre-Selection	Exactly two isolated leptons ($\ell = e, \mu$) with opposite charge $p_T^{\text{lead}} > 22\,\text{GeV}$, $p_T^{\text{sublead}} > 15\,\text{GeV}$ $|\eta_e| < 2.5$, $|\eta_\mu| < 2.5$, $p_T^{\text{jet}} > 30\,\text{GeV}$ $m_{\ell\ell} > 10\,\text{GeV}$ $E_T^{\text{miss, track}} > 20\,\text{GeV}$	
Background rejection	$N_{b\text{-jet},(p_T>20\,\text{GeV})} = 0$	
	$\Delta\phi_{\ell\ell,E_T^{\text{miss}}} > \pi/2$ $p_T^{\ell\ell} > 30\,\text{GeV}$	$\max(m_T^\ell) > 50\,\text{GeV}$ $m_{\tau\tau} < m_Z - 25\,\text{GeV}$
	$m_T > 80\,\text{GeV}$	
$H \to WW^* \to \ell\nu\ell\nu$ topology	$m_{\ell\ell} < 55\,\text{GeV}$ $\Delta\phi_{\ell\ell} < 1.8$	

For the signal region category containing zero jets, a p_T threshold of 30 GeV is used to define the jet-counting criterion, meaning that the region has zero jets with $p_T > 30$ GeV. The azimuthal angle between the dilepton system and the missing transverse momentum, $\Delta\phi_{\ell\ell,E_T^{\text{miss}}}$, is required to be larger than $\pi/2$. Since the leptons and E_T^{miss} are typically back to back for signal events, this requirement removes potential pathological events in which the E_T^{miss} points in the direction of the lepton pair because of misidentified objects. The transverse momentum of the dilepton system, $p_T^{\ell\ell}$, is required to be at least 30 GeV in order to reject events in which a Z boson decays into leptonically decaying τ-leptons.

For the signal region category containing exactly one jet that satisfies $p_T > 30$ GeV, the larger of the two lepton transverse masses, each defined as $m_T^\ell = \sqrt{2 p_T^\ell E_T^{\text{miss}}(1 - \cos(\phi_\ell - \phi_{E_T^{\text{miss}}}))}$, is required to exceed 50 GeV. Processes with at least one real W boson typically have a large value of m_T^ℓ for at least one of the two leptons, so a lower bound on this variable suppresses $Z/\gamma^* \to \tau\tau$ and multi-jet events. The 1-jet region also requires the di-τ candidate invariant mass, $m_{\tau\tau}$, as computed using the collinear approximation [109], to be less than $m_Z - 25$ GeV in order to remove $Z/\gamma^* \to \tau\tau$ background events.[2]

The signal region, divided into 0-jet and 1-jet categories, exploits the lepton kinematics to enhance a signal similar to that predicted by the SM. The azimuthal opening angle between the leptons, $\Delta\phi_{\ell\ell}$, is required to be less than 1.8 radians because the charged leptons in leptonic $H \to WW^* \to \ell\nu\ell\nu$ tend to be more collimated than those from non-resonant WW background. This is due to the spin-zero initial state of the resonant process and the $V - A$ structure of the weak interaction. Both the 0-jet and 1-jet categories also require that the dilepton invariant mass, $m_{\ell\ell}$, be less than 55 GeV. Table 2 summarizes all the require-

ments imposed on the signal region. The overall acceptance of the signal region, as defined by the number of events in the signal region, divided by the number of events passing the pre-selection, is 28%.

4.3 'Truth' objects

The particle-level objects are simulated before particles traverse the detector, and can be found in the signal samples after the parton shower generation step. Collinear photons, for which the angular separation between the photon and particle-level lepton is $\Delta R < 0.1$, are added to the four-momentum of the lepton. The electrons and muons with $|\eta| < 2.7$ and transverse momentum higher than 10 GeV, and jets with $|\eta| < 4.5$ and transverse momentum higher than 20 GeV, are selected at the first selection stage.

Simulated particle-level jets are built from all stable particles with $c\tau > 10$ mm, including neutrinos, photons, and leptons from hadron decays or produced in the shower. However, all decay products from the Higgs boson decay and the leptonic decays of associated vector bosons are removed from the inputs to the jet algorithm. The jets are reconstructed using the anti-k_t algorithm [103] with a radius parameter $R = 0.4$ implemented in the FastJet package [110]. After this first selection stage, an overlap removal procedure is applied to objects that are near each other and mimic the SR selection. A particle-level electron is rejected if it is in the vicinity of a muon with $\Delta R(e, \mu) < 0.1$, or a jet with $0.2 < \Delta R(e, j) < 0.4$. Conversely, a jet is rejected if there is an electron within $\Delta R(e, j) < 0.2$. A muon is rejected if there is a jet within $\Delta R(\mu, j) < 0.4$. The MC 'truth'-level E_T^{miss} arises from neutrinos, and is calculated from preselected objects, as well as jets that are not required to satisfy the pre-selection criteria. At the second selection stage, further selection criteria are applied to the particle-level objects. A higher jet-p_T requirement of 30 GeV is applied, while elec-

---

[2] m_Z refers to the mass of the Z boson, i.e. 91.18 GeV.

Table 3 Event selection criteria used to define the control regions in the analysis. The pre-selection requirements were applied in all six control regions. The definitions of $m_{\tau\tau}$, m_{T}^{ℓ}, and the jet-counting p_{T} thresholds are the same as for the signal regions. The selection criteria that are reversed or different in the CR in order to make it orthogonal to the SR are marked in bold

CR	$N_{\mathrm{jet},(p_{\mathrm{T}}>30\,\mathrm{GeV})} = 0$	$N_{\mathrm{jet},(p_{\mathrm{T}}>30\,\mathrm{GeV})} = 1$
$qq \to WW$	$N_{b\text{-jet},(p_{\mathrm{T}}>20\,\mathrm{GeV})} = 0$ $\Delta\phi_{\ell\ell,E_{\mathrm{T}}^{\mathrm{miss}}} > \pi/2$ $p_{\mathrm{T}}^{\ell\ell} > 30$ GeV **$55 < m_{\ell\ell} < 110$ GeV** **$\Delta\phi_{\ell\ell} < 2.6$**	**$m_{\ell\ell} > 80$ GeV** **$\lvert m_{\tau\tau} - m_Z \rvert > 25$ GeV** $\max\left(m_{\mathrm{T}}^{\ell}\right) > 50$ GeV
$t\bar{t}/Wt$	**$N_{b\text{-jet},(20\,\mathrm{GeV}<p_{\mathrm{T}}<30\,\mathrm{GeV})} > 0$** $\Delta\phi_{\ell\ell,E_{\mathrm{T}}^{\mathrm{miss}}} > \pi/2$ $p_{\mathrm{T}}^{\ell\ell} > 30$ GeV **$\Delta\phi_{\ell\ell} < 2.8$**	**$N_{b\text{-jet},(p_{\mathrm{T}}>30\,\mathrm{GeV})} = 1$** **$N_{b\text{-jet},(20\,\mathrm{GeV}<p_{\mathrm{T}}<30\,\mathrm{GeV})} = 0$** $m_{\tau\tau} < m_Z - 25$ GeV $\max\left(m_{\mathrm{T}}^{\ell}\right) > 50$ GeV
$Z/\gamma^* \to \tau\tau$	$N_{b\text{-jet},(p_{\mathrm{T}}>20\,\mathrm{GeV})} = 0$ **$m_{\ell\ell} < 80$ GeV** **no $E_{\mathrm{T}}^{\mathrm{miss,\,track}}$ requirement** **$\Delta\phi_{\ell\ell} > 2.8$**	$m_{\tau\tau} > m_Z - 25$ GeV $\max\left(m_{\mathrm{T}}^{\ell}\right) > 50$ GeV

trons and muons are required to satisfy $p_{\mathrm{T}} > 15$ GeV and be within $\lvert\eta\rvert < 2.5$. The particle-level objects selected at the second stage are used in the definition of the fiducial regions, constructed to mimic the signal region as closely as possible.

4.4 Fiducial region selection

The fiducial region (FR) selection is defined using particle-level objects, before the detector reconstruction is applied. This selection is designed to be as close as possible to the signal region in order to avoid large extrapolation uncertainties. To obtain the fiducial region, all the selections shown in Table 2 are applied at the particle level. Additionally, the absolute rapidity of the dilepton system, $\lvert y_{\ell\ell}\rvert$, is required to be less than 2.5, in order to match the constraints due to the coverage of the ATLAS detector. As shown in Table 2, the fiducial phase space at particle level includes a veto on jets containing b-quarks. If a jet is matched with a weakly decaying b-hadron, it is labelled as a b-jet. The overall correction factor, defined as the number of reconstructed signal events in the SR divided by the number of signal events in the fiducial region, is 35%. The number of events that pass into both the reconstructed signal region and fiducial region is 2250, the number of events that pass the reconstructed signal region and do not pass into the fiducial region is 352, the number of events that do not pass into the reconstructed signal region and pass into the fiducial region is 5117, and the number of events that fail to reach either region is 144109.

Table 4 Normalization factors for all background contributions constrained by control regions, as determined in the fit (described in Sect. 7) to the p_{T}^H observable

Background	Normalization factor
$qqWW$ $N_{\mathrm{jet}} = 0$	0.97 ± 0.07
$qqWW$ $N_{\mathrm{jet}} = 1$	0.91 ± 0.13
Z+jets $N_{\mathrm{jet}} = 0$	0.91 ± 0.07
Z+jets $N_{\mathrm{jet}} = 1$	1.02 ± 0.12
Top $N_{\mathrm{jet}} = 0$	1.07 ± 0.24
Top $N_{\mathrm{jet}} = 1$	1.03 ± 0.18

5 Background estimation

The contributions from SM processes that mimic the signal production are estimated using a variety of methods. One method involves defining a normalization factor by comparing data with MC events in regions rich in background, known as control regions (CRs). The normalization factor is a free parameter that is obtained when the fitting procedure (described in Sect. 7) is applied simultaneously to all signal and control regions. The background in the signal regions is then scaled by the normalization factor, ensuring the background modelling is normalized to the real data. The control regions are close to the signal regions, in order to minimize the extrapolation uncertainties, but have one or two selection criteria reversed in order to ensure a high purity of background events and orthogonality with respect to the signal

regions. Backgrounds estimated from control regions include those containing two W bosons, which closely resemble the signal and include top-quark production ($t\bar{t}$ and Wt) and WW production. A control region is also used to estimate the backgrounds from the $Z/\gamma^* \to \tau\tau$ process, which resembles the signal when the τ-leptons decay leptonically. The selections used to define the control regions are shown in Table 3 for the 0-jet and 1-jet categories, and Table 4 shows the corresponding normalization factors.

The presence of jets originating from b-quarks is used to identify processes containing top quarks. The 0-jet top control region contains a requirement that $\Delta\phi_{\ell\ell} < 2.8$ in order to remain alligned with the signal region, while retaining high statistics. The 1-jet top control region removes events with low-p_T b-jets ($N_{b\text{-jet},(20\,\mathrm{GeV} < p_T < 30\,\mathrm{GeV})}$) in order to ensure that the ratio of $t\bar{t}$ to Wt is similar to that in the signal region and thus minimize the influence of secondary shape differences. The purity of the 0-jet (1-jet) top control region, defined as the ratio of the top-quark component to the total expectation, is 89% (98%).

In the WW and $Z/\gamma^* \to \tau\tau$ control regions the requirement that no b-jets with $p_T > 20$ GeV be present is applied in order to reduce the top-quark contamination in those regions. The defining feature of regions containing WW background is a selection on the dilepton invariant mass ($m_{\ell\ell}$), as shown in Table 3. The 0-jet WW control region has a requirement that $\Delta\phi_{\ell\ell} < 2.8$ in order to keep the region closely alligned to the signal region, while maximizing statistics. The WW control region containing one jet also reduces the $Z/\gamma^* \to \tau\tau$ contamination by using the same $m_{\tau\tau}$ and $\max(m_T^\ell)$ selections that are applied in the signal region. The $Z/\gamma^* \to \tau\tau$ control regions are defined by requiring leptons from the τ decay to be well separated ($\Delta\phi_{\ell\ell} > 2.8$), and the invariant mass of the leptons to be low ($m_{\ell\ell} < 80$ GeV) to eliminate contamination from $Z \to ee/\mu\mu$ events. In addition, the $Z/\gamma^* \to \tau\tau$ regions have no $E_T^{\mathrm{miss,\ track}}$ requirement. The purity of the 0-jet (1-jet) WW CR is 67% (34%). The lower purity in the 1-jet region is acceptable because the ratio of WW events to top-quark events in the control region is close to that in the SR. The purity of the $Z/\gamma^* \to \tau\tau$ region is 94% and 76% in the 0-jet and 1-jet regions respectively. Table 4 shows the normalization factors extracted from each control region after the fitting procedure is applied to the p_T^H distribution.

Distributions of $m_{\ell\ell}$ and $\cos\theta^*$ in the top and $Z/\gamma^* \to \tau\tau$ control regions of the 0-jet channel are shown in Fig. 1, alongside the distribution of $m_{\ell\ell}$ in a loose region including both the WW control region and the signal region in the 1-jet channel. The normalization factors obtained from the fitting procedure are applied to distributions in the figure.

Backgrounds from processes such as W+jets and multi-jet production have large cross sections, and can be mistaken for signal events in the rare cases where a jet is misidenti-fied as an isolated lepton. These backgrounds are estimated using a data-driven method known as the extrapolation-factor method, and are labelled as 'Mis-Id' in the figures. This method is described in detail in Ref. [6].

The remaining backgrounds include WZ, $W\gamma$, ZZ and VVV, have small cross sections, and are estimated from simulation. Finally, Higgs boson production via processes such as vector-boson fusion, and in association with vector bosons or top-quark pairs, are fixed to their SM predictions and treated as background. This is because these additional production mechanisms have a negligible impact on the final results when treated as part of the signal model.

6 Measured yields, uncertainties and distributions

To obtain differential fiducial cross sections, the reconstruction-level signal and background expectations are fitted to the data, and the resulting information is corrected for detector effects to the particle level. A signal region is defined for each bin of each observable, from which the number of signal events N_S is extracted from a fit to the data. A combined fit is performed to the m_T distribution in the range 80 to 160 GeV in bins of 10 GeV. This combined fit includes single-bin WW, top, and $Z/\gamma^* \to \tau\tau$ control regions. Normalization factors used to normalize the backgrounds in the signal regions are extracted from the combined fit. The fit is performed for each slice of the measured observables. Normalization factors are compatible across all observables.

The fit is performed using the profile likelihood method (see, e.g., Ref. [111]), where the likelihood is constructed as the product of likelihoods from individual signal and control regions, as well as the product of all bins in those regions. All background estimates, both the data-driven estimate and those obtained from MC simulation, are added to the Poisson expectations. The systematic uncertainties are included as nuisance parameters, constrained by a Gaussian term.

The analysis is affected by theoretical uncertainties in the MC modelling of the signal and background, as well as experimental uncertainties related to the detector measurements. The signal and background expectations depend on nuisance parameters, which correspond to systematic uncertainties. The ggF signal uncertainties are a small contribution since the measurement is made in a fiducial region, making it independent of the type of signal model assumed. Uncertainties in the shape of the ggF signal distribution are minimized since the measurement is made in individual bins of kinematic variables. The uncertainties on the ggF cross-section predictions do not impact the measurements. The only remaining signal uncertainties are the uncertainties that affect the detector level corrections. An example of such an uncertainty is the jet shower shape uncertainty, since changes in how jets are reconstructed can affect truth-level and reconstruction-level
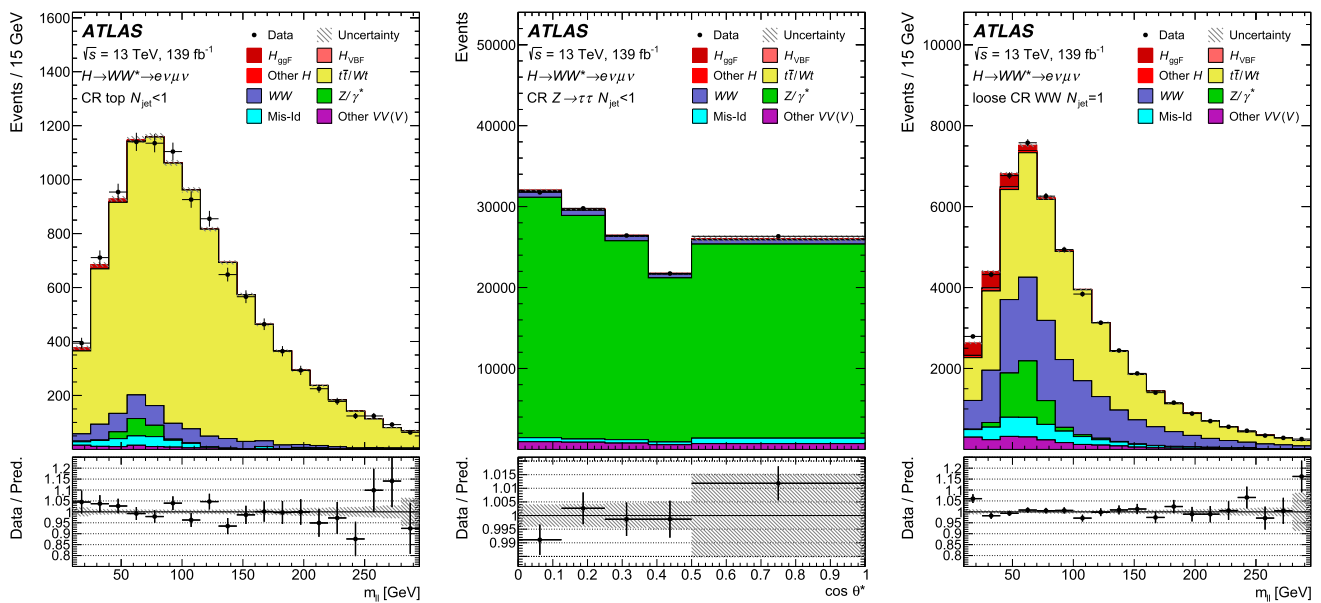
Fig. 1 Distributions of $m_{\ell\ell}$ in the top control region of the 0-jet channel (left), $\cos\theta^*$ in the $Z/\gamma^* \to \tau\tau$ control regions of the 0-jet channel (centre), and $m_{\ell\ell}$ in a loose region including both the WW control region and the signal region in the 1-jet channel (right). The MC backgrounds are normalized by normalization factors obtained from signal plus background fits to the observable that is being plotted. Model uncertainties shown are obtained from the fit result using a reweighting technique

quantities differently. These residual uncertainties are taken into account. The uncertainties in non-ggF Higgs production processes are treated in the same way as the uncertainties in the other backgrounds, and cross-section uncertainties are accounted for.

Various uncertainties related to detector measurements are considered. Uncertainties associated with identifying, reconstructing and calibrating objects such as electrons, muons, jets and missing transverse momentum, as well as tagging jets as originating from b-quarks are evaluated. The systematic uncertainty associated with the energy/momentum scale and resolution of objects is estimated by performing a scaling or smearing of the energy/momentum, and observing its effect on the yields and shape of the distribution of selected events in the final state. The systematic uncertainty is evaluated by comparing the $\pm 1\sigma$ variations with the nominal prediction. The missing transverse momentum is constructed from various objects, as described in Sect. 4.1, and has uncertainties associated with those objects. Uncertainties in the measured efficiencies for electron and muon triggers and pile-up are included as systematic uncertainties. The uncertainty in the combined 2015–2018 integrated luminosity is 1.7% [112], obtained using the LUCID-2 detector [113] for the primary luminosity measurements.

The theoretical uncertainties in the MC modelling take into account QCD scale uncertainties, parton shower (PS) and underlying event (UE) modelling, and parton distribution function (PDF) uncertainties. To calculate the QCD scale uncertainties, the renormalization ($\mu_{\rm r}$) and factorization ($\mu_{\rm f}$)

scales are varied in order to estimate the impact of missing higher-order corrections in fixed-order perturbative predictions. To estimate the QCD scale uncertainty for the Higgs boson signal, the Stewart–Tackmann method [114] is followed. For the backgrounds originating from WW bosons, top production, and $Z/\gamma^* \to \tau\tau$, the scale uncertainty is evaluated using the envelope of seven-point $\mu_{\rm r}$, $\mu_{\rm f}$ variations, with $\mu_{\rm r}$ and $\mu_{\rm f}$ each varying by factors of 0.5 and 2, subject to the constraint that $0.5 \leq \mu_{\rm r}/\mu_{\rm f} \leq 2.0$, and the maximum variation of the event yields is taken as the uncertainty.

The PDF uncertainties are calculated following the standard PDF4LHC prescriptions [115].

The uncertainties related to the UE and PS, as well as generator uncertainties, are estimated using alternative generators, and taken into account for the WW, top and $Z/\gamma^* \to \tau\tau$ backgrounds. In addition to that, for WW and top backgrounds, the uncertainties associated with matching NLO matrix elements to parton showers are estimated. For the WW background, an uncertainty is estimated to account for the fact that 0–1 additional jets are generated at NLO, while 2–4 additional jets are generated at LO. An additional uncertainty applied to single-top processes is estimated by comparing samples using different diagram removal schemes to account for interference between Wt and top-pair production [61].

A pruning procedure is used in order to improve the stability of the likelihood maximization by neglecting sources of small uncertainties. For this, any systematic uncertainty that induces a yield change of less than 0.1% for a given pro-
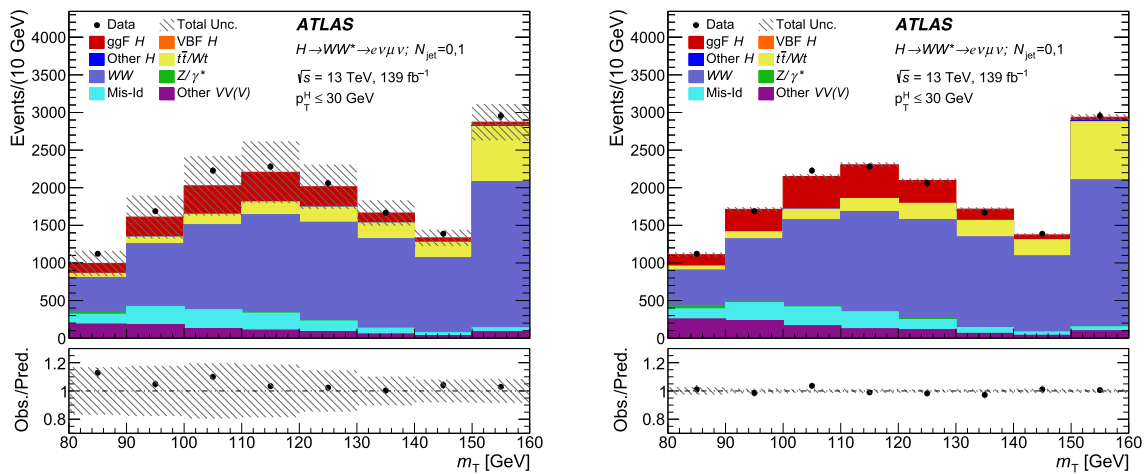
Fig. 2 Pre-fit (left) and post-fit (right) distribution of the transverse mass m_T of the Higgs boson in the first bin of the transverse momentum p_T^H: 0–30 GeV for $N_{jet} = 0, 1$. The last bin in m_T contains the overflow of events with $m_T > 160$ GeV
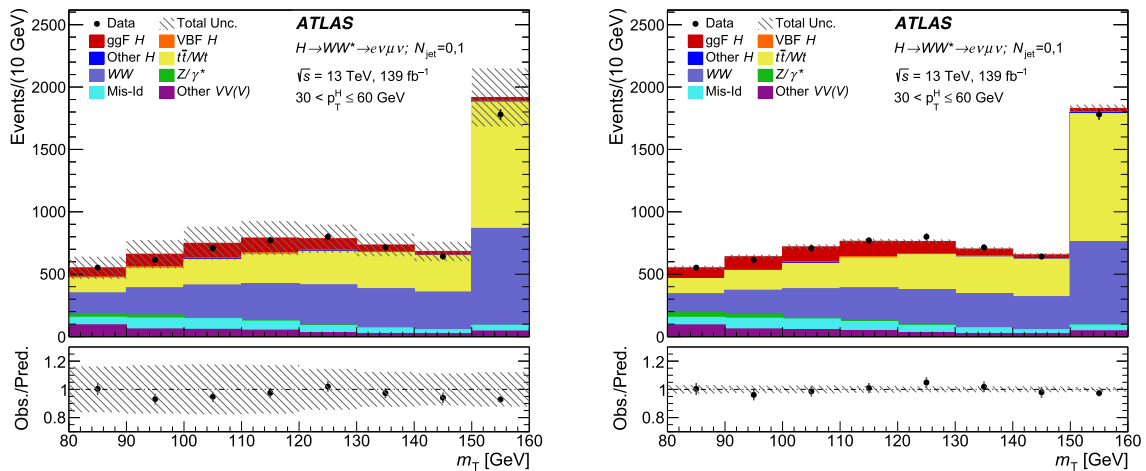
Fig. 3 Pre-fit (left) and post-fit (right) distribution of the transverse mass m_T of the Higgs boson in the second bin of the transverse momentum p_T^H: 30–60 GeV for $N_{jet} = 0, 1$. The last bin in m_T contains the overflow of events with $m_T > 160$ GeV
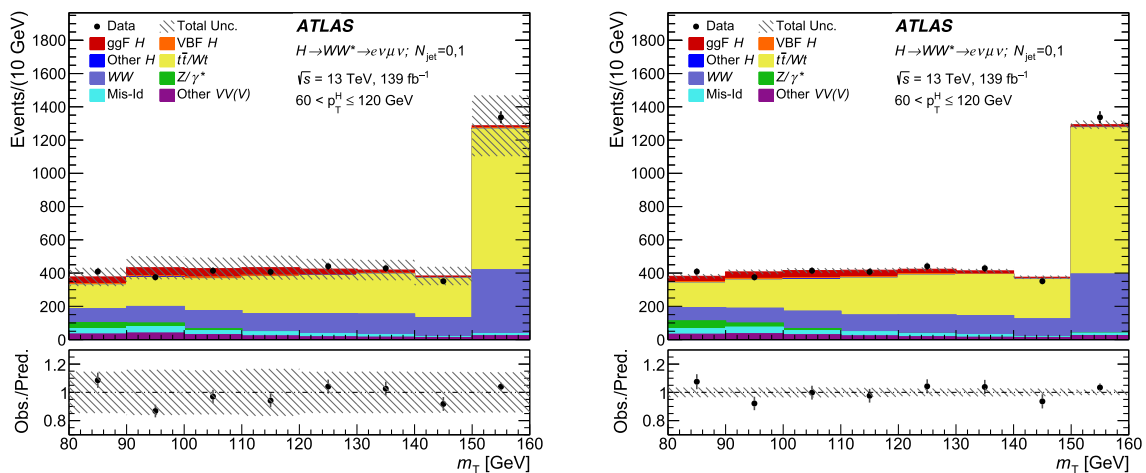
Fig. 4 Pre-fit (left) and post-fit (right) distribution of the transverse mass m_T of the Higgs boson in the third bin of the transverse momentum p_T^H: 60–120 GeV for $N_{jet} = 0, 1$. The last bin in m_T contains the overflow of events with $m_T > 160$ GeV

cess in an observable bin is neglected for that bin and that process. Furthermore, for any systematic uncertainty which is very likely to be compatible with a pure normalization effect across m_T bins (with a p-value $p > 95\%$), the shape component is neglected.

7 Unfolding

The reconstruction-level measurements are extrapolated to their particle-level quantities using a procedure known as unfolding [116]. This procedure uses Monte Carlo signal samples to define the correlation between reconstruction-level and particle-level quantities. These correlations are described in terms of a response matrix C, such that

$$\vec{n}_{\text{reco}} = C \cdot \vec{n}_{\text{particle-level}} + \vec{n}_{\text{out-of-fiducial}},$$

where $\vec{n}_{\text{reco}}$ is the vector of event counts in bins of the reconstruction-level quantity, $\vec{n}_{\text{particle-level}}$ is the vector of event counts in bins of the particle-level quantity, and $\vec{n}_{\text{out-of-fiducial}}$ is the vector of signal events that pass the selection at the reconstruction level but are not inside the fiducial region defined at the particle level. In practice, the response matrix is derived from the migration matrix, a two-dimensional distribution of simulated events encoding the correlation between the particle- and reconstruction-level quantities, by normalizing each element to the total number of events in the corresponding particle-level bin. In this way, acceptance, resolution and efficiency effects are encoded in the matrix. Assuming that the response derived from simulation is representative of the detector response in real data, the particle-level distributions in data can be obtained by applying the inverse of the response matrix to the measured data.

The practical application of this procedure faces a challenge related to the lack of regularization: the bin migrations between particle and reconstruction levels induce off-diagonal entries in the response matrix, leading to negative off-diagonal entries in its inverse and ultimately to the amplification of uncertainties.

Two different approaches to alleviate this are presented here. The first approach is an unfolding procedure that uses a Tikhonov-regularized [117] in-likelihood unfolding algorithm. The likelihood used extracts the reconstruction-level signal yields by means of signal strengths μ_j multiplying the expected event yields $s_{j,m}^{r,\text{exp}}$ in m_T bin m and observable bin j, and is of the form

$$\mathcal{L}(\vec{\mu}, \vec{\theta}) = \prod_{j=1}^{N_{\text{bin}}} \prod_{m=1}^{N_{m_T}} P\left(N_j | \mu_j s_{j,m}^{r,\text{exp}}(\vec{\theta}) + \sum_{n=1}^{N_{\text{bg}}} \mu_n^b b_{j,m,n}(\vec{\theta})\right)$$
$$\times \left\{ \prod_{c=1}^{N_{\text{CR}}} P(N_c | s_c^{r,\text{exp}}(\vec{\theta}) + \sum_{n=1}^{N_{\text{bg}}} \mu_n^b b_{c,n}(\vec{\theta})) \right\} \times \prod_{k=1}^{N_\theta} N(\tilde{\theta}_k | \theta_k).$$

In the Poisson terms P, the quantities N_j and N_c are the numbers of observed events in bin j of the signal region, and in control region c, respectively; $s_c^{r,\text{exp}}$ is the expected event count in CR c; and $b_{j,m,n}$ and $b_{c,n}$ are the expected event counts in observable bin j and m_T bin m of the SR and in CR c, respectively, of the n-th background process. Finally, μ_n^b is the normalization factor for the n-th background process (and is fixed to 1 for backgrounds not estimated using CRs). The N_θ nuisance parameters in the Gaussian terms N are represented by $\vec{\theta}$. The SR is further subdivided into $e\mu$ and μe, depending on which of the two leptons has the higher p_T, but this is not shown explicitly in the above expression. Also, when not considering the N_{jet} observable, the $N_{\text{jet}} = 0$ and $N_{\text{jet}} = 1$ SRs are treated separately in the fit; this further subdivision is not displayed explicitly either.

The signal $s_j^r = \mu_j s_j^{r,\text{exp}}$ of the reconstruction-level distribution in the j-th observable bin can be rewritten as

$$s_j^r = \sum_i s_i^t C_{ij} + f_j$$

where s_i^t is the signal yield in the particle-level bin i, f_j is the number of reconstructed events that are not in the fiducial region

$$f_j = s_j^{r,\text{exp}} - \sum_i M_{ij}$$

and C_{ij} is the response matrix

$$C_{ij} = M_{ij} / s_i^{t,\text{exp}}$$

given by the migration matrix M_{ij} and the predicted particle-level yield $s_i^{t,\text{exp}}$. The quantities $s^{r,\text{exp}}$, $s^{t,\text{exp}}$, and M are obtained from Monte Carlo predictions, with full dependencies on nuisance parameters from theory and experimental sources, i.e. $s^{r,\text{exp}} = s^{r,\text{exp}}(\vec{\theta})$, $s^{t,\text{exp}} = s^{t,\text{exp}}(\vec{\theta})$, and $M = M(\vec{\theta})$, and these dependencies are fully maintained throughout the likelihood maximization.

A Tikhonov regularization term is included in the likelihood as a penalty term, taking the form

$$P(\vec{x}) = \exp\left(-\tau \cdot \left(\sum_{i=2}^{N_{\text{bin}}-1} ((x_{i-1} - x_i) - (x_i - x_{i+1}))^2\right)\right)$$

with x being the quantity for which the curvature should be regularized. For this analysis, the measured particle-level signal strength, $x_i = s_i^t / s_i^{t,\text{exp}}$, is chosen as the regularized quantity (see also, e.g., Ref. [118]). This type of regularization is chosen for all single-differential distributions in this analysis. For the double-differential cross-section measurements, independent values of τ are chosen for each of the
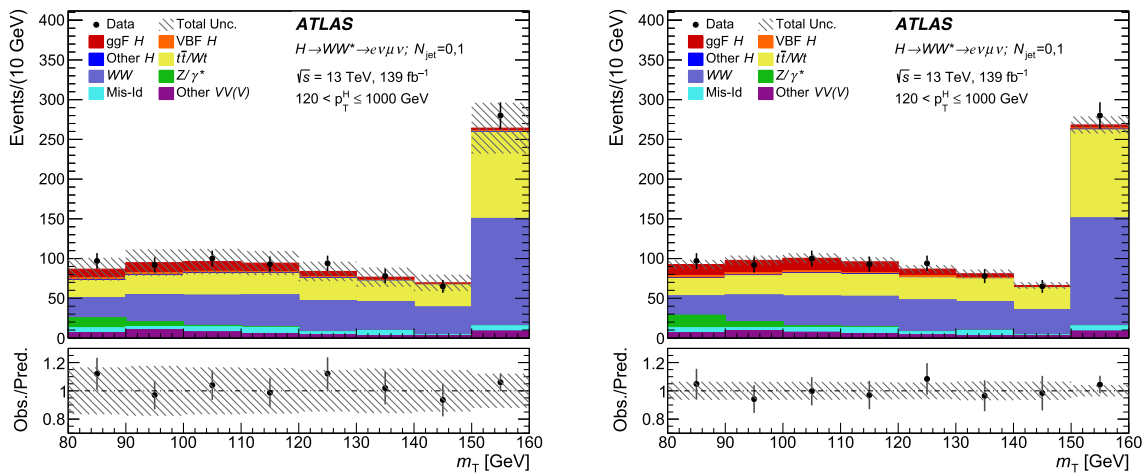
Fig. 5 Pre-fit (left) and post-fit (right) distribution of the transverse mass m_T of the Higgs boson in the last bin of the transverse momentum p_T^H: 120–1000 GeV for $N_{jet} = 0, 1$. The last bin in m_T contains the overflow of events with $m_T > 160$ GeV

two jet multiplicity bins. No regularization across jet bins is performed, as two bins are not enough to define a curvature.

The choice of a value for the regularization parameter τ is a trade-off between minimizing statistical fluctuations on the one hand, and the potential bias induced by adding an artificial constraint to the measurement on the other. This compromise is reached by first constructing distributions with the number of signal plus background events in each particle-level bin, fluctuated randomly by its respective Poisson uncertainty. The 'toy' distributions are then unfolded using the original response matrix in order to obtain the unfolded particle-level distribution. A bias is then calculated by subtracting the original particle-level events from the unfolded particle-level events for 1000 toy simulations for each value of the regularization parameter τ. The average of the bias for all these toy simulations is compared with the statistical uncertainty for each value of τ for each SR bin, and a value for τ is chosen so as to attain the lowest bias relative to uncertainty for most of the bins. Values of τ near 1 were investigated since previous studies using this technique showed this range to be optimal. The final τ values range from 0.25 to 1.5. For the example of the p_T^H variable, a τ value of 0.25 was chosen, and corresponds to values of the maximum bias divided by the uncertainty of 0.06, 0.01, 0.01, and 0.02 for the lowest to highest bins, respectively.

A second unfolding procedure was performed as a cross-check and yielded similar results. This procedure extracts the reconstructed differential cross sections from the same statistical model, but then performs an iterative Bayesian unfolding (IBU), which uses the number of iterations as the regularization parameter. Further details of this method and the results obtained using it are provided in the Appendix.

The statistical and systematic uncertainties are propagated to the final result consistently, including their effects on the detector response. The entries of the response matrix are sub-

Fig. 6 Measured differential fiducial cross section for p_T^H in the 0+1-jet fiducial region using the regularized in-likelihood unfolding method. Uncertainty bars on the data points include statistical and systematic uncertainties from experimental and theory sources as well as background normalization effects and shape effects from background and signal. Uncertainty bands on the predictions shown are dominated by normalization effects on the signal arising from showering, PDF models, α_s and the QCD scale. The legend includes p-values quantifying the level of agreement between the data and the predictions, including all sources of uncertainty. The systematic uncertainties of the data are shown separately
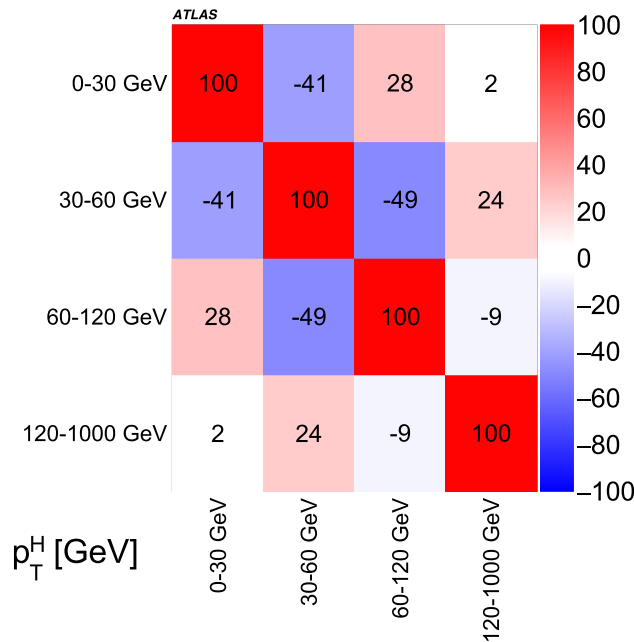
ject to correlated uncertainties among the matrix elements, which are incorporated into the statistical model for the in-likelihood procedure. For the iterative Bayesian unfolding procedure, the post-fit values of all nuisance parameters are propagated to the detector response, and the uncertainties are included in the bin-by-bin covariances and checked for coverage using toy distributions. Cross-section normalization uncertainties from theory that affect the signal are excluded from the measurement and instead are included in the predictions for comparison, while effects on the shape are fully propagated alongside the experimental uncertainties.

Fig. 7 Measured differential fiducial cross section for $m_{\ell\ell}$ (left) and $y_{\ell\ell}$ (right) in the 0+1-jet fiducial region using the regularized in-likelihood unfolding method. Uncertainty bars on the data points include statistical and systematic uncertainties from experimental and theory sources as well as background normalization effects and shape effects from background and signal. Uncertainty bars on the predictions shown are dominated by normalization effects on the signal arising from showering, PDF models, α_s and the QCD scale. The legend includes p-values quantifying the level of agreement between the data and the predictions, including all sources of uncertainty. The systematic uncertainties of the data are shown separately

Fig. 8 Measured differential fiducial cross section for $p_T^{\ell\ell}$ (left) and $\Delta\phi_{\ell\ell}$ (right) in the 0+1-jet fiducial region using the regularized in-likelihood unfolding method. Uncertainty bars on the data points include statistical and systematic uncertainties from experimental and theory sources as well as background normalization effects and shape effects from background and signal. Uncertainty bands on the predictions shown are dominated by normalization effects on the signal arising from showering, PDF models, α_s and the QCD scale. The legend includes p-values quantifying the level of agreement between the data and the predictions, including all sources of uncertainty. The systematic uncertainties of the data are shown separately

Several tests were performed to assess the robustness of the unfolding procedure. The purpose of the tests is to determine whether the unfolding procedure is biased by variations in the input samples that account for different spectral shapes, different Monte Carlo generators, new-physics contributions and systematic correlations. For the first tests, fluctuated MC truth-level distributions were created by fluctuating individual observable bins within their respective Poisson uncertainties. The fluctuated distributions are folded, and then unfolded, and the resulting unfolded distributions are found to closely match the original fluctuated truth-level distribution, showing that no biases were introduced. The same migration matrix, derived from SM ggF simulation, is used to fold and unfold the distributions. Since the migration matrix is only composed of Monte Carlo signal events, biases could be introduced by correlated nuisance parameters that only affect the signal. Thus, for the second tests, toy datasets generated with random values of the nuisance parameters demonstrated that no such biases are introduced in the construction of the migration matrix.

Fig. 9 Measured differential fiducial cross section for $p_T^{\ell 0}$ (left) and $\cos\theta^*$ (right) in the 0+1-jet fiducial region using the regularized in-likelihood unfolding method. Uncertainty bars on the data points include statistical and systematic uncertainties from experimental and theory sources as well as background normalization effects and shape effects from background and signal. Uncertainty bands on the predictions

shown are dominated by normalization effects on the signal arising from showering, PDF models, α_s and the QCD scale. The legend includes p-values quantifying the level of agreement between the data and the predictions, including all sources of uncertainty. The systematic uncertainties of the data are shown separately
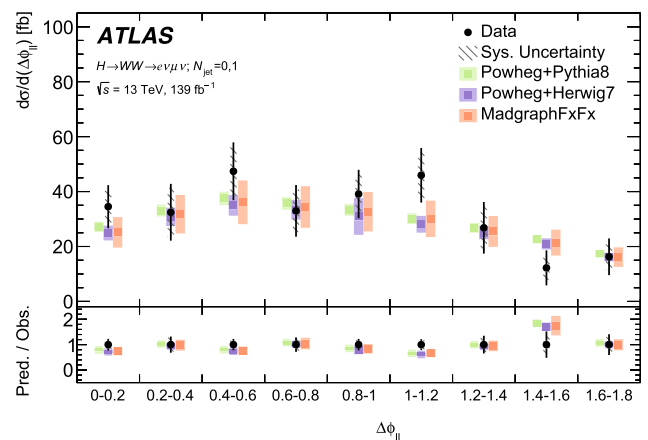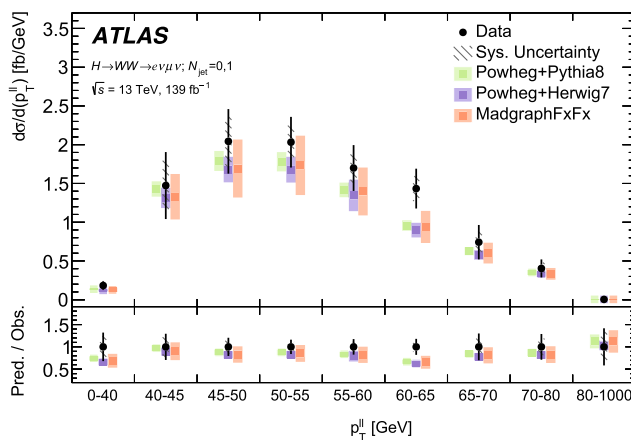

Fig. 10 Measured differential fiducial cross section for $|y_{j0}|$ in the 1-jet fiducial region using the regularized in-likelihood unfolding method. Uncertainty bars on the data points include statistical and systematic uncertainties from experimental and theory sources as well as background normalization effects and shape effects from background and signal. Uncertainty bands on the predictions shown are dominated by normalization effects on the signal arising from showering, PDF models, α_s and the QCD scale. The legend includes p-values quantifying the level of agreement between the data and the predictions, including all sources of uncertainty. The systematic uncertainties of the data are shown separately

8 Results

The results of the measurement are illustrated in the figures in this section. The m_T distributions are obtained for all bins of each observable: $|y_{j0}|$, p_T^H, $p_T^{\ell 0}$, $p_T^{\ell\ell}$, $m_{\ell\ell}$, $y_{\ell\ell}$, $\Delta\phi_{\ell\ell}$, and $\cos\theta^*$. Figures 2, 3, 4 and 5 show examples of the pre- and post-fit m_T distributions at the reconstruction level for bins of the p_T^H observable, which are inputs to the unfolding procedure. The number of bins and bin edges were chosen

in order to maximize the Signal/$\sqrt{\text{Background}}$ significance measure, while minimizing the bin migrations and statistical errors. In the distributions obtained after the fitting procedure is performed, all systematic uncertainties are included, and the background is normalised using the normalisation factors extracted from the control regions. The Higgs boson transverse momentum, p_T^H, is defined as the p_T of the combined two-lepton system and missing transverse momentum at the reconstruction and particle levels, and is binned in p_T bins in the ranges 0–30 GeV, 30–60 GeV, 60–120 GeV and 120–1000 GeV. The ggF Higgs production predictions are derived from Monte Carlo simulated samples normalized to the best SM predicted cross sections from Table 1. These figures show that the data agree with the Standard Model expectation for the Higgs boson signal and backgrounds within the uncertainties. After the fitting procedure is performed, there is a decrease in uncertainties due to the additional information that results from the comparison to data in both the signal and control regions. The fit induces correlations between the nuisance parameters, which reduce the total uncertainties in the post-fit distributions via the correlation matrix.

The final differential fiducial cross sections for each observable, obtained using the regularized in-likelihood unfolding method are shown in Figs. 6, 7, 8, 9, 10 for the single-differential distributions, and Figs. 11, 12, 13 for the double-differential distributions. Figure 14 shows the correlations of the unfolded cross sections in the signal regions in the different p_T^H intervals. The numbers in the legend on the right are shown in percentages.

The compatibility of the data and each set of predictions is characterized by the p-values, shown in the respective figure legends. These p-values are computed from the fit of the

Fig. 11 Measured differential fiducial cross section for $m_{\ell\ell}$ (left) and $\Delta\phi_{\ell\ell}$ (right) versus N_{jet} in the 0-jet and 1-jet fiducial regions using the regularized in-likelihood unfolding method. Uncertainty bars on the data points include statistical and systematic uncertainties from experimental and theory sources as well as background normalization effects and shape effects from background and signal. Uncertainty bands on

the predictions shown are dominated by normalization effects on the signal arising from showering, PDF models, α_s and the QCD scale. The legend includes p-values quantifying the level of agreement between the data and the predictions, including all sources of uncertainty. The systematic uncertainties of the data are shown separately

Fig. 12 Measured differential fiducial cross section for $y_{\ell\ell}$ (left) and $p_T^{\ell\ell}$ (right) versus N_{jet} in the 0-jet and 1-jet fiducial regions using the regularized in-likelihood unfolding method. Uncertainty bars on the data points include statistical and systematic uncertainties from experimental and theory sources as well as background normalization effects and shape effects from background and signal. Uncertainty bands on

the predictions shown are dominated by normalization effects on the signal arising from showering, PDF models, α_s and the QCD scale. The legend includes p-values quantifying the level of agreement between the data and the predictions, including all sources of uncertainty. The systematic uncertainties of the data are shown separately

respective predictions, including uncertainties in normalization and shape, to the observed data. The total cross sections (sum over all bins) are compatible with each other for all observables. The data and predictions agree very well, as demonstrated by the high p-values for all of the plots. No significant differences are observed between the measured cross sections and their Standard Model Monte Carlo predictions.

The uncertainties with the largest impact on the results include uncertainties related to jet and muon reconstruction. Theory uncertainties associated with the top-quark and WW

backgrounds, and with the difficulty of modelling $V\gamma$ processes also play a leading role. For the POWHEG+PYTHIA 8 prediction, the uncertainties were evaluated in several different regions of phase space and summed in quadrature as described in Ref. [6], whereas for the POWHEG+HERWIG 7 sample, they could only be evaluated inclusively for each bin, resulting in a slightly less precise evaluation. Other leading uncertainties include ones affecting the data-driven background estimates for misidentified objects, as well as uncertainties related to normalizing the backgrounds from control regions. The uncertainties are listed in Table 5, which shows ranges of values that correspond the different bins of the
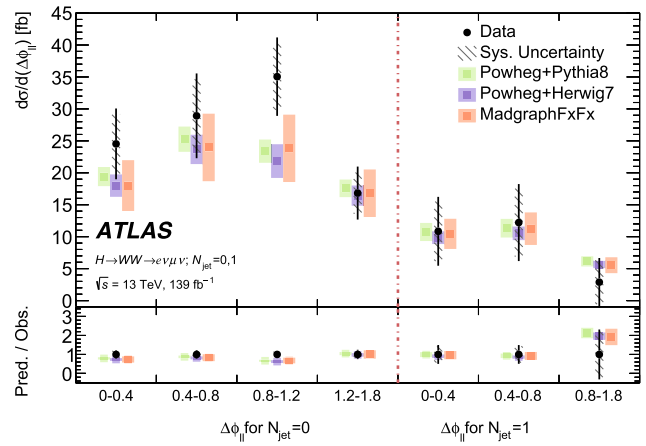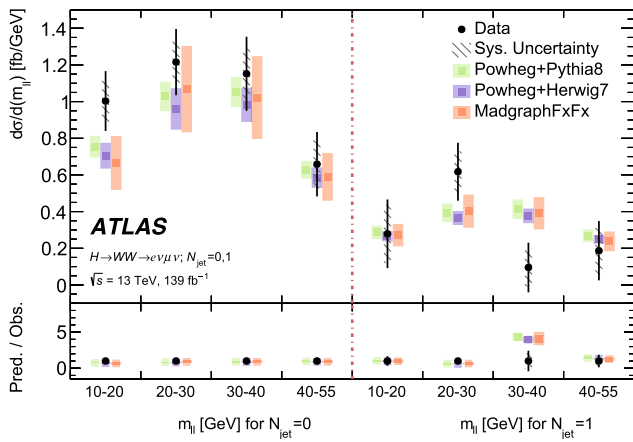
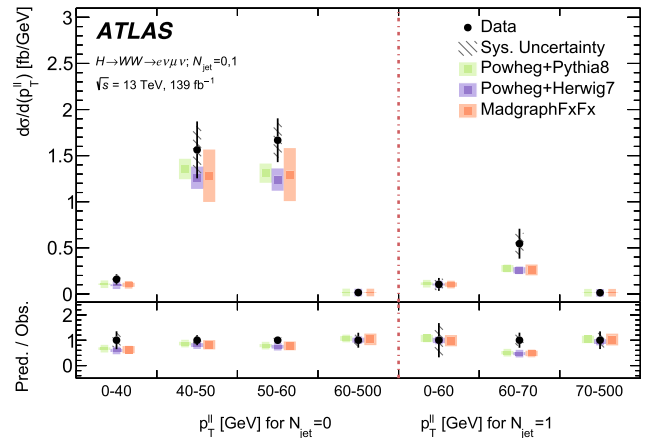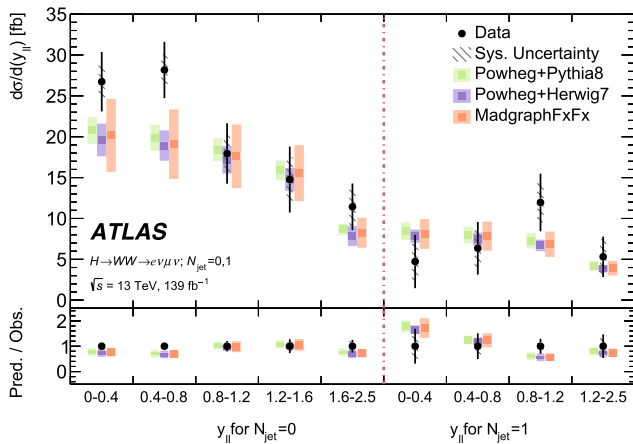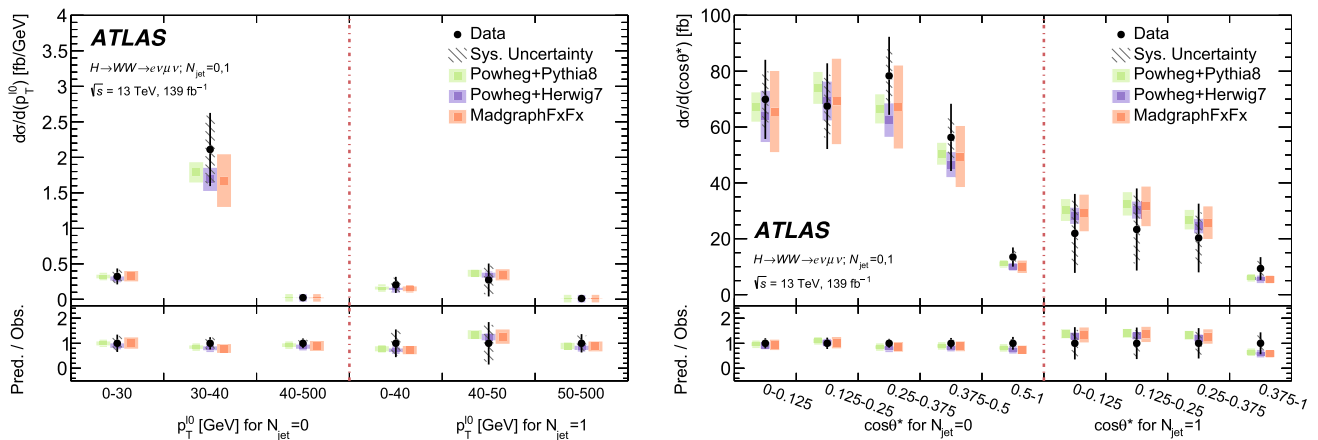**Fig. 13** Measured differential fiducial cross section for $p_T^{\ell 0}$ (left) and $\cos\theta^*$ (right) versus N_{jet} in the 0-jet and 1-jet fiducial regions using the regularized in-likelihood unfolding method. Uncertainty bars on the data points include statistical and systematic uncertainties from experimental and theory sources as well as background normalization effects and shape effects from background and signal. Uncertainty bands on

the predictions shown are dominated by normalization effects on the signal arising from showering, PDF models, α_s and the QCD scale. The legend includes p-values quantifying the level of agreement between the data and the predictions, including all sources of uncertainty. The systematic uncertainties of the data are shown separately

Fig. 14 Post-fit correlations of the observed cross sections for the bins of transverse momentum p_T^H. The legend on the right shows numbers in percentages

measured observables. Table 6 shows a detailed breakdown of the uncertainties for the p_T^H variable obtained after the final fitting procedure is performed.

The integrated fiducial cross section is obtained using the procedure described above but without binning in any observable (and consequently without any regularization). It is measured to be $56.0^{+10.0}_{-9.5}$ fb.

9 Conclusion

Measuring the Higgs boson's differential production cross section is an important aspect of measuring Higgs properties and further testing the Standard Model. This analysis has measured single- and double-differential cross sections for Higgs boson production via gluon–gluon fusion and decay into $WW^* \to e\nu\mu\nu$ in bins of the final-state transverse mass, m_T. The measurement was performed using the full LHC Run 2 dataset of 13 TeV proton–proton collisions collected with the ATLAS detector during 2015–2018, corresponding to an integrated luminosity of 139 fb^{-1}. The resulting m_T distributions and measurements of the differential cross sections in fiducial regions are presented for the $|y_{j0}|$, p_T^H, $p_T^{\ell 0}$, $p_T^{\ell\ell}$, $m_{\ell\ell}$, $y_{\ell\ell}$, $\Delta\phi_{\ell\ell}$, and $\cos\theta^*$ observables. Likelihood unfolding with Tikhonov regularisation is used to transform the reconstruction-level quantities to their particle-level distributions in each of these eight observables, and in each of the last six of them versus jet multiplicity. Performing the measurement at the particle level facilitates direct comparison with theoretical predictions and minimizes the impact of the signal uncertainties on the final results. The results agree extremely well with Standard Model expectations, derived using the POWHEG+PYTHIA 8 , POWHEG+HERWIG 7 and MAD-GRAPH5_AMC@NLO Monte Carlo generators. The leading uncertainties are related to jet and muon reconstruction, theoretical modelling of the WW and $V\gamma$ backgrounds, and data-driven background estimates for misidentified objects. The results improve upon those previously obtained by ATLAS, mainly by using more data and analysing a larger suite of observables. In addition, these results were obtained by using a fitting procedure, unlike the previous version of the anal-

Table 5 The statistical uncertainties of the data and Monte Carlo predictions, as well as experimental and theoretical uncertainties of the measured cross sections for each kinematic variable. The uncertainties vary depending on the m_T bin in which the cross sections are measured, as demonstrated by the range shown for each entry. The dominant sources of systematic uncertainties are discussed in the text

Variable	Data statistical (%)	MC statistical (%)	Experimental (%)	Theory (%)
$y_{\ell\ell}$	14–22	5.3–10	6.9–15	5.9–15
$p_T^{\ell\ell}$	15–29	6.4–14	8.2–31	6.8–27
$p_T^{\ell 0}$	13–28	6.3–13	9.3–28	14–34
$\Delta\phi_{\ell\ell}$	11–39	6.1–18	7.8–22	13–27
y_{j0}	23–51	12–26	21–54	26–58
$\cos\theta^*$	11–15	5.8–7.6	8.5–11	8.9–14
p_T^H	8.5–72	6.2–18	10–58	12–27
$m_{\ell\ell}$	12–25	5.6–11	7.5–15	7.3–20
$y_{\ell\ell}$ vs N_{jet}	9.0–62	3.9–25	8.0–20	5.0–53
$p_T^{\ell\ell}$ vs N_{jet}	9.8–36	4.7–20	12–41	9.9–50
$p_T^{\ell 0}$ vs N_{jet}	9.6–50	5.8–20	10–35	9.4–74
$\Delta\phi_{\ell\ell}$ vs N_{jet}	9.6–65	5.6–18	6.8–31	14–74
$\cos\theta^*$ vs N_{jet}	13–50	6.8–25	7.7–39	8.9–58
$m_{\ell\ell}$ vs N_{jet}	12–152	5.7–44	8.9–58	7.2–82

Table 6 Relative cross section uncertainties broken down for each bin in p_T^H

Contribution	0 – 30 GeV	30 – 60 GeV	60 – 120 GeV	120 – 1000 GeV
Total relative uncertainty	19	51	108	62
Total systematic uncertainty	17	41	81	45
Statistical uncertainties from data	8.5	29	72	43
Statistical uncertainties from simulation	6.2	15	17	18
Experimental systematic uncertainty	10	24	58	31
Flavour tagging	4.9	6.1	13	18
Jet Energy Scale	4.9	17	30	21
Jet Energy Resolution	4.8	8.4	12	10
Missing transverse energy	4.6	8.2	11	8.2
Muons	4.6	4.2	4.8	2.3
Electrons	3.2	2.2	2.5	1.1
Misidentified objects	3.9	10	3.3	1.3
Pile-up	3.8	1.2	6.9	4.4
Luminosity	2.7	4.5	3.5	2.8
Systematic uncertainty from theory	11	27	23	25
On gluon-fusion production	6.1	7.1	4.7	5.2
On Vector Boson Fusion production	2.4	1.8	2.7	3.2
On top quark production	4.3	20	18	21
On decays of $Z \to \tau\tau$	4.2	5.9	2.2	3.9
On the WW background	7.3	10	12	6.0
On other diboson processes	5.9	14	7.8	8.8
Background normalization factors	2.3	0.7	0.9	0.6

ysis, which relied on a simple subtraction of the expected background event yields from the observed event yields.

Data Availability Statement This manuscript has no associated data or the data will not be deposited. [Authors' comment: "All ATLAS scientific output is published in journals, and preliminary results are made available in Conference Notes. All are openly available, without restriction on use by external parties beyond copyright law and the standard conditions agreed by CERN. Data associated with journal publications are also made available: tables and data from plots (e.g. cross section values, likelihood profiles, selection efficiencies, cross section limits, ...) are stored in appropriate repositories such as HEPDATA (http://hepdata.cedar.ac.uk/). ATLAS also strives to make additional material related to the paper available that allows a reinterpretation of the data in the context of new theoretical models. For example, an extended encapsulation of the analysis is often provided for measurements in the framework of RIVET (http://rivet.hepforge.org/)." This information is taken from the ATLAS Data Access Policy, which is a public document that can be downloaded from http://opendata.cern.ch/record/413 [opendata.cern.ch]].

Appendix: Iterative Bayesian unfolding

A secondary unfolding method is used as a cross-check, in which the unfolded truth distribution is obtained iteratively using Bayes' theorem. Bayes' theorem can be used to estimate the probability of a specific cause, C, given an effect, E, using the equation:

$$P(C_i|E_j, I) = \frac{P(E_j|C_i, I) \cdot P(C_i|I)}{\sum_{k=1}^{M} P(E_j|C_k, I) \cdot P(C_k|I)}$$

where I is our prior knowledge of probabilities of causes C_i. If n_j events are measured in bin j, the number of truth events in bin i, is then given by

$$P(\mu_i|n_j) = \frac{P(C_i|E_j, I) \cdot n_j}{\epsilon_i}$$

where the efficiency, ϵ_i, is defined as

$$\epsilon_i = \sum_{j=1} P(E_j|C_i, I).$$
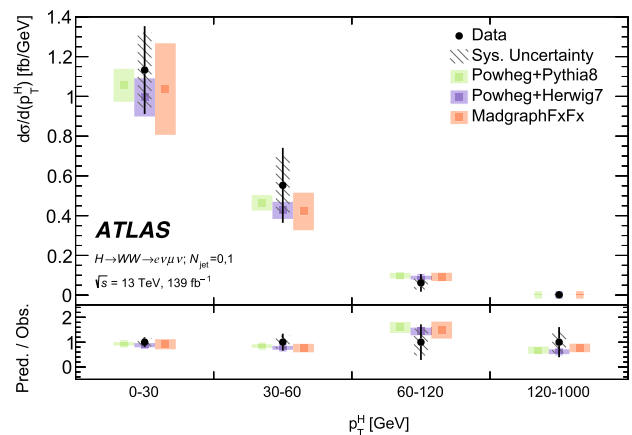
Fig. 15 Differential fiducial cross section for p_T^H in the 0+1-jet fiducial region using the iterative Bayesian unfolding method. Uncertainty bars on the data points include statistical and systematic uncertainties from experimental and theory sources as well as background normalization effects and shape effects from background and signal. Uncertainty bands on the predictions shown are dominated by normalization effects on the signal arising from showering, PDF models, α_s and the QCD scale. The systematic uncertainties of the data are shown separately

The number of truth events per bin is measured iteratively, and at each iteration the prior distribution $P(C_i, I)$, becomes the measured distribution. The number of iterations is optimized using a procedure intended to prevent statistical fluctuations from being interpreted as features in the true distribution. As the number of iterations increases, the bias towards the truth distribution is reduced, but the statistical uncertainty is increased. To find a balance between these two factors, two-dimensional plots of 'fluctuation' versus 'bias' are constructed. Distributions are constructed by fluctuat-

ing the number of events in each truth bin by its respective Poisson uncertainty, and then folding it using the nominal response matrix. The true values in the fluctuated, folded distribution are intended to represent the measured distribution. These distributions are then unfolded, using the nominal response matrix. The fluctuation axis is then defined by the relation: fluctuated truth distribution minus the original truth distribution divided by the original truth distribution. The bias axis is defined by the relation: unfolded truth distribution minus the fluctuated truth distribution divided by
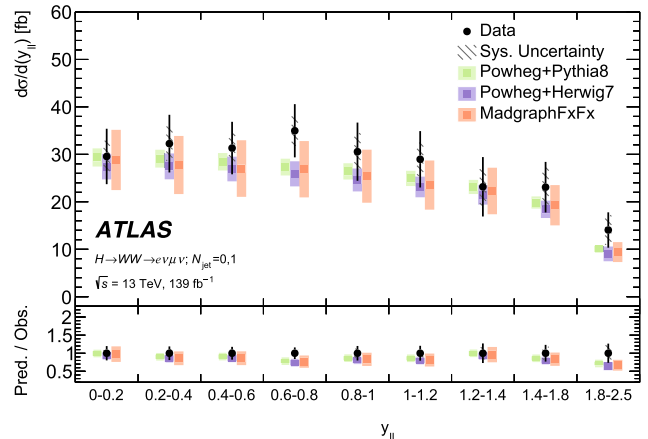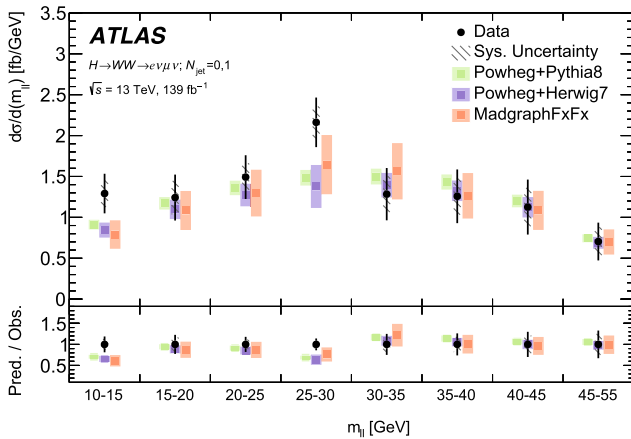
Fig. 16 Differential fiducial cross section for $m_{\ell\ell}$ (left) and $y_{\ell\ell}$ (right) in the 0+1-jet fiducial region using the iterative Bayesian unfolding method. Uncertainty bars on the data points include statistical and systematic uncertainties from experimental and theory sources as well as background normalization effects and shape effects from background

and signal. Uncertainty bands on the predictions shown are dominated by normalization effects on the signal arising from showering, PDF models, α_s and the QCD scale. The systematic uncertainties of the data are shown separately

Fig. 17 Differential fiducial cross section for $p_T^{\ell\ell}$ (left) and $\Delta\phi_{\ell\ell}$ (right) in the 0+1-jet fiducial region using the iterative bayesian unfolding method. Uncertainty bars on the data points include statistical and systematic uncertainties from experimental and theory sources as well as background normalization effects and shape effects from background

and signal. Uncertainty bands on the predictions shown are dominated by normalization effects on the signal arising from showering, PDF models, α_s and the QCD scale. The systematic uncertainties of the data are shown separately
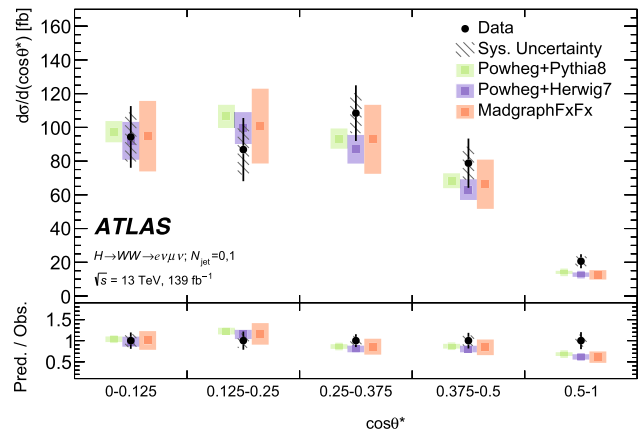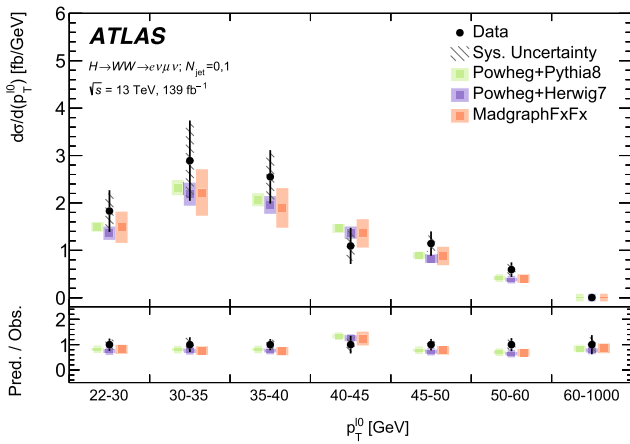
Fig. 18 Differential fiducial cross section for $p_T^{\ell 0}$ (left) and $\cos\theta^*$ (right) in the 0+1-jet fiducial region using the iterative Bayesian unfolding method. Uncertainty bars on the data points include statistical and systematic uncertainties from experimental and theory sources as well as background normalization effects and shape effects from background

and signal. Uncertainty bands on the predictions shown are dominated by normalization effects on the signal arising from showering, PDF models, α_s and the QCD scale. The systematic uncertainties of the data are shown separately
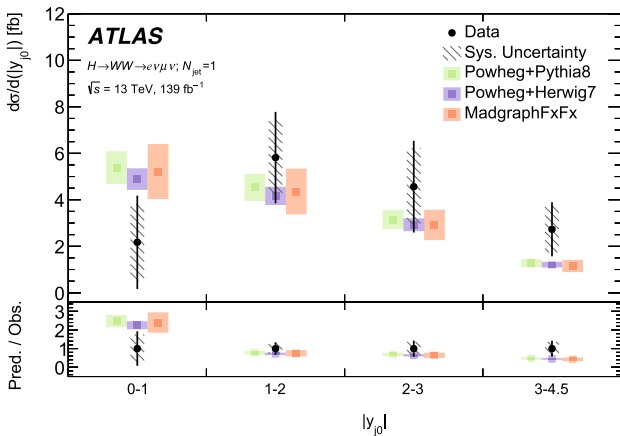
Fig. 19 Differential fiducial cross section for $|y_{j0}|$ in the 0+1-jet fiducial region using the iterative Bayesian unfolding method. Uncertainty bars on the data points include statistical and systematic uncertainties from experimental and theory sources as well as background normalization effects and shape effects from background and signal. Uncertainty bands on the predictions shown are dominated by normalization effects on the signal arising from showering, PDF models, α_s and the QCD scale. The systematic uncertainties of the data are shown separately

This appendix contains the unfolded distributions of different observables binned to match the final binnings employed in the analysis. The differential cross sections shown allow a comparison of the results from the two unfolding procedures. The two unfolding procedures produce results that are consistent with each other, demonstrating that the choice of regularization which is different between the two methods, does not have an impact on the results.

The differential fiducial cross sections for each observable, obtained using the iterative Bayesian unfolding method, are shown in Figs. 15, 16, 17, 18 and 19 for the single-differential distributions, and Figs. 20, 21 and 22 for the double-differential distributions.

the fluctuated truth distribution. The bias is calculated at the points where the fluctuation equals the uncertainty in the two-dimensional fluctuation-versus-bias distributions. Since this intersection occurs twice (when the fluctuation equals the negative uncertainty and when the fluctuation equals the positive uncertainty), the mean of these two values is taken as the bias. Finally, for each observable, the number of iterations is chosen such that the ratio of the bias to the uncertainty is less than a certain threshold for all bins. The number of iterations chosen varies from 2 to 18 depending on the observable.

Fig. 20 Differential fiducial cross section for $m_{\ell\ell}$ (left) and $\Delta\phi_{\ell\ell}$ (right) versus N_{jet} in the 0-jet and 1-jet fiducial regions using the iterative Bayesian unfolding method. Uncertainty bars on the data points include statistical and systematic uncertainties from experimental and theory sources as well as background normalization effects and shape effects from background and signal. Uncertainty bands on the predictions shown are dominated by normalization effects on the signal arising from showering, PDF models, α_s and the QCD scale. The systematic uncertainties of the data are shown separately

Fig. 21 Differential fiducial cross section for $y_{\ell\ell}$ (left) and $p_T^{\ell\ell}$ (right) versus N_{jet} in the 0-jet and 1-jet fiducial regions using the iterative Bayesian unfolding method. Uncertainty bars on the data points include statistical and systematic uncertainties from experimental and theory sources as well as background normalization effects and shape effects from background and signal. Uncertainty bands on the predictions shown are dominated by normalization effects on the signal arising from showering, PDF models, α_s and the QCD scale. The systematic uncertainties of the data are shown separately

Fig. 22 Differential fiducial cross section for $p_T^{\ell 0}$ (left) and $\cos\theta^*$ (right) versus N_{jet} in the 0-jet and 1-jet fiducial regions using the iterative Bayesian unfolding method. Uncertainty bars on the data points include statistical and systematic uncertainties from experimental and theory sources as well as background normalization effects and shape effects from background and signal. Uncertainty bands on the predictions shown are dominated by normalization effects on the signal arising from showering, PDF models, α_s and the QCD scale. The systematic uncertainties of the data are shown separately

References

1. ATLAS Collaboration, Observation of a new particle in the search for the Standard Model Higgs boson with the ATLAS detector at the LHC. Phys. Lett. B **1**, 716 (2012). https://doi.org/10.1016/j.physletb.2012.08.020

2. CMS Collaboration, Observation of a new boson at a mass of 125 GeV with the CMS experiment at the LHC. Phys. Lett. B **30**, 716 (2012). https://doi.org/10.1016/j.physletb.2012.08.021. arXiv:1207.7235 [hep-ex]

3. ATLAS Collaboration, A detailed map of Higgs boson interactions by the ATLAS experiment ten years after the discovery. Nature **52**, 607 (2022). https://doi.org/10.1038/s41586-022-04893-w. arXiv:2207.00092 [hep-ex]

4. CMS Collaboration, A portrait of the Higgs boson by the CMS experiment ten years after the discovery. Nature **60**, 607 (2022). https://doi.org/10.1038/s41586-022-04892-x. arXiv:2207.00043 [hep-ex]

5. ATLAS Collaboration, Measurement of fiducial differential cross sections of gluon-fusion production of Higgs bosons decaying to $WW^* \rightarrow e\nu\mu\nu$ with the ATLAS detector at $\sqrt{s} = 8\,TeV$. JHEP **08**, 104 (2016). https://doi.org/10.1007/JHEP08(2016)104. arXiv:1604.02997 [hep-ex]

6. ATLAS Collaboration, Measurements of Higgs boson production by gluon-gluon fusion and vector-boson fusion using $H \rightarrow WW^* \rightarrow e\nu\mu\nu$ decays in pp collisions at $\sqrt{s} = 13\,TeV$ with the ATLAS detector (2022). arXiv:2207.00338 [hep-ex]

7. CMS Collaboration, Measurement of the inclusive and differential Higgs boson production cross sections in the leptonic WW decay mode at $\sqrt{s} = 13\,TeV$. JHEP **03**, 003 (2021). https://doi.org/10.1007/JHEP03(2021)003. arXiv:2007.01984 [hep-ex]

8. ATLAS Collaboration, Measurement of the total and differential Higgs boson production crosssections at $\sqrt{s} = 13\,TeV$ with the ATLAS detector by combining the $H \rightarrow ZZ \rightarrow 4\ell$ and $H \rightarrow \gamma\gamma$ decay channels (2022). arXiv:2207.08615 [hep-ex]

9. CMS Collaboration, Measurement and interpretation of differential cross sections for Higgs boson production at $\sqrt{s} = 13\,TeV$. Phys. Lett. B **369**, 792 (2019). https://doi.org/10.1016/j.physletb.2019.03.059. arXiv:1812.06504 [hep-ex]

10. W. Buchmüller, D. Wyler, Effective lagrangian analysis of new interactions and flavour conservation. Nucl. Phys. B **268**, 621 (1986). https://doi.org/10.1016/0550-3213(86)90262-2. ((**issn: 0550-3213**))

11. B. Grzadkowski, M. Iskrzyñski, M. Misiak, J. Rosiek, Dimension-six terms in the Standard Model Lagrangian. JHEP **10** (2010). https://doi.org/10.1007/jhep10(2010)085. arXiv:1008.4884 [hep-ph]

12. G. Bozzi, S. Catani, D. de Florian, M. Grazzini, Higgs boson production at the LHC: transverse momentum resummation and rapidity dependence. Nucl. Phys. B **791**, 1 (2008). https://doi.org/10.1016/j.nuclphysb.2007.09.034. arXiv:0705.3887 [hep-ph]

13. A.J. Barr, Measuring slepton spin at the LHC. JHEP **02**, 042 (2006). https://doi.org/10.1088/1126-6708/2006/02/042. arXiv:hep-ph/0511115

14. ATLAS Collaboration, The ATLAS Experiment at the CERN Large Hadron Collider. JINST **3**, S08003 (2008). https://doi.org/10.1088/1748-0221/3/08/S08003

15. ATLAS Collaboration, ATLAS Insertable B-Layer: Technical Design Report, ATLAS-TDR-19; CERN-LHCC-2010-013 (2010). https://cds.cern.ch/record/1291633 [Addendum: ATLAS-TDR-19-ADD-1; CERN-LHCC-2012-009 (2012). https://cds.cern.ch/record/1451888]

16. B. Abbott et al., Production and integration of the ATLAS Insertable B-Layer. JINST **13**, T05008 (2018). https://doi.org/10.1088/1748-0221/13/05/T05008. arXiv:1803.00844 [physics.ins-det]

17. ATLAS Collaboration, The ATLAS Collaboration Software and Firmware, ATL-SOFT-PUB-2021- 001 (2021). https://cds.cern.ch/record/2767187

18. K. Hamilton, P. Nason, E. Re, G. Zanderighi, NNLOPS simulation of Higgs boson production. JHEP **10**, 222 (2013). https://doi.org/10.1007/JHEP10(2013)222. arXiv:1309.0017 [hep-ph]

19. K. Hamilton, P. Nason, G. Zanderighi, Finite quark-mass effects in the NNLOPSPOWHEG+MiNLO Higgs generator. JHEP **05**, 140 (2015). https://doi.org/10.1007/JHEP05(2015)140. arXiv:1501.04637 [hep-ph]

20. S. Alioli, P. Nason, C. Oleari, E. Re, A general framework for implementing NLO calculations in shower Monte Carlo pro-

grams: the POWHEG BOX. JHEP **06**, 043 (2010). https://doi.org/10.1007/JHEP06(2010)043

21. P. Nason, A new method for combining NLO QCD with shower Monte Carlo algorithms. JHEP **11**, 040 (2004). https://doi.org/10.1088/1126-6708/2004/11/040. arXiv:hep-ph/0409146

22. S. Frixione, P. Nason, C. Oleari, Matching NLO QCD computations with parton shower simulations: the POWHEG method. JHEP **11**, 070 (2007). https://doi.org/10.1088/1126-6708/2007/11/070. arXiv:0709.2092 [hep-ph]

23. T. Sjöstrand, S. Mrenna, P.Z. Skands, A brief introduction to PYTHIA 8.1. Comput. Phys. Commun. **852**, 178 (2008). https://doi.org/10.1016/j.cpc.2008.01.036

24. K. Hamilton, P. Nason, G. Zanderighi, MINLO: multi-scale improved NLO. JHEP **10**, 155 (2012). https://doi.org/10.1007/JHEP10(2012)155. arXiv:1206.3572 [hep-ph]

25. J.M. Campbell et al., NLO Higgs boson production plus one and two jets using the POWHEG BOX, MadGraph4 and MCFM. JHEP **07**, 092 (2012). https://doi.org/10.1007/JHEP07(2012)092. arXiv:1202.5475 [hep-ph]

26. K. Hamilton, P. Nason, C. Oleari, G. Zanderighi, Merging H/W/Z + 0 and 1 jet at NLO with no merging scale: a path to parton shower + NNLO matching. JHEP **05**, 082 (2013). https://doi.org/10.1007/JHEP05(2013)082. arXiv:1212.4504 [hep-ph]

27. S. Catani, M. Grazzini, Next-to-next-to-leading-order subtraction formalism in hadron collisions and its application to higgsboson production at the large hadron collider. Phys. Rev. Lett. **98**, 222002 (2007). https://doi.org/10.1103/PhysRevLett.98.222002. arXiv:hep-ph/0703012 [hep-ph]

28. G. Bozzi, S. Catani, D. de Florian, M. Grazzini, Transverse-momentum resummation and the spectrum of the Higgs boson at the LHC. Nucl. Phys. B **737**, 73 (2006). https://doi.org/10.1016/j.nuclphysb.2005.12.022. arXiv:hep-ph/0508068

29. D. de Florian, G. Ferrera, M. Grazzini, D. Tommasini, Transverse-momentum resummation: Higgs boson production at the Tevatron and the LHC. JHEP **11**, 064 (2011). https://doi.org/10.1007/JHEP11(2011)064. arXiv:1109.2109 [hep-ph]

30. ATLAS Collaboration, Measurement of the Z/γ^* boson transverse momentum distribution in pp collisions at $\sqrt{s} = 7 TeV$ with the ATLAS detector. JHEP **09**, 145 (2014). https://doi.org/10.1007/JHEP09(2014)145. arXiv:1406.3660 [hep-ex]

31. D. de Florian et al., Handbook of LHC Higgs Cross Sections: 4. Deciphering the Nature of the Higgs Sector (2016). https://doi.org/10.23731/CYRM-2017-002. arXiv:1610.07922 [hep-ph]

32. C. Anastasiou et al., High precision determination of the gluon fusion Higgs boson cross-section at the LHC. JHEP **05**, 058 (2016). https://doi.org/10.1007/JHEP05(2016)058. arXiv:1602.00695 [hep-ph]

33. C. Anastasiou, C. Duhr, F. Dulat, F. Herzog, B. Mistlberger, Higgs Boson gluon-fusion production in QCD at three loops. Phys. Rev. Lett. **114**, 212001 (2015). https://doi.org/10.1103/PhysRevLett.114.212001. arXiv:1503.06056 [hep-ph]

34. F. Dulat, A. Lazopoulos, B. Mistlberger, iHixs 2 - Inclusive Higgs cross sections. Comput. Phys. Commun. **233**, 243 (2018). https://doi.org/10.1016/j.cpc.2018.06.025. arXiv:1802.00827 [hep-ph]

35. R.V. Harlander, K.J. Ozeren, Finite top mass effects for hadronic Higgs production at next-to-next-to-leading order. JHEP **11**, 088 (2009). https://doi.org/10.1088/1126-6708/2009/11/088. arXiv:0909.3420 [hep-ph]

36. R.V. Harlander, K.J. Ozeren, Top mass effects in Higgs production at next-to-next-to-leading order QCD: Virtual corrections. Phys. Lett. B **679**, 467 (2009). https://doi.org/10.1016/j.physletb.2009.08.012. arXiv:0907.2997 [hep-ph]

37. R.V. Harlander, H. Mantler, S. Marzani, K.J. Ozeren, Higgs production in gluon fusion at next-to-next-to-leading order QCD for finite top mass. Eur. Phys. J. C **66**, 359 (2010). https://doi.org/10.1140/epjc/s10052-010-1258-x. arXiv:0912.2104 [hep-ph]

38. A. Pak, M. Rogal, M. Steinhauser, Finite top quark mass effects in NNLO Higgs boson production at LHC. JHEP **02**, 025 (2010). https://doi.org/10.1007/JHEP02(2010)025. arXiv:0911.4662 [hep-ph]

39. S. Actis, G. Passarino, C. Sturm, S. Uccirati, NLO electroweak corrections to Higgs boson production at hadron colliders. Phys. Lett. B **670**, 12 (2008). https://doi.org/10.1016/j.physletb.2008.10.018. arXiv:0809.1301 [hep-ph]

40. S. Actis, G. Passarino, C. Sturm, S. Uccirati, NNLO computational techniques: The cases $HH \to \gamma\gamma$ and $HH \to gg$. Nucl. Phys. B **811**, 182 (2009). https://doi.org/10.1016/j.nuclphysb.2008.11.024. arXiv:0809.3667 [hep-ph]

41. M. Bonetti, K. Melnikov, L. Tancredi, Higher order corrections to mixed QCD-EW contributions to Higgs boson production in gluon fusion. Phys. Rev. D **97**, 056017 (2018) [Erratum: Phys. Rev. D **97**, 099906 (2018)]. https://doi.org/10.1103/PhysRevD.97.056017. arXiv:1801.10403 [hep-ph]

42. J. Alwall et al., The automated computation of tree-level and next-to-leading order differential cross sections, and their matching to parton shower simulations. JHEP **07**, 079 (2014). https://doi.org/10.1007/JHEP07(2014)079. arXiv:1405.0301 [hep-ph]

43. NNPDF Collaboration, R.D. Ball et al., Parton distributions with LHC data. Nucl. Phys. B **867**, 244 (2013). https://doi.org/10.1016/j.nuclphysb.2012.10.003. arXiv:1207.1303 [hep-ph]

44. M. Ciccolini, A. Denner, S. Dittmaier, Strong and electroweak corrections to the production of a Higgs Boson + 2 jets via weak interactions at the large hadron collider. Phys. Rev. Lett. **99**, 161803 (2007). https://doi.org/10.1103/PhysRevLett.99.161803. arXiv:0707.0381 [hep-ph]

45. M. Ciccolini, A. Denner, S. Dittmaier, Electroweak and QCD corrections to Higgs production via vector-boson fusion at the CERN LHC. Phys. Rev. D **77**, 013002 (2008). https://doi.org/10.1103/PhysRevD.77.013002. arXiv:0710.4749 [hep-ph]

46. P. Bolzoni, F. Maltoni, S.-O. Moch, M. Zaro, Higgs boson production via vector-boson fusion at next-to-next-to-leading order in QCD. Phys. Rev. Lett. **105**, 011801 (2010). https://doi.org/10.1103/PhysRevLett.105.011801. arXiv:1003.4451 [hep-ph]

47. M.L. Ciccolini, S. Dittmaier, M. Krämer, Electroweak radiative corrections to associated WH and ZH production at hadron colliders. Phys. Rev. D **68**, 073003 (2003). https://doi.org/10.1103/PhysRevD.68.073003. arXiv:hep-ph/0306234

48. O. Brein, A. Djouadi, R. Harlander, NNLO QCD corrections to the Higgs–Strahlung processes at hadron colliders. Phys. Lett. B **579**, 149 (2004). https://doi.org/10.1016/j.physletb.2003.10.112. arXiv:hep-ph/0307206

49. O. Brein, R.V. Harlander, M. Wiesemann, T. Zirke, Top-quark mediated effects in hadronic Higgs–Strahlung. Eur. Phys. J. C **72**, 1868 (2012). https://doi.org/10.1140/epjc/s10052-012-1868-6. arXiv:1111.0761 [hep-ph]

50. L. Altenkamp, S. Dittmaier, R.V. Harlander, H. Rzehak, T.J.E. Zirke, Gluon-induced Higgsstrahlung at next-to-leading order QCD. JHEP **02**, 078 (2013). https://doi.org/10.1007/JHEP02(2013)078. arXiv:1211.5015 [hep-ph]

51. A. Denner, S. Dittmaier, S. Kallweit and A. Mück, HAWK 2.0: a Monte Carlo program for Higgs production in vector-boson fusion and Higgs strahlung at hadron colliders. Comput. Phys. Commun. **195**, 161 (2015). https://doi.org/10.1016/j.cpc.2015.04.021. arXiv:1412.5390 [hep-ph]

52. O. Brein, R.V. Harlander, T.J.E. Zirke, vh@nnlo—Higgs Strahlung at hadron colliders. Comput. Phys. Commun. **184**, 998 (2013). https://doi.org/10.1016/j.cpc.2012.11.002. arXiv:1210.5347 [hep-ph]

53. R.V. Harlander, A. Kulesza, V. Theeuwes, T. Zirke, Soft gluon resummation for gluon-induced Higgs Strahlung. JHEP **11**, 082 (2014). https://doi.org/10.1007/JHEP11(2014)082. arXiv:1410.0217 [hep-ph]

54. J. Butterworth et al., PDF4LHC recommendations for LHC Run II. J. Phys. G **43**, 023001 (2016). https://doi.org/10.1088/0954-3899/43/2/023001. arXiv:1510.03865 [hep-ph]

55. A. Djouadi, J. Kalinowski, M. Spira, HDECAY: a program for Higgs boson decays in the Standard Model and its supersymmetric extension. Comput. Phys. Commun. **108**, 56 (1998). https://doi.org/10.1016/S0010-4655(97)00123-9. arXiv:hep-ph/9704448

56. M. Spira, QCD effects in Higgs physics. Fortsch. Phys. **46**, 203 (1998). https://doi.org/10.1002/(SICI)1521-3978(199804)46:3<203::AID-PROP203>3.0.CO;2-4. arXiv:hep-ph/9705337

57. A. Djouadi, M.M. Mühlleitner, M. Spira, Decays of supersymmetric particles: the program SUSY-HIT (SUspect-SdecaY-Hdecay-InTerface). Acta Phys. Polon. B **38**, 635 (2007). arXiv:hep-ph/0609292

58. A. Bredenstein, A. Denner, S. Dittmaier, M.M. Weber, Radiative corrections to the semileptonic and hadronic Higgs-boson decays $HH \rightarrow WW/ZZ \rightarrow 4$ fermions. JHEP **02**, 080 (2007). https://doi.org/10.1088/1126-6708/2007/02/080. arXiv:hep-ph/0611234

59. A. Bredenstein, A. Denner, S. Dittmaier, M.M. Weber, Precise predictions for the Higgs-boson decay $H \rightarrow WW/ZZ \rightarrow 4$ leptons. Phys. Rev. D **74**, 013004 (2006). https://doi.org/10.1103/PhysRevD.74.013004. arXiv:hep-ph/0604011

60. A. Bredenstein, A. Denner, S. Dittmaier, M.M. Weber, Precision calculations for the Higgs decays $H \rightarrow ZZ/WW \rightarrow 4$ leptons. Nucl. Phys. Proc. Suppl. **160**, 131 (2006). https://doi.org/10.1016/j.nuclphysbps.2006.09.104. arXiv:hep-ph/0607060

61. S. Frixione, E. Laenen, P. Motylinski, C. White, B.R. Webber, Single-top hadroproduction in association with a W boson. JHEP **07**, 029 (2008). https://doi.org/10.1088/1126-6708/2008/07/029. arXiv:0805.3067 [hep-ph]

62. M. Czakon, P. Fiedler, A. Mitov, Total top-quark pair-production cross section at hadron colliders through $O(\alpha_S^4)$. Phys. Rev. Lett. **110**, 252004 (2013). https://doi.org/10.1103/PhysRevLett.110.252004. arXiv:1303.6254 [hep-ph]

63. J.M. Campbell, R.K. Ellis, MCFM for the Tevatron and the LHC. Nucl. Phys. B Proc. Suppl. **10–15**, 205 (2010). https://doi.org/10.1016/j.nuclphysbps.2010.08.011. arXiv:1007.3492 [hep-ph]

64. ATLAS Collaboration, ATLAS Pythia 8 tunes to 7 TeV data, ATL-PHYS-PUB-2014-021 (2014). https://cds.cern.ch/record/1966419

65. T. Sjöstrand et al., An introduction to PYTHIA 8.2. Comput. Phys. Commun. **191**, 159 (2015). https://doi.org/10.1016/j.cpc.2015.01.024. arXiv:1410.3012 [hep-ph]

66. P. Nason, C. Oleari, NLO Higgs boson production via vector-boson fusion matched with shower in POWHEG. JHEP **02**, 037 (2010). https://doi.org/10.1007/JHEP02(2010)037. arXiv:0911.5299 [hep-ph]

67. R. Frederix, S. Frixione, Merging meets matching in MC@NLO. JHEP **12**, 061 (2012). https://doi.org/10.1007/JHEP12(2012)061. arXiv:1209.6215 [hep-ph]

68. J. Bellm et al., Herwig 7.0/Herwig++ 3.0 release note. Eur. Phys. J. C **76**, 196 (2016). https://doi.org/10.1140/epjc/s10052-016-4018-8. arXiv:1512.01178 [hep-ph]

69. E. Bothmann et al., Event generation with Sherpa 2.2. SciPost Phys. **7**, 034 (2019). https://doi.org/10.21468/SciPostPhys.7.3.034. arXiv:1905.09127 [hep-ph]

70. The NNPDF Collaboration, R.D. Ball et al., Parton distributions for the LHC run II. JHEP **04**, 040 (2015). https://doi.org/10.1007/JHEP04(2015)040. arXiv:1410.8849 [hep-ph]

71. T. Gleisberg, S. Höche, Comix, a new matrix element generator. JHEP **12**, 039 (2008). https://doi.org/10.1088/1126-6708/2008/12/039. arXiv:0808.3674 [hep-ph]

72. S. Schumann, F. Krauss, A parton shower algorithm based on Catani–Seymour dipole factorisation. JHEP **03**, 038

73. S. Höche, F. Krauss, M. Schönherr, F. Siegert, A critical appraisal of NLO+PS matching methods. JHEP **09**, 049 (2012). https://doi.org/10.1007/JHEP09(2012)049. arXiv:1111.1220 [hep-ph]

74. S. Höche, F. Krauss, M. Schönherr, F. Siegert, QCD matrix elements + parton showers. The NLO case. JHEP **04**, 027 (2013). https://doi.org/10.1007/JHEP04(2013)027. arXiv:1207.5030 [hep-ph]

75. S. Catani, F. Krauss, B.R. Webber, R. Kuhn, QCD matrix elements + parton showers. JHEP **11**, 063 (2001). https://doi.org/10.1088/1126-6708/2001/11/063. arXiv:hep-ph/0109231

76. S. Höche, F. Krauss, S. Schumann, F. Siegert, QCD matrix elements and truncated showers. JHEP **05**, 053 (2009). https://doi.org/10.1088/1126-6708/2009/05/053. arXiv:0903.1219 [hep-ph]

77. F. Buccioni et al., OpenLoops 2. Eur. Phys. J. C **79**, 866 (2019). https://doi.org/10.1140/epjc/s10052-019-7306-2. arXiv:1907.13071 [hep-ph]

78. F. Cascioli, P. Maierhöfer, S. Pozzorini, Scattering amplitudes with open loops. Phys. Rev. Lett. **108**, 111601 (2012). https://doi.org/10.1103/PhysRevLett.108.111601. arXiv:1111.5206 [hep-ph]

79. A. Denner, S. Dittmaier, L. Hofer, Collier: a fortran-based complex one-loop library in extended regularizations. Comput. Phys. Commun. **212**, 220 (2017). https://doi.org/10.1016/j.cpc.2016.10.013. arXiv:1604.06792 [hep-ph]

80. S. Hoeche, S. Schumann, F. Siegert, Hard photon production and matrix-element parton-shower merging. Phys. Rev. D **81**, 034026 (2010). https://doi.org/10.1103/PhysRevD.81.034026. arXiv:0912.3501 [hep-ph]

81. F. Caola, K. Melnikov, R. Rontsch, L. Tancredi, QCD corrections to W^+W^- production through gluon fusion. Phys. Lett. B **754**, 275 (2016). https://doi.org/10.1016/j.physletb.2016.01.046. arXiv:1511.08617 [hep-ph]

82. F. Cascioli et al., Precise Higgs-background predictions: merging NLO QCD and squared quarkloop corrections to four-lepton + 0,1 jet production. JHEP **01**, 046 (2014). https://doi.org/10.1007/JHEP01(2014)046. arXiv:1309.0500 [hep-ph]

83. M. Beneke, P. Falgari, S. Klein, C. Schwinn, Hadronic top-quark pair production with NNLL threshold resummation. Nucl. Phys. B **855**, 695 (2012). https://doi.org/10.1016/j.nuclphysb.2011.10.021. arXiv:1109.1536 [hep-ph]

84. M. Cacciari, M. Czakon, M. Mangano, A. Mitov, P. Nason, Top-pair production at hadron colliders with next-to-next-to-leading logarithmic soft-gluon resummation. Phys. Lett. B **710**, 612 (2012). https://doi.org/10.1016/j.physletb.2012.03.013. arXiv:1111.5869 [hep-ph]

85. P. Bärnreuther, M. Czakon, A. Mitov, Percent-level-precision physics at the Tevatron: next-to- next-to-leading order QCD corrections to $q\bar{q} \rightarrow t\bar{t} + X$ Phys. Rev. Lett. **109**, 132001 (2012). https://doi.org/10.1103/PhysRevLett.109.132001. arXiv:1204.5201 [hep-ph]

86. M. Czakon, A. Mitov, NNLO corrections to top-pair production at hadron colliders: the all-fermionic scattering channels. JHEP **12**, 054 (2012). https://doi.org/10.1007/JHEP12(2012)054. arXiv:1207.0236 [hep-ph]

87. M. Czakon, A. Mitov, NNLO corrections to top pair production at hadron colliders: the quark-gluon reaction. JHEP **01**, 080 (2013). https://doi.org/10.1007/JHEP01(2013)080. arXiv:1210.6832 [hep-ph]

88. M. Czakon, P. Fiedler, A. Mitov, Total top-quark pair-production cross section at hadron colliders through $O(\alpha_S^4)$. Phys. Rev. Lett. **110**, 252004 (2013). https://doi.org/10.1103/PhysRevLett.110.252004. arXiv:1303.6254 [hep-ph]

89. M. Czakon, A. Mitov, Top++: a program for the calculation of the top-pair cross-section at hadron colliders. Comput. Phys.

Commun. **185**, 2930 (2014). https://doi.org/10.1016/j.cpc.2014.06.021. arXiv:1112.5675 [hep-ph]

90. N. Kidonakis, Two-loop soft anomalous dimensions for single top quark associated production with a W^- or H^-. Phys. Rev. D **82**, 054018 (2010). https://doi.org/10.1103/PhysRevD.82.054018. arXiv:1005.4451 [hep-ph]

91. N. Kidonakis, Top quark production, in *Proceedings, Helmholtz International Summer School on Physics of Heavy Quarks and Hadrons (HQ 2013)* (JINR, Dubna, Russia, 15th–28th July 2013) 139. https://doi.org/10.3204/DESY-PROC-2013-03/Kidonakis. arXiv:1311.0283 [hep-ph]

92. C. Anastasiou, L. Dixon, K. Melnikov, F. Petriello, High-precision QCD at hadron colliders: electroweak gauge boson rapidity distributions at next-to-next-to leading order. Phys. Rev. D **69**, 094008 (2004). https://doi.org/10.1103/PhysRevD.69.094008. arXiv:hep-ph/0312266

93. ATLAS Collaboration, Measurement of the inelastic proton–proton cross section at $\sqrt{s} = 13\,TeV$ with the ATLAS detector at the LHC. Phys. Rev. Lett **117**, 182002 (2016). arXiv:1606.02625 [hep-ex]

94. ATLAS Collaboration, The ATLAS simulation infrastructure. Eur. Phys. J. C **70**, 823 (2010). https://doi.org/10.1140/epjc/s10052-010-1429-9. arXiv:1005.4568 [physics.ins-det]

95. S. Agostinelli et al., GEANT4—a simulation toolkit. Nucl. Instrum. Meth. A **506**, 250 (2003). https://doi.org/10.1016/S0168-9002(03)01368-8

96. ATLAS Collaboration, ATLAS data quality operations and performance for 2015–2018 data-taking. JINST **15**, P04003 (2020). https://doi.org/10.1088/1748-0221/15/04/P04003. arXiv:1911.04632 [physics.ins-det]

97. ATLAS Collaboration, Performance of electron and photon triggers in ATLAS during LHC Run 2. Eur. Phys. J. C **47**, 80 (2020). https://doi.org/10.1140/epjc/s10052-019-7500-2. arXiv:1909.00761 [hep-ex]

98. ATLAS Collaboration, Performance of the ATLAS muon triggers in Run 2. JINST **15**, P09015 (2020). https://doi.org/10.1088/1748-0221/15/09/p09015. arXiv:2004.13447 [hep-ex]

99. ATLAS Collaboration, Electron reconstruction and identification in the ATLAS experiment using the 2015 and 2016 LHC proton-proton collision data at $\sqrt{s} = 13\,TeV$, Eur. Phys. J. C **79**, 639 (2019). https://doi.org/10.1140/epjc/s10052-019-7140-6. arXiv:1902.04655 [hep-ex]

100. ATLAS Collaboration, Electron and photon performance measurements with the ATLAS detector using the 2015-2017 LHC proton–proton collision data. JINST **14**, P12006 (2019). https://doi.org/10.1088/1748-0221/14/12/P12006. arXiv:1908.00005 [hep-ex]

101. ATLAS Collaboration, Muon reconstruction and identification efficiency in ATLAS using the full Run 2 pp collision data set at $\sqrt{s} = 13\,TeV$, Eur. Phys. J. C **81**, 578 (2021). https://doi.org/10.1140/epjc/s10052-021-09233-2. arXiv:2012.00578 [hep-ex]

102. ATLAS Collaboration, Muon reconstruction performance of the ATLAS detector in proton-proton collision data at $\sqrt{s} = 13\,TeV$. Eur. Phys. J. C **76**, 292 (2016). https://doi.org/10.1140/epjc/s10052-016-4120-y. arXiv:1603.05598 [hep-ex]

103. M. Cacciari, G.P. Salam, G. Soyez, The anti-k_t jet clustering algorithm. JHEP **04**, 063 (2008). https://doi.org/10.1088/1126-6708/2008/04/063. arXiv:0802.1189 [hep-ph]

104. ATLAS Collaboration, Jet energy scale and resolution measured in proton-proton collisions at $\sqrt{s} = 13\,TeV$ with the ATLAS detector. Eur. Phys. J. C **81**, 689 (2020). https://doi.org/10.1140/epjc/s10052-021-09402-3. arXiv:2007.02645 [hep-ex]

105. ATLAS Collaboration, Jet reconstruction and performance using particle flow with the ATLAS detector. Eur. Phys. J. C **77**, 466 (2017). https://doi.org/10.1140/epjc/s10052-017-5031-2. arXiv:1703.10485 [hep-ex]

106. ATLAS Collaboration, Performance of pile-up mitigation techniques for jets in pp collisions at $\sqrt{s} = 8\,TeV$ using the ATLAS detector. Eur. Phys. J. C **76**, 581 (2016). https://doi.org/10.1140/epjc/s10052-016-4395-z. arXiv:1510.03823 [hep-ex]

107. ATLAS Collaboration, Optimisation and performance studies of the ATLAS b-tagging algorithms for the 2017-18 LHC run, ATL-PHYS-PUB-2017-013 (2017). https://cds.cern.ch/record/2273281

108. ATLAS Collaboration, Performance of missing transverse momentum reconstruction with the ATLAS detector using proton–proton collisions at $\sqrt{s} = 13$ TeV. Eur. Phys. J. C **78**, 903 (2018). https://doi.org/10.1140/epjc/s10052-018-6288-9. arXiv:1802.08168 [hep-ex]

109. T. Plehn, D.L. Rainwater, D. Zeppenfeld, A method for identifying $H \rightarrow tau\,tau \rightarrow e^{+-}\mu^{-+}+$ missing p(T) at the CERN LHC. Phys. Rev. D **61**, 093005 (2000). https://doi.org/10.1103/PhysRevD.61.093005. arXiv:hep-ph/9911385

110. M. Cacciari, G.P. Salam, G. Soyez, FastJet user manual. Eur. Phys. J. C **72**, 1896 (2012). https://doi.org/10.1140/epjc/s10052-012-1896-2. arXiv:1111.6097 [hep-ph]

111. A.L. Stuart, J.K. Ord, S.C. Arnold, Kendall's advanced theory of statistics, Vol. 2A: Classical inference and the linear model (1999)

112. ATLAS Collaboration, Luminosity determination in pp collisions at $\sqrt{s} = 13\,TeV$ using the ATLAS detector at the LHC, ATLAS-CONF-2019-021 (2019). https://cds.cern.ch/record/2677054

113. G. Avoni et al., The new LUCID-2 detector for luminosity measurement and monitoring in ATLAS. JINST **13**, P07017 (2018). https://doi.org/10.1088/1748-0221/13/07/P07017

114. I.W. Stewart, F.J. Tackmann, Theory uncertainties for Higgs mass and other searches using jet bins. Phys. Rev. D **85** (2012). https://doi.org/10.1103/physrevd.85.034011. arXiv:1107.2117 [hep-ph]

115. J. Butterworth et al., PDF4LHC recommendations for LHC Run II. J. Phys. G **43** (2016). arXiv:1510.03865 [hep-ph]

116. L. Brenner et al., Comparison of unfolding methods using RooFitUnfold. Int. J. Mod. Phys. A **35**, 2050145 (2020). https://doi.org/10.1142/S0217751X20501456. arXiv:1910.14654 [physics.data-an]

117. A. Tikhonov, Solution of incorrectly formulated problems and the regularization method. Sov. Math. Dokl. **5**, 1035/1038 (1963). https://ci.nii.ac.jp/naid/10004315593/en/

118. ATLAS Collaboration, Measurements of the Higgs boson inclusive and differential fiducial cross sections in the 4ℓ. decay channel at $\sqrt{s} = 13\,TeV$. Eur. Phys. J. C **80**, 942 (2020). https://doi.org/10.1140/epjc/s10052-020-8223-0. arXiv:2004.03969 [hep-ex]

119. ATLAS Collaboration, ATLAS Computing Acknowledgements, ATL-SOFT-PUB-2021-003 (2021). https://cds.cern.ch/record/2776662

ATLAS Collaboration[*]

G. Aad[102], B. Abbott[120], K. Abeling[55], S. H. Abidi[29], A. Aboulhorma[35e], H. Abramowicz[151], H. Abreu[150], Y. Abulaiti[117], A. C. Abusleme Hoffman[137a], B. S. Acharya[69a,69b,p], C. Adam Bourdarios[4], L. Adamczyk[85a], L. Adamek[155], S. V. Addepalli[26], J. Adelman[115], A. Adiguzel[21c], S. Adorni[56], T. Adye[134], A. A. Affolder[136], Y. Afik[36], M. N. Agaras[13], J. Agarwala[73a,73b], A. Aggarwal[100], C. Agheorghiesei[27c], J. A. Aguilar-Saavedra[130f], A. Ahmad[36], F. Ahmadov[38,aa], W. S. Ahmed[104], S. Ahuja[95], X. Ai[48], G. Aielli[76a,76b], M. Ait Tamlihat[35e], B. Aitbenchikh[35a], I. Aizenberg[169], M. Akbiyik[100], T. P. A. Åkesson[98], A. V. Akimov[37], K. Al Khoury[41], G. L. Alberghi[23b], J. Albert[165], P. Albicocco[53], S. Alderweireldt[52], M. Aleksa[36], I. N. Aleksandrov[38], C. Alexa[27b], T. Alexopoulos[10], A. Alfonsi[114], F. Alfonsi[23b], M. Alhroob[120], B. Ali[132], S. Ali[148], M. Aliev[37], G. Alimonti[71a], W. Alkakhi[55], C. Allaire[66], B. M. M. Allbrooke[146], C. A. Allendes Flores[137f], P. P. Allport[20], A. Aloisio[72a,72b], F. Alonso[90], C. Alpigiani[138], M. Alvarez Estevez[99], A. Alvarez Fernandez[100], M. G. Alviggi[72a,72b], M. Aly[101], Y. Amaral Coutinho[82b], A. Ambler[104], C. Amelung[36], M. Amerl[101], C. G. Ames[109], D. Amidei[106], S. P. Amor Dos Santos[130a], K. R. Amos[163], V. Ananiev[125], C. Anastopoulos[139], T. Andeen[11], J. K. Anders[36], S. Y. Andrean[47a,47b], A. Andreazza[71a,71b], S. Angelidakis[9], A. Angerami[41,ad], A. V. Anisenkov[37], A. Annovi[74a], C. Antel[56], M. T. Anthony[139], E. Antipov[145], M. Antonelli[53], D. J. A. Antrim[17a], F. Anulli[75a], M. Aoki[83], T. Aoki[153], J. A. Aparisi Pozo[163], M. A. Aparo[146], L. Aperio Bella[48], C. Appelt[18], N. Aranzabal[36], V. Araujo Ferraz[82a], C. Arcangeletti[53], A. T. H. Arce[51], E. Arena[92], J-F. Arguin[108], S. Argyropoulos[54], J.-H. Arling[48], A. J. Armbruster[36], O. Arnaez[4], H. Arnold[114], Z. P. Arrubarrena Tame[109], G. Artoni[75a,75b], H. Asada[111], K. Asai[118], S. Asai[153], N. A. Asbah[61], J. Assahsah[35d], K. Assamagan[29], R. Astalos[28a], R. J. Atkin[33a], M. Atkinson[162], N. B. Atlay[18], H. Atmani[62b], P. A. Atmasiddha[106], K. Augsten[132], S. Auricchio[72a,72b], A. D. Auriol[20], V. A. Austrup[171], G. Avner[150], G. Avolio[36], K. Axiotis[56], G. Azuelos[108,ah], D. Babal[28a], H. Bachacou[135], K. Bachas[152,s], A. Bachiu[34], F. Backman[47a,47b], A. Badea[61], P. Bagnaia[75a,75b], M. Bahmani[18], A. J. Bailey[163], V. R. Bailey[162], J. T. Baines[134], C. Bakalis[10], O. K. Baker[172], E. Bakos[15], D. Bakshi Gupta[8], R. Balasubramanian[114], E. M. Baldin[37], P. Balek[133], E. Ballabene[71a,71b], F. Balli[135], L. M. Baltes[63a], W. K. Balunas[32], J. Balz[100], E. Banas[86], M. Bandieramonte[129], A. Bandyopadhyay[24], S. Bansal[24], L. Barak[151], E. L. Barberio[105], D. Barberis[57a,57b], M. Barbero[102], G. Barbour[96], K. N. Barends[33a], T. Barillari[110], M-S. Barisits[36], T. Barklow[143], P. Baron[122], D. A. Baron Moreno[101], A. Baroncelli[62a], G. Barone[29], A. J. Barr[126], L. Barranco Navarro[47a,47b], F. Barreiro[99], J. Barreiro Guimarães da Costa[14a], U. Barron[151], M. G. Barros Teixeira[130a], S. Barsov[37], F. Bartels[63a], R. Bartoldus[143], A. E. Barton[91], P. Bartos[28a], A. Basan[100], M. Baselga[49], I. Bashta[77a,77b], A. Bassalat[66,b], M. J. Basso[155], C. R. Basson[101], R. L. Bates[59], S. Batlamous[35e], J. R. Batley[32], B. Batool[141], M. Battaglia[136], D. Battulga[18], M. Bauce[75a,75b], P. Bauer[24], J. B. Beacham[51], T. Beau[127], P. H. Beauchemin[158], F. Becherer[54], P. Bechtle[24], H. P. Beck[19,r], K. Becker[167], A. J. Beddall[21d], V. A. Bednyakov[38], C. P. Bee[145], L. J. Beemster[15], T. A. Beermann[36], M. Begalli[82d], M. Begel[29], A. Behera[145], J. K. Behr[48], C. Beirao Da Cruz E Silva[36], J. F. Beirer[36,55], F. Beisiegel[24], M. Belfkir[159], G. Bella[151], L. Bellagamba[23b], A. Bellerive[34], P. Bellos[20], K. Beloborodov[37], N. L. Belyaev[37], D. Benchekroun[35a], F. Bendebba[35a], Y. Benhammou[151], M. Benoit[29], J. R. Bensinger[26], S. Bentvelsen[114], L. Beresford[36], M. Beretta[53], E. Bergeaas Kuutmann[161], N. Berger[4], B. Bergmann[132], J. Beringer[17a], S. Berlendis[7], G. Bernardi[5], C. Bernius[143], F. U. Bernlochner[24], T. Berry[95], P. Berta[133], A. Berthold[50], I. A. Bertram[91], S. Bethke[110], A. Betti[75a,75b], A. J. Bevan[94], M. Bhamjee[33c], S. Bhatta[145], D. S. Bhattacharya[166], P. Bhattarai[26], V. S. Bhopatkar[121], R. Bi[29,ak], R. M. Bianchi[129], O. Biebel[109], R. Bielski[123], M. Biglietti[77a], T. R. V. Billoud[132], M. Bindi[55], A. Bingul[21b], C. Bini[75a,75b], A. Biondini[92], C. J. Birch-sykes[101], G. A. Bird[20,134], M. Birman[169], M. Biros[133], T. Bisanz[36], E. Bisceglie[43a,43b], D. Biswas[170], A. Bitadze[101], K. Bjørke[125], I. Bloch[48], C. Blocker[26], A. Blue[59], U. Blumenschein[94], J. Blumenthal[100], G. J. Bobbink[114], V. S. Bobrovnikov[37], M. Boehler[54], D. Bogavac[36], A. G. Bogdanchikov[37], C. Bohm[47a], V. Boisvert[95], P. Bokan[48], T. Bold[85a], M. Bomben[5], M. Bona[94], M. Boonekamp[135], C. D. Booth[95], A. G. Borbély[59], H. M. Borecka-Bielska[108], L. S. Borgna[96], G. Borissov[91], D. Bortoletto[126], D. Boscherini[23b], M. Bosman[13], J. D. Bossio Sola[36], K. Bouaouda[35a], N. Bouchhar[163], J. Boudreau[129], E. V. Bouhova-Thacker[91], D. Boumediene[40], R. Bouquet[5], A. Boveia[119], J. Boyd[36], D. Boye[29], I. R. Boyko[38], J. Bracinik[20], N. Brahimi[62d], G. Brandt[171], O. Brandt[32], F. Braren[48], B. Brau[103], J. E. Brau[123], K. Brendlinger[48], R. Brener[169],

L. Brenner[114], R. Brenner[161], S. Bressler[169], D. Britton[59], D. Britzger[110], I. Brock[24], G. Brooijmans[41], W. K. Brooks[137f], E. Brost[29], L. M. Brown[165], T. L. Bruckler[126], P. A. Bruckman de Renstrom[86], B. Brüers[48], D. Bruncko[28b,*], A. Bruni[23b], G. Bruni[23b], M. Bruschi[23b], N. Bruscino[75a,75b], T. Buanes[16], Q. Buat[138], A. G. Buckley[59], I. A. Budagov[38,*], M. K. Bugge[125], O. Bulekov[37], B. A. Bullard[143], S. Burdin[92], C. D. Burgard[49], A. M. Burger[40], B. Burghgrave[8], J. T. P. Burr[32], C. D. Burton[11], J. C. Burzynski[142], E. L. Busch[41], V. Büscher[100], P. J. Bussey[59], J. M. Butler[25], C. M. Buttar[59], J. M. Butterworth[96], W. Buttinger[134], C. J. Buxo Vazquez[107], A. R. Buzykaev[37], G. Cabras[23b], S. Cabrera Urbán[163], D. Caforio[58], H. Cai[129], Y. Cai[14a,14d], V. M. M. Cairo[36], O. Cakir[3a], N. Calace[36], P. Calafiura[17a], G. Calderini[127], P. Calfayan[68], G. Callea[59], L. P. Caloba[82b], D. Calvet[40], S. Calvet[40], T. P. Calvet[102], M. Calvetti[74a,74b], R. Camacho Toro[127], S. Camarda[36], D. Camarero Munoz[26], P. Camarri[76a,76b], M. T. Camerlingo[72a,72b], D. Cameron[125], C. Camincher[165], M. Campanelli[96], A. Camplani[42], V. Canale[72a,72b], A. Canesse[104], M. Cano Bret[80], J. Cantero[163], Y. Cao[162], F. Capocasa[26], M. Capua[43a,43b], A. Carbone[71a,71b], R. Cardarelli[76a], J. C. J. Cardenas[8], F. Cardillo[163], T. Carli[36], G. Carlino[72a], J. I. Carlotto[13], B. T. Carlson[129,t], E. M. Carlson[156a,165], L. Carminati[71a,71b], M. Carnesale[75a,75b], S. Caron[113], E. Carquin[137f], S. Carrá[71a,71b], G. Carratta[23a,23b], F. Carrio Argos[33g], J. W. S. Carter[155], T. M. Carter[52], M. P. Casado[13,j], A. F. Casha[155], M. Caspar[48], E. G. Castiglia[172], F. L. Castillo[63a], L. Castillo Garcia[13], V. Castillo Gimenez[163], N. F. Castro[130a,130e], A. Catinaccio[36], J. R. Catmore[125], V. Cavaliere[29], N. Cavalli[23a,23b], V. Cavasinni[74a,74b], E. Celebi[21a], F. Celli[126], M. S. Centonze[70a,70b], K. Cerny[122], A. S. Cerqueira[82a], A. Cerri[146], L. Cerrito[76a,76b], F. Cerutti[17a], A. Cervelli[23b], G. Cesarini[53], S. A. Cetin[21d], Z. Chadi[35a], D. Chakraborty[115], M. Chala[130f], J. Chan[170], W. Y. Chan[153], J. D. Chapman[32], B. Chargeishvili[149b], D. G. Charlton[20], T. P. Charman[94], M. Chatterjee[19], S. Chekanov[6], S. V. Chekulaev[156a], G. A. Chelkov[38,a], A. Chen[106], B. Chen[151], B. Chen[165], H. Chen[14c], H. Chen[29], J. Chen[62c], J. Chen[142], S. Chen[153], S. J. Chen[14c], X. Chen[62c], X. Chen[14b,ag], Y. Chen[62a], C. L. Cheng[170], H. C. Cheng[64a], S. Cheong[143], A. Cheplakov[38], E. Cheremushkina[48], E. Cherepanova[114], R. Cherkaoui El Moursli[35e], E. Cheu[7], K. Cheung[65], L. Chevalier[135], V. Chiarella[53], G. Chiarelli[74a], N. Chiedde[102], G. Chiodini[70a], A. S. Chisholm[20], A. Chitan[27b], M. Chitishvili[163], M. V. Chizhov[38], K. Choi[11], A. R. Chomont[75a,75b], Y. Chou[103], E. Y. S. Chow[114], T. Chowdhury[33g], L. D. Christopher[33g], K. L. Chu[64a], M. C. Chu[64a], X. Chu[14a,14d], J. Chudoba[131], J. J. Chwastowski[86], D. Cieri[110], K. M. Ciesla[85a], V. Cindro[93], A. Ciocio[17a], F. Cirotto[72a,72b], Z. H. Citron[169,m], M. Citterio[71a], D. A. Ciubotaru[27b], B. M. Ciungu[155], A. Clark[56], P. J. Clark[52], J. M. Clavijo Columbie[48], S. E. Clawson[101], C. Clement[47a,47b], J. Clercx[48], L. Clissa[23a,23b], Y. Coadou[102], M. Cobal[69a,69c], A. Coccaro[57b], R. F. Coelho Barrue[130a], R. Coelho Lopes De Sa[103], S. Coelli[71a], H. Cohen[151], A. E. C. Coimbra[71a,71b], B. Cole[41], J. Collot[60], P. Conde Muiño[130a,130g], M. P. Connell[33c], S. H. Connell[33c], I. A. Connelly[59], E. I. Conroy[126], F. Conventi[72a,ai], H. G. Cooke[20], A. M. Cooper-Sarkar[126], F. Cormier[164], L. D. Corpe[36], M. Corradi[75a,75b], F. Corriveau[104,y], A. Cortes-Gonzalez[18], M. J. Costa[163], F. Costanza[4], D. Costanzo[139], B. M. Cote[119], G. Cowan[95], J. W. Cowley[32], K. Cranmer[117], S. Crépé-Renaudin[60], F. Crescioli[127], M. Cristinziani[141], M. Cristoforetti[78a,78b,d], V. Croft[114], G. Crosetti[43a,43b], A. Cueto[36], T. Cuhadar Donszelmann[160], H. Cui[14a,14d], Z. Cui[7], W. R. Cunningham[59], F. Curcio[43a,43b], P. Czodrowski[36], M. M. Czurylo[63b], M. J. Da Cunha Sargedas De Sousa[62a], J. V. Da Fonseca Pinto[82b], C. Da Via[101], W. Dabrowski[85a], T. Dado[49], S. Dahbi[33g], T. Dai[106], C. Dallapiccola[103], M. Dam[42], G. D'amen[29], V. D'Amico[109], J. Damp[100], J. R. Dandoy[128], M. F. Daneri[30], M. Danninger[142], V. Dao[36], G. Darbo[57b], S. Darmora[6], S. J. Das[29,ak], S. D'Auria[71a,71b], C. David[156b], T. Davidek[133], B. Davis-Purcell[34], I. Dawson[94], K. De[8], R. De Asmundis[72a], N. De Biase[48], S. De Castro[23a,23b], N. De Groot[113], P. de Jong[114], H. De la Torre[107], A. De Maria[14c], A. De Salvo[75a], U. De Sanctis[76a,76b], A. De Santo[146], J. B. De Vivie De Regie[60], D. V. Dedovich[38], J. Degens[114], A. M. Deiana[44], F. Del Corso[23a,23b], J. Del Peso[99], F. Del Rio[63a], F. Deliot[135], C. M. Delitzsch[49], M. Della Pietra[72a,72b], D. Della Volpe[56], A. Dell'Acqua[36], L. Dell'Asta[71a,71b], M. Delmastro[4], P. A. Delsart[60], S. Demers[172], M. Demichev[38], S. P. Denisov[37], L. D'Eramo[115], D. Derendarz[86], F. Derue[127], P. Dervan[92], K. Desch[24], K. Dette[155], C. Deutsch[24], F. A. Di Bello[57a,57b], A. Di Ciaccio[76a,76b], L. Di Ciaccio[4], A. Di Domenico[75a,75b], C. Di Donato[72a,72b], A. Di Girolamo[36], G. Di Gregorio[5], A. Di Luca[78a,78b], B. Di Micco[77a,77b], R. Di Nardo[77a,77b], C. Diaconu[102], F. A. Dias[114], T. Dias Do Vale[142], M. A. Diaz[137a,137b], F. G. Diaz Capriles[24], M. Didenko[163], E. B. Diehl[106], L. Diehl[54], S. Díez Cornell[48], C. Diez Pardos[141], C. Dimitriadi[24,161], A. Dimitrievska[17a], I-M. Dinu[27b], S. J. Dittmeier[63b], F. Dittus[36], F. Djama[102], T. Djobava[149b], J. I. Djuvsland[16], C. Doglioni[98,101],

J. Dolejsi[133], Z. Dolezal[133], M. Donadelli[82c], B. Dong[107], J. Donini[40], A. D'Onofrio[77a,77b], M. D'Onofrio[92], J. Dopke[134], A. Doria[72a], M. T. Dova[90], A. T. Doyle[59], M. A. Draguet[126], E. Drechsler[142], E. Dreyer[169], I. Drivas-koulouris[10], A. S. Drobac[158], M. Drozdova[56], D. Du[62a], T. A. du Pree[114], F. Dubinin[37], M. Dubovsky[28a], E. Duchovni[169], G. Duckeck[109], O. A. Ducu[27b], D. Duda[110], A. Dudarev[36], E. R. Duden[26], M. D'uffizi[101], L. Duflot[66], M. Dührssen[36], C. Dülsen[171], A. E. Dumitriu[27b], M. Dunford[63a], S. Dungs[49], K. Dunne[47a,47b], A. Duperrin[102], H. Duran Yildiz[3a], M. Düren[58], A. Durglishvili[149b], B. L. Dwyer[115], G. I. Dyckes[17a], M. Dyndal[85a], S. Dysch[101], B. S. Dziedzic[86], Z. O. Earnshaw[146], B. Eckerova[28a], S. Eggebrecht[55], M. G. Eggleston[51], E. Egidio Purcino De Souza[127], L. F. Ehrke[56], G. Eigen[16], K. Einsweiler[17a], T. Ekelof[161], P. A. Ekman[98], Y. El Ghazali[35b], H. El Jarrari[35e,148], A. El Moussaouy[35a], V. Ellajosyula[161], M. Ellert[161], F. Ellinghaus[171], A. A. Elliot[94], N. Ellis[36], J. Elmsheuser[29], M. Elsing[36], D. Emeliyanov[134], Y. Enari[153], I. Ene[17a], S. Epari[13], J. Erdmann[49], P. A. Erland[86], M. Errenst[171], M. Escalier[66], C. Escobar[163], E. Etzion[151], G. Evans[130a], H. Evans[68], M. O. Evans[146], A. Ezhilov[37], S. Ezzarqtouni[35a], F. Fabbri[59], L. Fabbri[23a,23b], G. Facini[96], V. Fadeyev[136], R. M. Fakhrutdinov[37], S. Falciano[75a], L. F. Falda Ulhoa Coelho[36], P. J. Falke[24], S. Falke[36], J. Faltova[133], Y. Fan[14a], Y. Fang[14a,14d], M. Fanti[71a,71b], M. Faraj[69a,69b], Z. Farazpay[97], A. Farbin[8], A. Farilla[77a], T. Farooque[107], S. M. Farrington[52], F. Fassi[35e], D. Fassouliotis[9], M. Faucci Giannelli[76a,76b], W. J. Fawcett[32], L. Fayard[66], P. Federic[133], P. Federicova[131], O. L. Fedin[37,a], G. Fedotov[37], M. Feickert[170], L. Feligioni[102], A. Fell[139], D. E. Fellers[123], C. Feng[62b], M. Feng[14b], Z. Feng[114], M. J. Fenton[160], A. B. Fenyuk[37], L. Ferencz[48], R. A. M. Ferguson[91], S. I. Fernandez Luengo[137f], J. Ferrando[48], A. Ferrari[161], P. Ferrari[113,114], R. Ferrari[73a], D. Ferrere[56], C. Ferretti[106], F. Fiedler[100], A. Filipčič[93], E. K. Filmer[1], F. Filthaut[113], M. C. N. Fiolhais[130a,130c,c], L. Fiorini[163], F. Fischer[141], W. C. Fisher[107], T. Fitschen[101], I. Fleck[141], P. Fleischmann[106], T. Flick[171], L. Flores[128], M. Flores[33d,ae], L. R. Flores Castillo[64a], F. M. Follega[78a,78b], N. Fomin[16], J. H. Foo[155], B. C. Forland[68], A. Formica[135], A. C. Forti[101], E. Fortin[102], A. W. Fortman[61], M. G. Foti[17a], L. Fountas[9,k], D. Fournier[66], H. Fox[91], P. Francavilla[74a,74b], S. Francescato[61], S. Franchellucci[56], M. Franchini[23a,23b], S. Franchino[63a], D. Francis[36], L. Franco[113], L. Franconi[19], M. Franklin[61], G. Frattari[26], A. C. Freegard[94], W. S. Freund[82b], Y. Y. Frid[151], N. Fritzsche[50], A. Froch[54], D. Froidevaux[36], J. A. Frost[126], Y. Fu[62a], M. Fujimoto[118], E. Fullana Torregrosa[163,*], J. Fuster[163], A. Gabrielli[23a,23b], A. Gabrielli[155], P. Gadow[48], G. Gagliardi[57a,57b], L. G. Gagnon[17a], G. E. Gallardo[126], E. J. Gallas[126], B. J. Gallop[134], R. Gamboa Goni[94], K. K. Gan[119], S. Ganguly[153], J. Gao[62a], Y. Gao[52], F. M. Garay Walls[137a,137b], B. Garcia[29,ak], C. García[163], J. E. García Navarro[163], M. Garcia-Sciveres[17a], R. W. Gardner[39], D. Garg[80], R. B. Garg[143,q], C. A. Garner[155], S. J. Gasiorowski[138], P. Gaspar[82b], G. Gaudio[73a], V. Gautam[13], P. Gauzzi[75a,75b], I. L. Gavrilenko[37], A. Gavrilyuk[37], C. Gay[164], G. Gaycken[48], E. N. Gazis[10], A. A. Geanta[27b,27e], C. M. Gee[136], C. Gemme[57b], M. H. Genest[60], S. Gentile[75a,75b], S. George[95], W. F. George[20], T. Geralis[46], L. O. Gerlach[55], P. Gessinger-Befurt[36], M. E. Geyik[171], M. Ghneimat[141], K. Ghorbanian[94], A. Ghosal[141], A. Ghosh[160], A. Ghosh[7], B. Giacobbe[23b], S. Giagu[75a,75b], P. Giannetti[74a], A. Giannini[62a], S. M. Gibson[95], M. Gignac[136], D. T. Gil[85b], A. K. Gilbert[85a], B. J. Gilbert[41], D. Gillberg[34], G. Gilles[114], N. E. K. Gillwald[48], L. Ginabat[127], D. M. Gingrich[2,ah], M. P. Giordani[69a,69c], P. F. Giraud[135], G. Giugliarelli[69a,69c], D. Giugni[71a], F. Giuli[36], I. Gkialas[9,k], L. K. Gladilin[37], C. Glasman[99], G. R. Gledhill[123], M. Glisic[123], I. Gnesi[43b,g], Y. Go[29,ak], M. Goblirsch-Kolb[26], B. Gocke[49], D. Godin[108], B. Gokturk[21a], S. Goldfarb[105], T. Golling[56], M. G. D. Gololo[33g], D. Golubkov[37], J. P. Gombas[107], A. Gomes[130a,130b], G. Gomes Da Silva[141], A. J. Gomez Delegido[163], R. Gonçalo[130a,130c], G. Gonella[123], L. Gonella[20], A. Gongadze[38], F. Gonnella[20], J. L. Gonski[41], R. Y. González Andana[52], S. González de la Hoz[163], S. Gonzalez Fernandez[13], R. Gonzalez Lopez[92], C. Gonzalez Renteria[17a], R. Gonzalez Suarez[161], S. Gonzalez-Sevilla[56], G. R. Gonzalvo Rodriguez[163], L. Goossens[36], P. A. Gorbounov[37], B. Gorini[36], E. Gorini[70a,70b], A. Gorišek[93], A. T. Goshaw[51], M. I. Gostkin[38], S. Goswami[121], C. A. Gottardo[36], M. Gouighri[35b], V. Goumarre[48], A. G. Goussiou[138], N. Govender[33c], I. Grabowska-Bold[85a], K. Graham[34], E. Gramstad[125], S. Grancagnolo[18], M. Grandi[146], V. Gratchev[37,*], P. M. Gravila[27f], F. G. Gravili[70a,70b], H. M. Gray[17a], M. Greco[70a,70b], C. Grefe[24], I. M. Gregor[48], P. Grenier[143], C. Grieco[13], A. A. Grillo[136], K. Grimm[31,n], S. Grinstein[13,v], J.-F. Grivaz[66], E. Gross[169], J. Grosse-Knetter[55], C. Grud[106], J. C. Grundy[126], L. Guan[106], W. Guan[170], C. Gubbels[164], J. G. R. Guerrero Rojas[163], G. Guerrieri[69a,69b], F. Guescini[110], R. Gugel[100], J. A. M. Guhit[106], A. Guida[48], T. Guillemin[4], E. Guilloton[134,167], S. Guindon[36], F. Guo[14a,14d], J. Guo[62c], L. Guo[66], Y. Guo[106], R. Gupta[48], S. Gurbuz[24], S. S. Gurdasani[54], G. Gustavino[36], M. Guth[56], P. Gutierrez[120], L. F. Gutierrez Zagazeta[128], C. Gutschow[96], C. Gwenlan[126], C. B. Gwilliam[92],

E. S. Haaland[125], A. Haas[117], M. Habedank[48], C. Haber[17a], H. K. Hadavand[8], A. Hadef[100], S. Hadzic[110], E. H. Haines[96], M. Haleem[166], J. Haley[121], J. J. Hall[139], G. D. Hallewell[102], L. Halser[19], K. Hamano[165], H. Hamdaoui[35e], M. Hamer[24], G. N. Hamity[52], E. J. Hampshire[95], J. Han[62b], K. Han[62a], L. Han[14c], L. Han[62a], S. Han[17a], Y. F. Han[155], K. Hanagaki[83], M. Hance[136], D. A. Hangal[41,ad], H. Hanif[142], M. D. Hank[128], R. Hankache[101], J. B. Hansen[42], J. D. Hansen[42], P. H. Hansen[42], K. Hara[157], D. Harada[56], T. Harenberg[171], S. Harkusha[37], Y. T. Harris[126], N. M. Harrison[119], P. F. Harrison[167], N. M. Hartman[143], N. M. Hartmann[109], Y. Hasegawa[140], A. Hasib[52], S. Haug[19], R. Hauser[107], M. Havranek[132], C. M. Hawkes[20], R. J. Hawkings[36], S. Hayashida[111], D. Hayden[107], C. Hayes[106], R. L. Hayes[114], C. P. Hays[126], J. M. Hays[94], H. S. Hayward[92], F. He[62a], Y. He[154], Y. He[127], N. B. Heatley[94], V. Hedberg[98], A. L. Heggelund[125], N. D. Hehir[94], C. Heidegger[54], K. K. Heidegger[54], W. D. Heidorn[81], J. Heilman[34], S. Heim[48], T. Heim[17a], J. G. Heinlein[128], J. J. Heinrich[123], L. Heinrich[110,af], J. Hejbal[131], L. Helary[48], A. Held[170], S. Hellesund[125], C. M. Helling[164], S. Hellman[47a,47b], C. Helsens[36], R. C. W. Henderson[91], L. Henkelmann[32], A. M. Henriques Correia[36], H. Herde[98], Y. Hernández Jiménez[145], L. M. Herrmann[24], T. Herrmann[50], G. Herten[54], R. Hertenberger[109], L. Hervas[36], N. P. Hessey[156a], H. Hibi[84], S. J. Hillier[20], F. Hinterkeuser[24], M. Hirose[124], S. Hirose[157], D. Hirschbuehl[171], T. G. Hitchings[101], B. Hiti[93], J. Hobbs[145], R. Hobincu[27e], N. Hod[169], M. C. Hodgkinson[139], B. H. Hodkinson[32], A. Hoecker[36], J. Hofer[48], T. Holm[24], M. Holzbock[110], L. B. A. H. Hommels[32], B. P. Honan[101], J. Hong[62c], T. M. Hong[129], J. C. Honig[54], B. H. Hooberman[162], W. H. Hopkins[6], Y. Horii[111], S. Hou[148], A. S. Howard[93], J. Howarth[59], J. Hoya[6], M. Hrabovsky[122], A. Hrynevich[48], T. Hryn'ova[4], P. J. Hsu[65], S.-C. Hsu[138], Q. Hu[41], Y. F. Hu[14a,14d,aj], D. P. Huang[96], S. Huang[64b], X. Huang[14c], Y. Huang[62a], Y. Huang[14a], Z. Huang[101], Z. Hubacek[132], M. Huebner[24], F. Huegging[24], T. B. Huffman[126], M. Huhtinen[36], S. K. Huiberts[16], R. Hulsken[104], N. Huseynov[12,a], J. Huston[107], J. Huth[61], R. Hyneman[143], G. Iacobucci[56], G. Iakovidis[29], I. Ibragimov[141], L. Iconomidou-Fayard[66], P. Iengo[72a,72b], R. Iguchi[153], T. Iizawa[56], Y. Ikegami[83], A. Ilg[19], N. Ilic[155], H. Imam[35a], T. Ingebretsen Carlson[47a,47b], G. Introzzi[73a,73b], M. Iodice[77a], V. Ippolito[75a,75b], M. Ishino[153], W. Islam[170], C. Issever[18,48], S. Istin[21a,am], H. Ito[168], J. M. Iturbe Ponce[64a], R. Iuppa[78a,78b], A. Ivina[169], J. M. Izen[45], V. Izzo[72a], P. Jacka[131,132], P. Jackson[1], R. M. Jacobs[48], B. P. Jaeger[142], C. S. Jagfeld[109], P. Jain[54], G. Jäkel[171], K. Jakobs[54], T. Jakoubek[169], J. Jamieson[59], K. W. Janas[85a], A. E. Jaspan[92], M. Javurkova[103], F. Jeanneau[135], L. Jeanty[123], J. Jejelava[149a,ab], P. Jenni[54,h], C. E. Jessiman[34], S. Jézéquel[4], C. Jia[62b], J. Jia[145], X. Jia[61], X. Jia[14a,14d], Z. Jia[14c], Y. Jiang[62a], S. Jiggins[48], J. Jimenez Pena[110], S. Jin[14c], A. Jinaru[27b], O. Jinnouchi[154], P. Johansson[139], K. A. Johns[7], J. W. Johnson[136], D. M. Jones[32], E. Jones[167], P. Jones[32], R. W. L. Jones[91], T. J. Jones[92], R. Joshi[119], J. Jovicevic[15], X. Ju[17a], J. J. Junggeburth[36], T. Junkermann[63a], A. Juste Rozas[13,v], S. Kabana[137e], A. Kaczmarska[86], M. Kado[110], H. Kagan[119], M. Kagan[143], A. Kahn[41], A. Kahn[128], C. Kahra[100], T. Kaji[168], E. Kajomovitz[150], N. Kakati[169], C. W. Kalderon[29], A. Kamenshchikov[155], S. Kanayama[154], N. J. Kang[136], D. Kar[33g], K. Karava[126], M. J. Kareem[156b], E. Karentzos[54], I. Karkanias[152,f], S. N. Karpov[38], Z. M. Karpova[38], V. Kartvelishvili[91], A. N. Karyukhin[37], E. Kasimi[152,f], J. Katzy[48], S. Kaur[34], K. Kawade[140], T. Kawamoto[135], G. Kawamura[55], E. F. Kay[165], F. I. Kaya[158], S. Kazakos[13], V. F. Kazanin[37], Y. Ke[145], J. M. Keaveney[33a], R. Keeler[165], G. V. Kehris[61], J. S. Keller[34], A. S. Kelly[96], D. Kelsey[146], J. J. Kempster[146], K. E. Kennedy[41], P. D. Kennedy[100], O. Kepka[131], B. P. Kerridge[167], S. Kersten[171], B. P. Kerševan[93], S. Keshri[66], L. Keszeghova[28a], S. Ketabchi Haghighat[155], M. Khandoga[127], A. Khanov[121], A. G. Kharlamov[37], T. Kharlamova[37], E. E. Khoda[138], T. J. Khoo[18], G. Khoriauli[166], J. Khubua[149b], Y. A. R. Khwaira[66], M. Kiehn[36], A. Kilgallon[123], D. W. Kim[47a,47b], E. Kim[154], Y. K. Kim[39], N. Kimura[96], A. Kirchhoff[55], C. Kirfel[24], J. Kirk[134], A. E. Kiryunin[110], T. Kishimoto[153], D. P. Kisliuk[155], C. Kitsaki[10], O. Kivernyk[24], M. Klassen[63a], C. Klein[34], L. Klein[166], M. H. Klein[106], M. Klein[92], S. B. Klein[56], U. Klein[92], P. Klimek[36], A. Klimentov[29], F. Klimpel[110], T. Klioutchnikova[36], P. Kluit[114], S. Kluth[110], E. Kneringer[79], T. M. Knight[155], A. Knue[54], R. Kobayashi[87], M. Kocian[143], P. Kodyš[133], D. M. Koeck[146], P. T. Koenig[24], T. Koffas[34], M. Kolb[135], I. Koletsou[4], T. Komarek[122], K. Köneke[54], A. X. Y. Kong[1], T. Kono[118], N. Konstantinidis[96], B. Konya[98], R. Kopeliansky[68], S. Koperny[85a], K. Korcyl[86], K. Kordas[152,f], G. Koren[151], A. Korn[96], S. Korn[55], I. Korolkov[13], N. Korotkova[37], B. Kortman[114], O. Kortner[110], S. Kortner[110], W. H. Kostecka[115], V. V. Kostyukhin[141], A. Kotsokechagia[135], A. Kotwal[51], A. Koulouris[36], A. Kourkoumeli-Charalampidi[73a,73b], C. Kourkoumelis[9], E. Kourlitis[6], O. Kovanda[146], R. Kowalewski[165], W. Kozanecki[135], A. S. Kozhin[37], V. A. Kramarenko[37], G. Kramberger[93], P. Kramer[100], M. W. Krasny[127], A. Krasznahorkay[36], J. A. Kremer[100], T. Kresse[50], J. Kretzschmar[92], K. Kreul[18], P. Krieger[155],

S. Krishnamurthy[103], M. Krivos[133], K. Krizka[20], K. Kroeninger[49], H. Kroha[110], J. Kroll[131], J. Kroll[128], K. S. Krowpman[107], U. Kruchonak[38], H. Krüger[24], N. Krumnack[81], M. C. Kruse[51], J. A. Krzysiak[86], O. Kuchinskaia[37], S. Kuday[3a], S. Kuehn[36], R. Kuesters[54], T. Kuhl[48], V. Kukhtin[38], Y. Kulchitsky[37,a], S. Kuleshov[137b,137d], M. Kumar[33g], N. Kumari[102], A. Kupco[131], T. Kupfer[49], A. Kupich[37], O. Kuprash[54], H. Kurashige[84], L. L. Kurchaninov[156a], Y. A. Kurochkin[37], A. Kurova[37], M. Kuze[154], A. K. Kvam[103], J. Kvita[122], T. Kwan[104], N. G. Kyriacou[106], L. A. O. Laatu[102], C. Lacasta[163], F. Lacava[75a,75b], H. Lacker[18], D. Lacour[127], N. N. Lad[96], E. Ladygin[38], B. Laforge[127], T. Lagouri[137e], S. Lai[55], I. K. Lakomiec[85a], N. Lalloue[60], J. E. Lambert[120], S. Lammers[68], W. Lampl[7], C. Lampoudis[152,f], A. N. Lancaster[115], E. Lançon[29], U. Landgraf[54], M. P. J. Landon[94], V. S. Lang[54], R. J. Langenberg[103], A. J. Lankford[160], F. Lanni[36], K. Lantzsch[24], A. Lanza[73a], A. Lapertosa[57a,57b], J. F. Laporte[135], T. Lari[71a], F. Lasagni Manghi[23b], M. Lassnig[36], V. Latonova[131], A. Laudrain[100], A. Laurier[150], S. D. Lawlor[95], Z. Lawrence[101], M. Lazzaroni[71a,71b], B. Le[101], E. M. Le Boulicaut[51], B. Leban[93], A. Lebedev[81], M. LeBlanc[36], F. Ledroit-Guillon[60], A. C. A. Lee[96], G. R. Lee[16], S. C. Lee[148], S. Lee[47a,47b], T. F. Lee[92], L. L. Leeuw[33c], H. P. Lefebvre[95], M. Lefebvre[165], C. Leggett[17a], K. Lehmann[142], G. Lehmann Miotto[36], M. Leigh[56], W. A. Leight[103], A. Leisos[152,u], M. A. L. Leite[82c], C. E. Leitgeb[48], R. Leitner[133], K. J. C. Leney[44], T. Lenz[24], S. Leone[74a], C. Leonidopoulos[52], A. Leopold[144], C. Leroy[108], R. Les[107], C. G. Lester[32], M. Levchenko[37], J. Levêque[4], D. Levin[106], L. J. Levinson[169], M. P. Lewicki[86], D. J. Lewis[4], A. Li[5], B. Li[62b], C. Li[62a], C-Q. Li[62c], H. Li[62a], H. Li[62b], H. Li[14c], H. Li[62b], J. Li[62c], K. Li[138], L. Li[62c], M. Li[14a,14d], Q. Y. Li[62a], S. Li[14a,14d], S. Li[62c,62d,e], T. Li[62b], X. Li[104], Z. Li[62b], Z. Li[126], Z. Li[104], Z. Li[92], Z. Li[14a,14d], Z. Liang[14a], M. Liberatore[48], B. Liberti[76a], K. Lie[64c], J. Lieber Marin[82b], H. Lien[68], K. Lin[107], R. A. Linck[68], R. E. Lindley[7], J. H. Lindon[2], A. Linss[48], E. Lipeles[128], A. Lipniacka[16], A. Lister[164], J. D. Little[4], B. Liu[14a], B. X. Liu[142], D. Liu[62c,62d], J. B. Liu[62a], J. K. K. Liu[32], K. Liu[62c,62d], M. Liu[62a], M. Y. Liu[62a], P. Liu[14a], Q. Liu[62c,62d,138], X. Liu[62a], Y. Liu[14c,14d], Y. L. Liu[106], Y. W. Liu[62a], J. Llorente Merino[142], S. L. Lloyd[94], E. M. Lobodzinska[48], P. Loch[7], S. Loffredo[76a,76b], T. Lohse[18], K. Lohwasser[139], E. Loiacono[48], M. Lokajicek[131,*], J. D. Long[162], I. Longarini[160], L. Longo[70a,70b], R. Longo[162], I. Lopez Paz[67], A. Lopez Solis[48], J. Lorenz[109], N. Lorenzo Martinez[4], A. M. Lory[109], X. Lou[47a,47b], X. Lou[14a,14d], A. Lounis[66], J. Love[6], P. A. Love[91], G. Lu[14a,14d], M. Lu[80], S. Lu[128], Y. J. Lu[65], H. J. Lubatti[138], C. Luci[75a,75b], F. L. Lucio Alves[14c], A. Lucotte[60], F. Luehring[68], I. Luise[145], O. Lukianchuk[66], O. Lundberg[144], B. Lund-Jensen[144], N. A. Luongo[123], M. S. Lutz[151], D. Lynn[29], H. Lyons[92], R. Lysak[131], E. Lytken[98], V. Lyubushkin[38], T. Lyubushkina[38], M. M. Lyukova[145], H. Ma[29], L. L. Ma[62b], Y. Ma[96], D. M. Mac Donell[165], G. Maccarrone[53], J. C. MacDonald[139], R. Madar[40], W. F. Mader[50], J. Maeda[84], T. Maeno[29], M. Maerker[50], H. Maguire[139], A. Maio[130a,130b,130d], K. Maj[85a], O. Majersky[48], S. Majewski[123], N. Makovec[66], V. Maksimovic[15], B. Malaescu[127], Pa. Malecki[86], V. P. Maleev[37], F. Malek[60], D. Malito[43a,43b], U. Mallik[80], C. Malone[32], S. Maltezos[10], S. Malyukov[38], J. Mamuzic[13], G. Mancini[53], G. Manco[73a,73b], J. P. Mandalia[94], I. Mandić[93], L. Manhaes de Andrade Filho[82a], I. M. Maniatis[169], J. Manjarres Ramos[102,ac], D. C. Mankad[169], A. Mann[109], B. Mansoulie[135], S. Manzoni[36], A. Marantis[152,u], G. Marchiori[5], M. Marcisovsky[131], C. Marcon[71a,71b], M. Marinescu[20], M. Marjanovic[120], E. J. Marshall[91], Z. Marshall[17a], S. Marti-Garcia[163], T. A. Martin[167], V. J. Martin[52], B. Martin dit Latour[16], L. Martinelli[75a,75b], M. Martinez[13,v], P. Martinez Agullo[163], V. I. Martinez Outschoorn[103], P. Martinez Suarez[13], S. Martin-Haugh[134], V. S. Martoiu[27b], A. C. Martyniuk[96], A. Marzin[36], S. R. Maschek[110], D. Mascione[78a,78b], L. Masetti[100], T. Mashimo[153], J. Masik[101], A. L. Maslennikov[37], L. Massa[23b], P. Massarotti[72a,72b], P. Mastrandrea[74a,74b], A. Mastroberardino[43a,43b], T. Masubuchi[153], T. Mathisen[161], N. Matsuzawa[153], J. Maurer[27b], B. Maček[93], D. A. Maximov[37], R. Mazini[148], I. Maznas[152,f], M. Mazza[107], S. M. Mazza[136], C. Mc Ginn[29], J. P. Mc Gowan[104], S. P. Mc Kee[106], E. F. McDonald[105], A. E. McDougall[114], J. A. Mcfayden[146], G. Mchedlidze[149b], R. P. Mckenzie[33g], T. C. Mclachlan[48], D. J. Mclaughlin[96], K. D. McLean[165], S. J. McMahon[134], P. C. McNamara[105], C. M. Mcpartland[92], R. A. McPherson[165,y], T. Megy[40], S. Mehlhase[109], A. Mehta[92], D. Melini[150], B. R. Mellado Garcia[33g], A. H. Melo[55], F. Meloni[48], A. M. Mendes Jacques Da Costa[101], H. Y. Meng[155], L. Meng[91], S. Menke[110], M. Mentink[36], E. Meoni[43a,43b], C. Merlassino[126], L. Merola[72a,72b], C. Meroni[71a], G. Merz[106], O. Meshkov[37], J. Metcalfe[6], A. S. Mete[6], C. Meyer[68], J-P. Meyer[135], R. P. Middleton[134], L. Mijović[52], G. Mikenberg[169], M. Mikestikova[131], M. Mikuž[93], H. Mildner[139], A. Milic[36], C. D. Milke[44], D. W. Miller[39], L. S. Miller[34], A. Milov[169], D. A. Milstead[47a,47b], T. Min[14c], A. A. Minaenko[37], I. A. Minashvili[149b], L. Mince[59], A. I. Mincer[117], B. Mindur[85a],

M. Mineev[38], Y. Mino[87], L. M. Mir[13], M. Miralles Lopez[163], M. Mironova[126], M. C. Missio[113], T. Mitani[168], A. Mitra[167], V. A. Mitsou[163], O. Miu[155], P. S. Miyagawa[94], Y. Miyazaki[89], A. Mizukami[83], T. Mkrtchyan[63a], M. Mlinarevic[96], T. Mlinarevic[96], M. Mlynarikova[36], S. Mobius[55], K. Mochizuki[108], P. Moder[48], P. Mogg[109], A. F. Mohammed[14a,14d], S. Mohapatra[41], G. Mokgatitswane[33g], B. Mondal[141], S. Mondal[132], K. Mönig[48], E. Monnier[102], L. Monsonis Romero[163], J. Montejo Berlingen[83], M. Montella[119], F. Monticelli[90], N. Morange[66], A. L. Moreira De Carvalho[130a], M. Moreno Llácer[163], C. Moreno Martinez[56], P. Morettini[57b], S. Morgenstern[167], M. Morii[61], M. Morinaga[153], A. K. Morley[36], F. Morodei[75a,75b], L. Morvaj[36], P. Moschovakos[36], B. Moser[36], M. Mosidze[149b], T. Moskalets[54], P. Moskvitina[113], J. Moss[31,o], E. J. W. Moyse[103], O. Mtintsilana[33g], S. Muanza[102], J. Mueller[129], D. Muenstermann[91], R. Müller[19], G. A. Mullier[161], J. J. Mullin[128], D. P. Mungo[155], J. L. Munoz Martinez[13], D. Munoz Perez[163], F. J. Munoz Sanchez[101], M. Murin[101], W. J. Murray[134,167], A. Murrone[71a,71b], J. M. Muse[120], M. Muškinja[17a], C. Mwewa[29], A. G. Myagkov[37,a], A. J. Myers[8], A. A. Myers[129], G. Myers[68], M. Myska[132], B. P. Nachman[17a], O. Nackenhorst[49], A. Nag[50], K. Nagai[126], K. Nagano[83], J. L. Nagle[29,ak], E. Nagy[102], A. M. Nairz[36], Y. Nakahama[83], K. Nakamura[83], H. Nanjo[124], R. Narayan[44], E. A. Narayanan[112], I. Naryshkin[37], M. Naseri[34], C. Nass[24], G. Navarro[22a], J. Navarro-Gonzalez[163], R. Nayak[151], A. Nayaz[18], P. Y. Nechaeva[37], F. Nechansky[48], L. Nedic[126], T. J. Neep[20], A. Negri[73a,73b], M. Negrini[23b], C. Nellist[114], C. Nelson[104], K. Nelson[106], S. Nemecek[131], M. Nessi[36,i], M. S. Neubauer[162], F. Neuhaus[100], J. Neundorf[48], R. Newhouse[164], P. R. Newman[20], C. W. Ng[129], Y. W. Y. Ng[48], B. Ngair[35e], H. D. N. Nguyen[108], R. B. Nickerson[126], R. Nicolaidou[135], J. Nielsen[136], M. Niemeyer[55], N. Nikiforou[36], V. Nikolaenko[37,a], I. Nikolic-Audit[127], K. Nikolopoulos[20], P. Nilsson[29], I. Ninca[48], H. R. Nindhito[56], G. Ninio[151], A. Nisati[75a], N. Nishu[2], R. Nisius[110], J-E. Nitschke[50], E. K. Nkadimeng[33g], S. J. Noacco Rosende[90], T. Nobe[153], D. L. Noel[32], Y. Noguchi[87], T. Nommensen[147], M. A. Nomura[29], M. B. Norfolk[139], R. R. B. Norisam[96], B. J. Norman[34], J. Novak[93], T. Novak[48], L. Novotny[132], R. Novotny[112], L. Nozka[122], K. Ntekas[160], N. M. J. Nunes De Moura Junior[82b], E. Nurse[96], J. Ocariz[127], A. Ochi[84], I. Ochoa[130a], S. Oerdek[161], J. T. Offermann[39], A. Ogrodnik[85a], A. Oh[101], C. C. Ohm[144], H. Oide[83], R. Oishi[153], M. L. Ojeda[48], Y. Okazaki[87], M. W. O'Keefe[92], Y. Okumura[153], L. F. Oleiro Seabra[130a], S. A. Olivares Pino[137d], D. Oliveira Damazio[29], D. Oliveira Goncalves[82a], J. L. Oliver[160], M. J. R. Olsson[160], A. Olszewski[86], J. Olszowska[86,*], Ö. O. Öncel[54], D. C. O'Neil[142], A. P. O'Neill[19], A. Onofre[130a,130e], P. U. E. Onyisi[11], M. J. Oreglia[39], G. E. Orellana[90], D. Orestano[77a,77b], N. Orlando[13], R. S. Orr[155], V. O'Shea[59], R. Ospanov[62a], G. Otero y Garzon[30], H. Otono[89], P. S. Ott[63a], G. J. Ottino[17a], M. Ouchrif[35d], J. Ouellette[29], F. Ould-Saada[125], M. Owen[59], R. E. Owen[134], K. Y. Oyulmaz[21a], V. E. Ozcan[21a], N. Ozturk[8], S. Ozturk[21d], H. A. Pacey[32], K. Pachal[51], A. Pacheco Pages[13], C. Padilla Aranda[13], G. Padovano[75a,75b], S. Pagan Griso[17a], G. Palacino[68], A. Palazzo[70a,70b], S. Palestini[36], J. Pan[172], T. Pan[64a], D. K. Panchal[11], C. E. Pandini[114], J. G. Panduro Vazquez[95], H. Pang[14b], P. Pani[48], G. Panizzo[69a,69c], L. Paolozzi[56], C. Papadatos[108], S. Parajuli[44], A. Paramonov[6], C. Paraskevopoulos[10], D. Paredes Hernandez[64b], T. H. Park[155], M. A. Parker[32], F. Parodi[57a,57b], E. W. Parrish[115], V. A. Parrish[52], J. A. Parsons[41], U. Parzefall[54], B. Pascual Dias[108], L. Pascual Dominguez[151], F. Pasquali[114], E. Pasqualucci[75a], S. Passaggio[57b], F. Pastore[95], P. Pasuwan[47a,47b], P. Patel[86], U. M. Patel[51], J. R. Pater[101], T. Pauly[36], J. Pearkes[143], M. Pedersen[125], R. Pedro[130a], S. V. Peleganchuk[37], O. Penc[36], E. A. Pender[52], H. Peng[62a], K. E. Penski[109], M. Penzin[37], B. S. Peralva[82d], A. P. Pereira Peixoto[60], L. Pereira Sanchez[47a,47b], D. V. Perepelitsa[29,ak], E. Perez Codina[156a], M. Perganti[10], L. Perini[71a,71b,*], H. Pernegger[36], S. Perrella[36], A. Perrevoort[113], O. Perrin[40], K. Peters[48], R. F. Y. Peters[101], B. A. Petersen[36], T. C. Petersen[42], E. Petit[102], V. Petousis[132], C. Petridou[152,f], A. Petrukhin[141], M. Pettee[17a], N. E. Pettersson[36], A. Petukhov[37], K. Petukhova[133], A. Peyaud[135], R. Pezoa[137f], L. Pezzotti[36], G. Pezzullo[172], T. M. Pham[170], T. Pham[105], P. W. Phillips[134], M. W. Phipps[162], G. Piacquadio[145], E. Pianori[17a], F. Piazza[71a,71b], R. Piegaia[30], D. Pietreanu[27b], A. D. Pilkington[101], M. Pinamonti[69a,69c], J. L. Pinfold[2], B. C. Pinheiro Pereira[130a], C. Pitman Donaldson[96], D. A. Pizzi[34], L. Pizzimento[76a,76b], A. Pizzini[114], M.-A. Pleier[29], V. Plesanovs[54], V. Pleskot[133], E. Plotnikova[38], G. Poddar[4], R. Poettgen[98], L. Poggioli[127], D. Pohl[24], I. Pokharel[55], S. Polacek[133], G. Polesello[73a], A. Poley[142,156a], R. Polifka[132], A. Polini[23b], C. S. Pollard[167], Z. B. Pollock[119], V. Polychronakos[29], E. Pompa Pacchi[75a,75b], D. Ponomarenko[113], L. Pontecorvo[36], S. Popa[27a], G. A. Popeneciu[27d], D. M. Portillo Quintero[156a], S. Pospisil[132], P. Postolache[27c], K. Potamianos[126], P. A. Potepa[85a], I. N. Potrap[38], C. J. Potter[32], H. Potti[1], T. Poulsen[48], J. Poveda[163], M. E. Pozo Astigarraga[36], A. Prades Ibanez[163], M. M. Prapa[46], J. Pretel[54], D. Price[101], M. Primavera[70a], M. A. Principe Martin[99], R. Privara[122], M. L. Proffitt[138],

N. Proklova[128], K. Prokofiev[64c], G. Proto[76a,76b], S. Protopopescu[29], J. Proudfoot[6], M. Przybycien[85a], W. W. Przygoda[85b], J. E. Puddefoot[139], D. Pudzha[37], D. Pyatiizbyantseva[37], J. Qian[106], D. Qichen[101], Y. Qin[101], T. Qiu[52], A. Quadt[55], M. Queitsch-Maitland[101], G. Quetant[56], G. Rabanal Bolanos[61], D. Rafanoharana[54], F. Ragusa[71a,71b], J. L. Rainbolt[39], J. A. Raine[56], S. Rajagopalan[29], E. Ramakoti[37], K. Ran[48,14d], N. P. Rapheeha[33g], V. Raskina[127], D. F. Rassloff[63a], S. Rave[100], B. Ravina[55], I. Ravinovich[169], M. Raymond[36], A. L. Read[125], N. P. Readioff[139], D. M. Rebuzzi[73a,73b], G. Redlinger[29], K. Reeves[45], J. A. Reidelsturz[171], D. Reikher[151], A. Rej[141], C. Rembser[36], A. Renardi[48], M. Renda[27b], M. B. Rendel[110], F. Renner[48], A. G. Rennie[59], S. Resconi[71a], M. Ressegotti[57a,57b], E. D. Resseguie[17a], S. Rettie[36], J. G. Reyes Rivera[107], B. Reynolds[119], E. Reynolds[17a], M. Rezaei Estabragh[171], O. L. Rezanova[37], P. Reznicek[133], N. Ribaric[91], E. Ricci[78a,78b], R. Richter[110], S. Richter[47a,47b], E. Richter-Was[85b], M. Ridel[127], S. Ridouani[35d], P. Rieck[117], P. Riedler[36], M. Rijssenbeek[145], A. Rimoldi[73a,73b], M. Rimoldi[48], L. Rinaldi[23a,23b], T. T. Rinn[29], M. P. Rinnagel[109], G. Ripellino[161], I. Riu[13], P. Rivadeneira[48], J. C. Rivera Vergara[165], F. Rizatdinova[121], E. Rizvi[94], C. Rizzi[56], B. A. Roberts[167], B. R. Roberts[17a], S. H. Robertson[104,y], M. Robin[48], D. Robinson[32], C. M. Robles Gajardo[137f], M. Robles Manzano[100], A. Robson[59], A. Rocchi[76a,76b], C. Roda[74a,74b], S. Rodriguez Bosca[63a], Y. Rodriguez Garcia[22a], A. Rodriguez Rodriguez[54], A. M. Rodríguez Vera[156b], S. Roe[36], J. T. Roemer[160], A. R. Roepe-Gier[136], J. Roggel[171], O. Røhne[125], R. A. Rojas[103], B. Roland[54], C. P. A. Roland[68], J. Roloff[29], A. Romaniouk[37], E. Romano[73a,73b], M. Romano[23b], A. C. Romero Hernandez[162], N. Rompotis[92], L. Roos[127], S. Rosati[75a], B. J. Rosser[39], E. Rossi[4], E. Rossi[72a,72b], L. P. Rossi[57b], L. Rossini[48], R. Rosten[119], M. Rotaru[27b], B. Rottler[54], C. Rougier[102,ac], D. Rousseau[66], D. Rousso[32], G. Rovelli[73a,73b], A. Roy[162], S. Roy-Garand[155], A. Rozanov[102], Y. Rozen[150], X. Ruan[33g], A. Rubio Jimenez[163], A. J. Ruby[92], V. H. Ruelas Rivera[18], T. A. Ruggeri[1], F. Rühr[54], A. Ruiz-Martinez[163], A. Rummler[36], Z. Rurikova[54], N. A. Rusakovich[38], H. L. Russell[165], J. P. Rutherfoord[7], K. Rybacki[91], M. Rybar[133], E. B. Rye[125], A. Ryzhov[37], J. A. Sabater Iglesias[56], P. Sabatini[163], L. Sabetta[75a,75b], H.F-W. Sadrozinski[136], F. Safai Tehrani[75a], B. Safarzadeh Samani[146], M. Safdari[143], S. Saha[104], M. Sahinsoy[110], M. Saimpert[135], M. Saito[153], T. Saito[153], D. Salamani[36], A. Salnikov[143], J. Salt[163], A. Salvador Salas[13], D. Salvatore[43a,43b], F. Salvatore[146], A. Salzburger[36], D. Sammel[54], D. Sampsonidis[152,f], D. Sampsonidou[62c,62d], J. Sánchez[163], A. Sanchez Pineda[4], V. Sanchez Sebastian[163], H. Sandaker[125], C. O. Sander[48], J. A. Sandesara[103], M. Sandhoff[171], C. Sandoval[22b], D. P. C. Sankey[134], T. Sano[87], A. Sansoni[53], L. Santi[75a,75b], C. Santoni[40], H. Santos[130a,130b], S. N. Santpur[17a], A. Santra[169], K. A. Saoucha[139], J. G. Saraiva[130a,130d], J. Sardain[7], O. Sasaki[83], K. Sato[157], C. Sauer[63b], F. Sauerburger[54], E. Sauvan[4], P. Savard[155,ah], R. Sawada[153], C. Sawyer[134], L. Sawyer[97], I. Sayago Galvan[163], C. Sbarra[23b], A. Sbrizzi[23a,23b], T. Scanlon[96], J. Schaarschmidt[138], P. Schacht[110], D. Schaefer[39], U. Schäfer[100], A. C. Schaffer[44,66], D. Schaile[109], R. D. Schamberger[145], E. Schanet[109], C. Scharf[18], M. M. Schefer[19], V. A. Schegelsky[37], D. Scheirich[133], F. Schenck[18], M. Schernau[160], C. Scheulen[55], C. Schiavi[57a,57b], Z. M. Schillaci[26], E. J. Schioppa[70a,70b], M. Schioppa[43a,43b], B. Schlag[100], K. E. Schleicher[54], S. Schlenker[36], J. Schmeing[171], M. A. Schmidt[171], K. Schmieden[100], C. Schmitt[100], S. Schmitt[48], L. Schoeffel[135], A. Schoening[63b], P. G. Scholer[54], E. Schopf[126], M. Schott[100], J. Schovancova[36], S. Schramm[56], F. Schroeder[171], H-C. Schultz-Coulon[63a], M. Schumacher[54], B. A. Schumm[136], Ph. Schune[135], H. R. Schwartz[136], A. Schwartzman[143], T. A. Schwarz[106], Ph. Schwemling[135], R. Schwienhorst[107], A. Sciandra[136], G. Sciolla[26], F. Scuri[74a], F. Scutti[105], C. D. Sebastiani[92], K. Sedlaczek[49], P. Seema[18], S. C. Seidel[112], A. Seiden[136], B. D. Seidlitz[41], C. Seitz[48], J. M. Seixas[82b], G. Sekhniaidze[72a], S. J. Sekula[44], L. Selem[4], N. Semprini-Cesari[23a,23b], S. Sen[51], D. Sengupta[56], V. Senthilkumar[163], L. Serin[66], L. Serkin[69a,69b], M. Sessa[77a,77b], H. Severini[120], F. Sforza[57a,57b], A. Sfyrla[56], E. Shabalina[55], R. Shaheen[144], J. D. Shahinian[128], D. Shaked Renous[169], L. Y. Shan[14a], M. Shapiro[17a], A. Sharma[36], A. S. Sharma[164], P. Sharma[80], S. Sharma[48], P. B. Shatalov[37], K. Shaw[146], S. M. Shaw[101], Q. Shen[5,62c], P. Sherwood[96], L. Shi[96], C. O. Shimmin[172], Y. Shimogama[168], J. D. Shinner[95], I. P. J. Shipsey[126], S. Shirabe[60], M. Shiyakova[38,an], J. Shlomi[169], M. J. Shochet[39], J. Shojaii[105], D. R. Shope[125], S. Shrestha[119,al], E. M. Shrif[33g], M. J. Shroff[165], P. Sicho[131], A. M. Sickles[162], E. Sideras Haddad[33g], A. Sidoti[23b], F. Siegert[50], Dj. Sijacki[15], R. Sikora[85a], F. Sili[90], J. M. Silva[20], M. V. Silva Oliveira[36], S. B. Silverstein[47a], S. Simion[66], R. Simoniello[36], E. L. Simpson[59], H. Simpson[146], L. R. Simpson[106], N. D. Simpson[98], S. Simsek[21d], S. Sindhu[55], P. Sinervo[155], S. Singh[142], S. Singh[155], S. Sinha[48], S. Sinha[33g], M. Sioli[23a,23b], I. Siral[36], S.Yu. Sivoklokov[37,*], J. Sjölin[47a,47b], A. Skaf[55], E. Skorda[98], P. Skubic[120], M. Slawinska[86], V. Smakhtin[169], B. H. Smart[134], J. Smiesko[36], S.Yu. Smirnov[37],

Y. Smirnov[37], L. N. Smirnova[37,a], O. Smirnova[98], A. C. Smith[41], E. A. Smith[39], H. A. Smith[126], J. L. Smith[92], R. Smith[143], M. Smizanska[91], K. Smolek[132], A. Smykiewicz[86], A. A. Snesarev[37], H. L. Snoek[114], S. Snyder[29], R. Sobie[165,y], A. Soffer[151], C. A. Solans Sanchez[36], E.Yu. Soldatov[37], U. Soldevila[163], A. A. Solodkov[37], S. Solomon[54], A. Soloshenko[38], K. Solovieva[54], O. V. Solovyanov[40], V. Solovyev[37], P. Sommer[36], A. Sonay[13], W. Y. Song[156b], J. M. Sonneveld[114], A. Sopczak[132], A. L. Sopio[96], F. Sopkova[28b], V. Sothilingam[63a], S. Sottocornola[68], R. Soualah[116b], Z. Soumaimi[35e], D. South[48], S. Spagnolo[70a,70b], M. Spalla[110], D. Sperlich[54], G. Spigo[36], M. Spina[146], S. Spinali[91], D. P. Spiteri[59], M. Spousta[133], E. J. Staats[34], A. Stabile[71a,71b], R. Stamen[63a], M. Stamenkovic[114], A. Stampekis[20], M. Standke[24], E. Stanecka[86], M. V. Stange[50], B. Stanislaus[17a], M. M. Stanitzki[48], M. Stankaityte[126], B. Stapf[48], E. A. Starchenko[37], G. H. Stark[136], J. Stark[102,ac], D. M. Starko[156b], P. Staroba[131], P. Starovoitov[63a], S. Stärz[104], R. Staszewski[86], G. Stavropoulos[46], J. Steentoft[161], P. Steinberg[29], B. Stelzer[142,156a], H. J. Stelzer[129], O. Stelzer-Chilton[156a], H. Stenzel[58], T. J. Stevenson[146], G. A. Stewart[36], J. R. Stewart[121], M. C. Stockton[36], G. Stoicea[27b], M. Stolarski[130a], S. Stonjek[110], A. Straessner[50], J. Strandberg[144], S. Strandberg[47a,47b], M. Strauss[120], T. Strebler[102], P. Strizenec[28b], R. Ströhmer[166], D. M. Strom[123], L. R. Strom[48], R. Stroynowski[44], A. Strubig[47a,47b], S. A. Stucci[29], B. Stugu[16], J. Stupak[120], N. A. Styles[48], D. Su[143], S. Su[62a], W. Su[62c,62d,138], X. Su[62a,66], K. Sugizaki[153], V. V. Sulin[37], M. J. Sullivan[92], D. M. S. Sultan[78a,78b], L. Sultanaliyeva[37], S. Sultansoy[3b], T. Sumida[87], S. Sun[106], S. Sun[170], O. Sunneborn Gudnadottir[161], M. R. Sutton[146], M. Svatos[131], M. Swiatlowski[156a], T. Swirski[166], I. Sykora[28a], M. Sykora[133], T. Sykora[133], D. Ta[100], K. Tackmann[48,w], A. Taffard[160], R. Tafirout[156a], J. S. Tafoya Vargas[66], R. H. M. Taibah[127], R. Takashima[88], E. P. Takeva[52], Y. Takubo[83], M. Talby[102], A. A. Talyshev[37], K. C. Tam[64b], N. M. Tamir[151], A. Tanaka[153], J. Tanaka[153], R. Tanaka[66], M. Tanasini[57a,57b], J. Tang[62c], Z. Tao[164], S. Tapia Araya[137f], S. Tapprogge[100], A. Tarek Abouelfadl Mohamed[107], S. Tarem[150], K. Tariq[62b], G. Tarna[27b,102], G. F. Tartarelli[71a], P. Tas[133], M. Tasevsky[131], E. Tassi[43a,43b], A. C. Tate[162], G. Tateno[153], Y. Tayalati[35e,x], G. N. Taylor[105], W. Taylor[156b], H. Teagle[92], A. S. Tee[170], R. Teixeira De Lima[143], P. Teixeira-Dias[95], J. J. Teoh[155], K. Terashi[153], J. Terron[99], S. Terzo[13], M. Testa[53], R. J. Teuscher[155,y], A. Thaler[79], O. Theiner[56], N. Themistokleous[52], T. Theveneaux-Pelzer[102], O. Thielmann[171], D. W. Thomas[95], J. P. Thomas[20], E. A. Thompson[17a], P. D. Thompson[20], E. Thomson[128], E. J. Thorpe[94], Y. Tian[55], V. Tikhomirov[37,a], Yu.A. Tikhonov[37], S. Timoshenko[37], E. X. L. Ting[1], P. Tipton[172], S. H. Tlou[33g], A. Tnourji[40], K. Todome[23a,23b], S. Todorova-Nova[133], S. Todt[50], M. Togawa[83], J. Tojo[89], S. Tokár[28a], K. Tokushuku[83], O. Toldaiev[68], R. Tombs[32], M. Tomoto[83,111], L. Tompkins[143,q], K. W. Topolnicki[85b], P. Tornambe[103], E. Torrence[123], H. Torres[50], E. Torró Pastor[163], M. Toscani[30], C. Tosciri[39], M. Tost[11], D. R. Tovey[139], A. Traeet[16], I. S. Trandafir[27b], T. Trefzger[166], A. Tricoli[29], I. M. Trigger[156a], S. Trincaz-Duvoid[127], D. A. Trischuk[26], B. Trocmé[60], C. Troncon[71a], L. Truong[33c], M. Trzebinski[86], A. Trzupek[86], F. Tsai[145], M. Tsai[106], A. Tsiamis[152,f], P. V. Tsiareshka[37], S. Tsigaridas[156a], A. Tsirigotis[152,u], V. Tsiskaridze[145], E. G. Tskhadadze[149a], M. Tsopoulou[152,f], Y. Tsujikawa[87], I. I. Tsukerman[37], V. Tsulaia[17a], S. Tsuno[83], O. Tsur[150], D. Tsybychev[145], Y. Tu[64b], A. Tudorache[27b], V. Tudorache[27b], A. N. Tuna[36], S. Turchikhin[38], I. Turk Cakir[3a], R. Turra[71a], T. Turtuvshin[38,z], P. M. Tuts[41], S. Tzamarias[152,f], P. Tzanis[10], E. Tzovara[100], K. Uchida[153], F. Ukegawa[157], P. A. Ulloa Poblete[137c], E. N. Umaka[29], G. Unal[36], M. Unal[11], A. Undrus[29], G. Unel[160], J. Urban[28b], P. Urquijo[105], G. Usai[8], R. Ushioda[154], M. Usman[108], Z. Uysal[21b], L. Vacavant[102], V. Vacek[132], B. Vachon[104], K. O. H. Vadla[125], T. Vafeiadis[36], A. Vaitkus[96], C. Valderanis[109], E. Valdes Santurio[47a,47b], M. Valente[156a], S. Valentinetti[23a,23b], A. Valero[163], A. Vallier[102,ac], J. A. Valls Ferrer[163], D. R. Van Arneman[114], T. R. Van Daalen[138], P. Van Gemmeren[6], M. Van Rijnbach[36,125], S. Van Stroud[96], I. Van Vulpen[114], M. Vanadia[76a,76b], W. Vandelli[36], M. Vandenbroucke[135], E. R. Vandewall[121], D. Vannicola[151], L. Vannoli[57a,57b], R. Vari[75a], E. W. Varnes[7], C. Varni[17a], T. Varol[148], D. Varouchas[66], L. Varriale[163], K. E. Varvell[147], M. E. Vasile[27b], L. Vaslin[40], G. A. Vasquez[165], F. Vazeille[40], T. Vazquez Schroeder[36], J. Veatch[31], V. Vecchio[101], M. J. Veen[103], I. Veliscek[126], L. M. Veloce[155], F. Veloso[130a,130c], S. Veneziano[75a], A. Ventura[70a,70b], A. Verbytskyi[110], M. Verducci[74a,74b], C. Vergis[24], M. Verissimo De Araujo[82b], W. Verkerke[114], J. C. Vermeulen[114], C. Vernieri[143], P. J. Verschuuren[95], M. Vessella[103], M. C. Vetterli[142,ah], A. Vgenopoulos[152,f], N. Viaux Maira[137f], T. Vickey[139], O. E. Vickey Boeriu[139], G. H. A. Viehhauser[126], L. Vigani[63b], M. Villa[23a,23b], M. Villaplana Perez[163], E. M. Villhauer[52], E. Vilucchi[53], M. G. Vincter[34], G. S. Virdee[20], A. Vishwakarma[52], C. Vittori[36], I. Vivarelli[146], V. Vladimirov[167], E. Voevodina[110], F. Vogel[109], P. Vokac[132], J. Von Ahnen[48], E. Von Toerne[24], B. Vormwald[36], V. Vorobel[133], K. Vorobev[37], M. Vos[163],

K. Voss[141], J. H. Vossebeld[92], M. Vozak[114], L. Vozdecky[94], N. Vranjes[15], M. Vranjes Milosavljevic[15], M. Vreeswijk[114], R. Vuillermet[36], O. Vujinovic[100], I. Vukotic[39], S. Wada[157], C. Wagner[103], J. M. Wagner[17a], W. Wagner[171], S. Wahdan[171], H. Wahlberg[90], R. Wakasa[157], M. Wakida[111], J. Walder[134], R. Walker[109], W. Walkowiak[141], A. M. Wang[61], A. Z. Wang[170], C. Wang[100], C. Wang[62c], H. Wang[17a], J. Wang[64a], R.-J. Wang[100], R. Wang[61], R. Wang[6], S. M. Wang[148], S. Wang[62b], T. Wang[62a], W. T. Wang[80], X. Wang[14c], X. Wang[162], X. Wang[62c], Y. Wang[62d], Y. Wang[14c], Z. Wang[106], Z. Wang[51,62c,62d], Z. Wang[106], A. Warburton[104], R. J. Ward[20], N. Warrack[59], A. T. Watson[20], H. Watson[59], M. F. Watson[20], G. Watts[138], B. M. Waugh[96], C. Weber[29], H. A. Weber[18], M. S. Weber[19], S. M. Weber[63a], C. Wei[62a], Y. Wei[126], A. R. Weidberg[126], E. J. Weik[117], J. Weingarten[49], M. Weirich[100], C. Weiser[54], C. J. Wells[48], T. Wenaus[29], B. Wendland[49], T. Wengler[36], N. S. Wenke[110], N. Wermes[24], M. Wessels[63a], K. Whalen[123], A. M. Wharton[91], A. S. White[61], A. White[8], M. J. White[1], D. Whiteson[160], L. Wickremasinghe[124], W. Wiedenmann[170], C. Wiel[50], M. Wielers[134], C. Wiglesworth[42], L. A. M. Wiik-Fuchs[54], D. J. Wilbern[120], H. G. Wilkens[36], D. M. Williams[41], H. H. Williams[128], S. Williams[32], S. Willocq[103], B. J. Wilson[101], P. J. Windischhofer[39], F. Winklmeier[123], B. T. Winter[54], J. K. Winter[101], M. Wittgen[143], M. Wobisch[97], R. Wölker[126], J. Wollrath[160], M. W. Wolter[86], H. Wolters[130a,130c], V. W. S. Wong[164], A. F. Wongel[48], S. D. Worm[48], B. K. Wosiek[86], K. W. Woźniak[86], K. Wraight[59], J. Wu[14a,14d], M. Wu[64a], M. Wu[113], S. L. Wu[170], X. Wu[56], Y. Wu[62a], Z. Wu[62a,135], J. Wuerzinger[110], T. R. Wyatt[101], B. M. Wynne[52], S. Xella[42], L. Xia[14c], M. Xia[14b], J. Xiang[64c], X. Xiao[106], M. Xie[62a], X. Xie[62a], S. Xin[14a,14d], J. Xiong[17a], I. Xiotidis[146], D. Xu[14a], H. Xu[62a], H. Xu[62a], L. Xu[62a], R. Xu[128], T. Xu[106], Y. Xu[14b], Z. Xu[62b], Z. Xu[14a], B. Yabsley[147], S. Yacoob[33a], N. Yamaguchi[89], Y. Yamaguchi[154], H. Yamauchi[157], T. Yamazaki[17a], Y. Yamazaki[84], J. Yan[62c], S. Yan[126], Z. Yan[25], H. J. Yang[62c,62d], H. T. Yang[62a], S. Yang[62a], T. Yang[64c], X. Yang[62a], X. Yang[14a], Y. Yang[44], Y. Yang[62a], Z. Yang[62a,106], W-M. Yao[17a], Y. C. Yap[48], H. Ye[14c], H. Ye[55], J. Ye[44], S. Ye[29], X. Ye[62a], Y. Yeh[96], I. Yeletskikh[38], B. K. Yeo[17a], M. R. Yexley[91], P. Yin[41], K. Yorita[168], S. Younas[27b], C. J. S. Young[54], C. Young[143], Y. Yu[62a], M. Yuan[106], R. Yuan[62b,l], L. Yue[96], M. Zaazoua[35e], B. Zabinski[86], E. Zaid[52], T. Zakareishvili[149b], N. Zakharchuk[34], S. Zambito[56], J. A. Zamora Saa[137d,137b], J. Zang[153], D. Zanzi[54], O. Zaplatilek[132], C. Zeitnitz[171], H. Zeng[14a], J. C. Zeng[162], D. T. Zenger Jr[26], O. Zenin[37], T. Ženiš[28a], S. Zenz[94], S. Zerradi[35a], D. Zerwas[66], M. Zhai[14a,14d], B. Zhang[14c], D. F. Zhang[139], J. Zhang[62b], J. Zhang[6], K. Zhang[14a,14d], L. Zhang[14c], P. Zhang[14a,14d], R. Zhang[170], S. Zhang[106], T. Zhang[153], X. Zhang[62c], X. Zhang[62b], Y. Zhang[5,62c], Z. Zhang[17a], Z. Zhang[66], H. Zhao[138], P. Zhao[51], T. Zhao[62b], Y. Zhao[136], Z. Zhao[62a], A. Zhemchugov[38], X. Zheng[62a], Z. Zheng[143], D. Zhong[162], B. Zhou[106], C. Zhou[170], H. Zhou[7], N. Zhou[62c], Y. Zhou[7], C. G. Zhu[62b], H. L. Zhu[62a], J. Zhu[106], Y. Zhu[62c], Y. Zhu[62a], X. Zhuang[14a], K. Zhukov[37], V. Zhulanov[37], N. I. Zimine[38], J. Zinsser[63b], M. Ziolkowski[141], L. Živković[15], A. Zoccoli[23a,23b], K. Zoch[56], T. G. Zorbas[139], O. Zormpa[46], W. Zou[41], L. Zwalinski[36]

[1] Department of Physics, University of Adelaide, Adelaide, Australia

[2] Department of Physics, University of Alberta, Edmonton, AB, Canada

[3] (a)Department of Physics, Ankara University, Ankara, Türkiye; (b)Division of Physics, TOBB University of Economics and Technology, Ankara, Türkiye

[4] LAPP, Université Savoie Mont Blanc, CNRS/IN2P3, Annecy, France

[5] APC, Université Paris Cité, CNRS/IN2P3, Paris, France

[6] High Energy Physics Division, Argonne National Laboratory, Argonne, IL, USA

[7] Department of Physics, University of Arizona, Tucson, AZ, USA

[8] Department of Physics, University of Texas at Arlington, Arlington, TX, USA

[9] Physics Department, National and Kapodistrian University of Athens, Athens, Greece

[10] Physics Department, National Technical University of Athens, Zografou, Greece

[11] Department of Physics, University of Texas at Austin, Austin, TX, USA

[12] Institute of Physics, Azerbaijan Academy of Sciences, Baku, Azerbaijan

[13] Institut de Física d'Altes Energies (IFAE), Barcelona Institute of Science and Technology, Barcelona, Spain

[14] (a)Institute of High Energy Physics, Chinese Academy of Sciences, Beijing, China; (b)Physics Department, Tsinghua University, Beijing, China; (c)Department of Physics, Nanjing University, Nanjing, China; (d)University of Chinese Academy of Science (UCAS), Beijing, China

[15] Institute of Physics, University of Belgrade, Belgrade, Serbia

[16] Department for Physics and Technology, University of Bergen, Bergen, Norway

[17] (a)Physics Division, Lawrence Berkeley National Laboratory, Berkeley, CA, USA; (b)University of California, Berkeley, CA, USA

[18] Institut für Physik, Humboldt Universität zu Berlin, Berlin, Germany

[19] Albert Einstein Center for Fundamental Physics and Laboratory for High Energy Physics, University of Bern, Bern, Switzerland

[20] School of Physics and Astronomy, University of Birmingham, Birmingham, UK

[21] (a)Department of Physics, Bogazici University, Istanbul, Türkiye; (b)Department of Physics Engineering, Gaziantep University, Gaziantep, Türkiye; (c)Department of Physics, Istanbul University, Istanbul, Türkiye; (d)Istinye University, Sariyer, Istanbul, Türkiye

[22] (a)Facultad de Ciencias y Centro de Investigaciónes, Universidad Antonio Nariño, Bogotá, Colombia; (b)Departamento de Física, Universidad Nacional de Colombia, Bogotá, Colombia

[23] (a)Dipartimento di Fisica e Astronomia A. Righi, Università di Bologna, Bologna, Italy; (b)INFN Sezione di Bologna, Bologna, Italy

[24] Physikalisches Institut, Universität Bonn, Bonn, Germany

[25] Department of Physics, Boston University, Boston, MA, USA

[26] Department of Physics, Brandeis University, Waltham, MA, USA

[27] (a)Transilvania University of Brasov, Brasov, Romania; (b)Horia Hulubei National Institute of Physics and Nuclear Engineering, Bucharest, Romania; (c)Department of Physics, Alexandru Ioan Cuza University of Iasi, Iasi, Romania; (d)National Institute for Research and Development of Isotopic and Molecular Technologies, Physics Department, Cluj-Napoca, Romania; (e)University Politehnica Bucharest, Bucharest, Romania; (f)West University in Timisoara, Timisoara, Romania; (g)Faculty of Physics, University of Bucharest, Bucharest, Romania

[28] (a)Faculty of Mathematics, Physics and Informatics, Comenius University, Bratislava, Slovakia; (b)Department of Subnuclear Physics, Institute of Experimental Physics of the Slovak Academy of Sciences, Kosice, Slovak Republic

[29] Physics Department, Brookhaven National Laboratory, Upton, NY, USA

[30] Departamento de Física, y CONICET, Facultad de Ciencias Exactas y Naturales, Instituto de Física de Buenos Aires (IFIBA), Universidad de Buenos Aires, Buenos Aires, Argentina

[31] California State University, Fresno, CA, USA

[32] Cavendish Laboratory, University of Cambridge, Cambridge, UK

[33] (a)Department of Physics, University of Cape Town, Cape Town, South Africa; (b)iThemba Labs, Western Cape, South Africa; (c)Department of Mechanical Engineering Science, University of Johannesburg, Johannesburg, South Africa; (d)National Institute of Physics, University of the Philippines, Diliman, Philippines; (e)Department of Physics, University of South Africa, Pretoria, South Africa; (f)University of Zululand, KwaDlangezwa, South Africa ; (g)School of Physics, University of the Witwatersrand, Johannesburg, South Africa

[34] Department of Physics, Carleton University, Ottawa, ON, Canada

[35] (a)Faculté des Sciences Ain Chock, Réseau Universitaire de Physique des Hautes Energies, Université Hassan II, Casablanca, Morocco; (b)Faculté des Sciences, Université Ibn-Tofail, Kénitra, Morocco; (c)Faculté des Sciences Semlalia, Université Cadi Ayyad, LPHEA-Marrakech, Morocco; (d)LPMR, Faculté des Sciences, Université Mohamed Premier, Oujda, Morocco; (e)Faculté des sciences, Université Mohammed V, Rabat, Morocco; (f)Institute of Applied Physics, Mohammed VI Polytechnic University, Ben Guerir, Morocco

[36] CERN, Geneva, Switzerland

[37] Affiliated with an institute covered by a cooperation agreement with CERN, Geneva, Switzerland

[38] Affiliated with an international laboratory covered by a cooperation agreement with CERN, Geneva, Switzerland

[39] Enrico Fermi Institute, University of Chicago, Chicago, IL, USA

[40] LPC, Université Clermont Auvergne, CNRS/IN2P3, Clermont-Ferrand, France

[41] Nevis Laboratory, Columbia University, Irvington, NY, USA

[42] Niels Bohr Institute, University of Copenhagen, Copenhagen, Denmark

[43] (a)Dipartimento di Fisica, Università della Calabria, Rende, Italy; (b)INFN Gruppo Collegato di Cosenza, Laboratori Nazionali di Frascati, Frascati, Italy

[44] Physics Department, Southern Methodist University, Dallas, TX, USA

[45] Physics Department, University of Texas at Dallas, Richardson, TX, USA

[46] National Centre for Scientific Research "Demokritos", Agia Paraskevi, Greece

[47] (a)Department of Physics, Stockholm University, Stockholm, Sweden; (b)Oskar Klein Centre, Stockholm, Sweden

[48] Deutsches Elektronen-Synchrotron DESY, Hamburg and Zeuthen, Germany

[49] Fakultät Physik , Technische Universität Dortmund, Dortmund, Germany

[50] Institut für Kern- und Teilchenphysik, Technische Universität Dresden, Dresden, Germany

[51] Department of Physics, Duke University, Durham, NC, USA

[52] SUPA-School of Physics and Astronomy, University of Edinburgh, Edinburgh, UK

[53] INFN e Laboratori Nazionali di Frascati, Frascati, Italy

[54] Physikalisches Institut, Albert-Ludwigs-Universität Freiburg, Freiburg, Germany

[55] II. Physikalisches Institut, Georg-August-Universität Göttingen, Göttingen, Germany

[56] Département de Physique Nucléaire et Corpusculaire, Université de Genève, Geneva, Switzerland

[57] [a]Dipartimento di Fisica, Università di Genova, Genoa, Italy; [b]INFN Sezione di Genova, Genoa, Italy

[58] II. Physikalisches Institut, Justus-Liebig-Universität Giessen, Giessen, Germany

[59] SUPA-School of Physics and Astronomy, University of Glasgow, Glasgow, UK

[60] LPSC, Université Grenoble Alpes, CNRS/IN2P3, Grenoble INP, Grenoble, France

[61] Laboratory for Particle Physics and Cosmology, Harvard University, Cambridge, MA, USA

[62] [a]Department of Modern Physics and State Key Laboratory of Particle Detection and Electronics, University of Science and Technology of China, Hefei, China; [b]Institute of Frontier and Interdisciplinary Science and Key Laboratory of Particle Physics and Particle Irradiation (MOE), Shandong University, Qingdao, China; [c]School of Physics and Astronomy, Shanghai Jiao Tong University, Key Laboratory for Particle Astrophysics and Cosmology (MOE), SKLPPC, Shanghai, China; [d]Tsung-Dao Lee Institute, Shanghai, China

[63] [a]Kirchhoff-Institut für Physik, Ruprecht-Karls-Universität Heidelberg, Heidelberg, Germany; [b]Physikalisches Institut, Ruprecht-Karls-Universität Heidelberg, Heidelberg, Germany

[64] [a]Department of Physics, Chinese University of Hong Kong, Shatin, N.T., Hong Kong, China; [b]Department of Physics, University of Hong Kong, Hong Kong, China; [c]Department of Physics and Institute for Advanced Study, Hong Kong University of Science and Technology, Clear Water Bay, Kowloon, Hong Kong, China

[65] Department of Physics, National Tsing Hua University, Hsinchu, Taiwan

[66] IJCLab, Université Paris-Saclay, CNRS/IN2P3, 91405 Orsay, France

[67] Centro Nacional de Microelectrónica (IMB-CNM-CSIC), Barcelona, Spain

[68] Department of Physics, Indiana University, Bloomington, IN, USA

[69] [a]INFN Gruppo Collegato di Udine, Sezione di Trieste, Udine, Italy; [b]ICTP, Trieste, Italy; [c]Dipartimento Politecnico di Ingegneria e Architettura, Università di Udine, Udine, Italy

[70] [a]INFN Sezione di Lecce, Lecce, Italy; [b]Dipartimento di Matematica e Fisica, Università del Salento, Lecce, Italy

[71] [a]INFN Sezione di Milano, Milan, Italy; [b]Dipartimento di Fisica, Università di Milano, Milan, Italy

[72] [a]INFN Sezione di Napoli, Naples, Italy; [b]Dipartimento di Fisica, Università di Napoli, Naples, Italy

[73] [a]INFN Sezione di Pavia, Pavia, Italy; [b]Dipartimento di Fisica, Università di Pavia, Pavia, Italy

[74] [a]INFN Sezione di Pisa, Pisa, Italy; [b]Dipartimento di Fisica E. Fermi, Università di Pisa, Pisa, Italy

[75] [a]INFN Sezione di Roma, Rome, Italy; [b]Dipartimento di Fisica, Sapienza Università di Roma, Rome, Italy

[76] [a]INFN Sezione di Roma Tor Vergata, Rome, Italy; [b]Dipartimento di Fisica, Università di Roma Tor Vergata, Rome, Italy

[77] [a]INFN Sezione di Roma Tre, Rome, Italy; [b]Dipartimento di Matematica e Fisica, Università Roma Tre, Rome, Italy

[78] [a]INFN-TIFPA, Povo, Italy; [b]Università degli Studi di Trento, Trento, Italy

[79] Department of Astro and Particle Physics, Universität Innsbruck, Innsbruck, Austria

[80] University of Iowa, Iowa City, IA, USA

[81] Department of Physics and Astronomy, Iowa State University, Ames, IA, USA

[82] [a]Departamento de Engenharia Elétrica, Universidade Federal de Juiz de Fora (UFJF), Juiz de Fora, Brazil; [b]Universidade Federal do Rio De Janeiro COPPE/EE/IF, Rio de Janeiro, Brazil; [c]Instituto de Física, Universidade de São Paulo, São Paulo, Brazil; [d]Rio de Janeiro State University, Rio de Janeiro, Brazil

[83] KEK, High Energy Accelerator Research Organization, Tsukuba, Japan

[84] Graduate School of Science, Kobe University, Kobe, Japan

[85] [a]Faculty of Physics and Applied Computer Science, AGH University of Science and Technology, Krakow, Poland; [b]Marian Smoluchowski Institute of Physics, Jagiellonian University, Krakow, Poland

[86] Institute of Nuclear Physics, Polish Academy of Sciences, Krakow, Poland

[87] Faculty of Science, Kyoto University, Kyoto, Japan

[88] Kyoto University of Education, Kyoto, Japan

89 Research Center for Advanced Particle Physics and Department of Physics, Kyushu University, Fukuoka, Japan

90 Instituto de Física La Plata, Universidad Nacional de La Plata and CONICET, La Plata, Argentina

91 Physics Department, Lancaster University, Lancaster, UK

92 Oliver Lodge Laboratory, University of Liverpool, Liverpool, UK

93 Department of Experimental Particle Physics, Jožef Stefan Institute and Department of Physics, University of Ljubljana, Ljubljana, Slovenia

94 School of Physics and Astronomy, Queen Mary University of London, London, UK

95 Department of Physics, Royal Holloway University of London, Egham, UK

96 Department of Physics and Astronomy, University College London, London, UK

97 Louisiana Tech University, Ruston, LA, USA

98 Fysiska institutionen, Lunds universitet, Lund, Sweden

99 Departamento de Física Teorica C-15 and CIAFF, Universidad Autónoma de Madrid, Madrid, Spain

100 Institut für Physik, Universität Mainz, Mainz, Germany

101 School of Physics and Astronomy, University of Manchester, Manchester, UK

102 CPPM, Aix-Marseille Université, CNRS/IN2P3, Marseille, France

103 Department of Physics, University of Massachusetts, Amherst, MA, USA

104 Department of Physics, McGill University, Montreal, QC, Canada

105 School of Physics, University of Melbourne, Victoria, Australia

106 Department of Physics, University of Michigan, Ann Arbor, MI, USA

107 Department of Physics and Astronomy, Michigan State University, East Lansing, MI, USA

108 Group of Particle Physics, University of Montreal, Montreal, QC, Canada

109 Fakultät für Physik, Ludwig-Maximilians-Universität München, Munich, Germany

110 Max-Planck-Institut für Physik (Werner-Heisenberg-Institut), Munich, Germany

111 Graduate School of Science and Kobayashi-Maskawa Institute, Nagoya University, Nagoya, Japan

112 Department of Physics and Astronomy, University of New Mexico, Albuquerque, NM, USA

113 Institute for Mathematics, Astrophysics and Particle Physics, Radboud University/Nikhef, Nijmegen, The Netherlands

114 Nikhef National Institute for Subatomic Physics and University of Amsterdam, Amsterdam, The Netherlands

115 Department of Physics, Northern Illinois University, DeKalb, IL, USA

116 (a)New York University Abu Dhabi, Abu Dhabi, United Arab Emirates; (b)University of Sharjah, Sharjah, United Arab Emirates

117 Department of Physics, New York University, New York, NY, USA

118 Ochanomizu University, Otsuka, Bunkyo-ku, Tokyo, Japan

119 Ohio State University, Columbus, OH, USA

120 Homer L. Dodge Department of Physics and Astronomy, University of Oklahoma, Norman, OK, USA

121 Department of Physics, Oklahoma State University, Stillwater, OK, USA

122 Palacký University, Joint Laboratory of Optics, Olomouc, Czech Republic

123 Institute for Fundamental Science, University of Oregon, Eugene, OR, USA

124 Graduate School of Science, Osaka University, Osaka, Japan

125 Department of Physics, University of Oslo, Oslo, Norway

126 Department of Physics, Oxford University, Oxford, UK

127 LPNHE, Sorbonne Université, Université Paris Cité, CNRS/IN2P3, Paris, France

128 Department of Physics, University of Pennsylvania, Philadelphia, PA, USA

129 Department of Physics and Astronomy, University of Pittsburgh, Pittsburgh, PA, USA

130 (a)Laboratório de Instrumentação e Física Experimental de Partículas-LIP, Lisbon, Portugal; (b)Departamento de Física, Faculdade de Ciências, Universidade de Lisboa, Lisboa, Portugal; (c)Departamento de Física, Universidade de Coimbra, Coimbra, Portugal; (d)Centro de Física Nuclear da Universidade de Lisboa, Lisbon, Portugal; (e)Departamento de Física, Universidade do Minho, Braga, Portugal; (f)Departamento de Física Teórica y del Cosmos, Universidad de Granada, Granada, Spain; (g)Departamento de Física, Instituto Superior Técnico, Universidade de Lisboa, Lisbon, Portugal

131 Institute of Physics of the Czech Academy of Sciences, Prague, Czech Republic

132 Czech Technical University in Prague, Prague, Czech Republic

133 Faculty of Mathematics and Physics, Charles University, Prague, Czech Republic

134 Particle Physics Department, Rutherford Appleton Laboratory, Didcot, UK

135 IRFU, CEA, Université Paris-Saclay, Gif-sur-Yvette, France

[136] Santa Cruz Institute for Particle Physics, University of California Santa Cruz, Santa Cruz, CA, USA

[137] (a)Departamento de Física, Pontificia Universidad Católica de Chile, Santiago, Chile; (b)Millennium Institute for Subatomic physics at high energy frontier (SAPHIR), Santiago, Chile; (c)Instituto de Investigación Multidisciplinario en Ciencia y Tecnología y Departamento de Física, Universidad de La Serena, La Serena, Chile; (d)Department of Physics, Universidad Andres Bello, Santiago, Chile; (e)Instituto de Alta Investigación, Universidad de Tarapacá, Arica, Chile ; (f)Departamento de Física, Universidad Técnica Federico Santa María, Valparaíso, Chile

[138] Department of Physics, University of Washington, Seattle, WA, USA

[139] Department of Physics and Astronomy, University of Sheffield, Sheffield, UK

[140] Department of Physics, Shinshu University, Nagano, Japan

[141] Department Physik, Universität Siegen, Siegen, Germany

[142] Department of Physics, Simon Fraser University, Burnaby, BC, Canada

[143] SLAC National Accelerator Laboratory, Stanford, CA, USA

[144] Department of Physics, Royal Institute of Technology, Stockholm, Sweden

[145] Departments of Physics and Astronomy, Stony Brook University, Stony Brook, NY, USA

[146] Department of Physics and Astronomy, University of Sussex, Brighton, UK

[147] School of Physics, University of Sydney, Sydney, Australia

[148] Institute of Physics, Academia Sinica, Taipei, Taiwan

[149] (a)E. Andronikashvili Institute of Physics, Iv. Javakhishvili Tbilisi State University, Tbilisi, Georgia; (b)High Energy Physics Institute, Tbilisi State University, Tbilisi, Georgia; (c)University of Georgia, Tbilisi, Georgia

[150] Department of Physics, Technion, Israel Institute of Technology, Haifa, Israel

[151] Raymond and Beverly Sackler School of Physics and Astronomy, Tel Aviv University, Tel Aviv, Israel

[152] Department of Physics, Aristotle University of Thessaloniki, Thessaloniki, Greece

[153] International Center for Elementary Particle Physics and Department of Physics, University of Tokyo, Tokyo, Japan

[154] Department of Physics, Tokyo Institute of Technology, Tokyo, Japan

[155] Department of Physics, University of Toronto, Toronto, ON, Canada

[156] (a)TRIUMF, Vancouver, BC, Canada; (b)Department of Physics and Astronomy, York University, Toronto, ON, Canada

[157] Division of Physics and Tomonaga Center for the History of the Universe, Faculty of Pure and Applied Sciences, University of Tsukuba, Tsukuba, Japan

[158] Department of Physics and Astronomy, Tufts University, Medford, MA, USA

[159] United Arab Emirates University, Al Ain, United Arab Emirates

[160] Department of Physics and Astronomy, University of California Irvine, Irvine, CA, USA

[161] Department of Physics and Astronomy, University of Uppsala, Uppsala, Sweden

[162] Department of Physics, University of Illinois, Urbana, IL, USA

[163] Instituto de Física Corpuscular (IFIC), Centro Mixto Universidad de Valencia-CSIC, Valencia, Spain

[164] Department of Physics, University of British Columbia, Vancouver, BC, Canada

[165] Department of Physics and Astronomy, University of Victoria, Victoria, BC, Canada

[166] Fakultät für Physik und Astronomie, Julius-Maximilians-Universität Würzburg, Würzburg, Germany

[167] Department of Physics, University of Warwick, Coventry, UK

[168] Waseda University, Tokyo, Japan

[169] Department of Particle Physics and Astrophysics, Weizmann Institute of Science, Rehovot, Israel

[170] Department of Physics, University of Wisconsin, Madison, WI, USA

[171] Fakultät für Mathematik und Naturwissenschaften, Fachgruppe Physik, Bergische Universität Wuppertal, Wuppertal, Germany

[172] Department of Physics, Yale University, New Haven, CT, USA

[a] Also Affiliated with an institute covered by a cooperation agreement with CERN, Geneva, Switzerland

[b] Also at An-Najah National University, Nablus, Palestine

[c] Also at Borough of Manhattan Community College, City University of New York, New York, NY, USA

[d] Also at Bruno Kessler Foundation, Trento, Italy

[e] Also at Center for High Energy Physics, Peking University, Beijing, China

[f] Also at Center for Interdisciplinary Research and Innovation (CIRI-AUTH), Thessaloniki , Greece

[g] Also at Centro Studi e Ricerche Enrico Fermi, Rome, Italy

[h] Also at CERN, Geneva, Switzerland

[i] Also at Département de Physique Nucléaire et Corpusculaire, Université de Genève, Geneva, Switzerland

[j] Also at Departament de Fisica de la Universitat Autonoma de Barcelona, Barcelona, Spain

[k] Also at Department of Financial and Management Engineering, University of the Aegean, Chios, Greece

[l] Also at Department of Physics and Astronomy, Michigan State University, East Lansing, MI, USA

[m] Also at Department of Physics, Ben Gurion University of the Negev, Beer Sheva, Israel

[n] Also at Department of Physics, California State University, East Bay, USA

[o] Also at Department of Physics, California State University, Sacramento, USA

[p] Also at Department of Physics, King's College London, London, UK

[q] Also at Department of Physics, Stanford University, Stanford, CA, USA

[r] Also at Department of Physics, University of Fribourg, Fribourg, Switzerland

[s] Also at Department of Physics, University of Thessaly, Thessaly, Greece

[t] Also at Department of Physics, Westmont College, Santa Barbara, USA

[u] Also at Hellenic Open University, Patras, Greece

[v] Also at Institucio Catalana de Recerca i Estudis Avancats, ICREA, Barcelona, Spain

[w] Also at Institut für Experimentalphysik, Universität Hamburg, Hamburg, Germany

[x] Also at Institute of Applied Physics, Mohammed VI Polytechnic University, Ben Guerir, Morocco

[y] Also at Institute of Particle Physics (IPP), Canada

[z] Also at Institute of Physics and Technology, Ulaanbaatar, Mongolia

[aa] Also at Institute of Physics, Azerbaijan Academy of Sciences, Baku, Azerbaijan

[ab] Also at Institute of Theoretical Physics, Ilia State University, Tbilisi, Georgia

[ac] Also at L2IT, Université de Toulouse, CNRS/IN2P3, UPS, Toulouse, France

[ad] Also at Lawrence Livermore National Laboratory, Livermore, USA

[ae] Also at National Institute of Physics, University of the Philippines, Diliman, Philippines

[af] Also at Technical University of Munich, Munich, Germany

[ag] Also at The Collaborative Innovation Center of Quantum Matter (CICQM), Beijing, China

[ah] Also at TRIUMF, Vancouver, BC, Canada

[ai] Also at Università di Napoli Parthenope, Naples, Italy

[aj] Also at University of Chinese Academy of Sciences (UCAS), Beijing, China

[ak] Also at Department of Physics, University of Colorado Boulder, Colorado, USA

[al] Also at Washington College, Chestertown, MD, USA

[am] Also at Physics Department, Yeditepe University, Istanbul, Türkiye

[an] Also at Institute for Nuclear Research and Nuclear Energy (INRNE) of the Bulgarian Academy of Sciences, Sofia, Bulgaria

[*] Deceased